POLITECNICO DI MILANO

Facoltà di Ingegneria Industriale

Corso di Laurea Magistrale in

Ingegneria Aeronautica

Structural Design Optimization of the SAR Plate Assembly Through Genetic Algorithms

Relatore: Prof. Sergio RICCI

Correlatore: Giuseppe TORRACO

Tesi di Laurea di:

Ezgi KIRMAN   Matr. 735209

❝ Man can will nothing unless he has first understood that he must count no one but himself; that he is alone, abandoned on earth in the midst of his infinite responsibilities, without help, with no other aim than the one he sets himself, with no other destiny than the one he forges for himself on this earth. ❞

Jean Paul Sartre

Ringraziamenti

Contents

List of Figures

List of Tables

Nomenclature

χ Midplane curvature

ϵ_0 Natural frequency of the shock absorber

λ Rate of transmission

ν Poisson's ratio

ρ Density

σ_1 Applied ultimate stress in longitudinal direction

σ_2 Applied ultimate stress in transverse direction

σ_c Maximum applied compression stress

σ_{tu} Ultimate tensile strength

σ_{ty} Tensile yield strength

τ_{12} Applied ultimate shear stress

ε_0 Midplane membrane strains

A_d Area of the rotor disc

CAD Computer aided design

CoG Centre of gravity

D_{11} Flexural rigidity of the laminate

E_{xx} Elastic modulus along the longitudinal direction

E_{yy} Elastic modulus along the transverse direction

F Applied force

F_{cc} Ultimate allowable crippling strength

F_{cu} Ultimate allowable compression strength along longitudinal direction

f_e^1 First natural frequency of the empty plate

f_l^1 First natural frequency of the fully loaded plate

FEM Finite element model

FI Failure index

g Gravitational acceleration

G_{xy} Shear modulus

k Rigidity of the system

LH Left hand side

M Moment per unit length

m Mass of the system

M_e Mass of the empty plate

MS Margin of safety

MS_{ult} Margin of safety at ultimate load

N Force per unit length

P_{ideal} Ideal power required to hover

$R_{x_{down}}$ Maximum reaction force at lower constraints along x

$R_{x_{up}}$ Maximum reaction force at upper constraints along x

$R_{y_{down}}$ Maximum reaction force at lower constraints along y

$R_{y_{up}}$ Maximum reaction force at upper constraints along y

$R_{z_{down}}$ Maximum reaction force at lower constraints along z

RH Right hand side

S_{12} Allowable ultimate stress for in plane shear

T Thrust produced by the rotor

t Total thickness of the laminate

V_i Induced velocity at the rotor

W Total weight

w_0 Characteristic damping rate

X_c Allowable ultimate stress in compression along the longitudinal direction

X_t Allowable ultimate stress in tension along the longitudinal direction

Y_c Allowable ultimate stress in compression along the transverse direction

Y_t Allowable ultimate stress in tension along the transverse direction

Abstract

Advances in computational technologies allow further improvements regarding the efficiency of the preliminary design phase. Specialized softwares enable the integration and the optimization of a process flow with the scope of reducing time and costs while significantly improving product performance, quality, and reliability. This thesis work consists of an *Isight* application with the aim of automation and optimization of a structural design process of the SAR Plate Assembly. The multiobjective optimization problem that regards this specific helicopter component is handled through the use of 4 different genetic algorithms. Once the procedure of finite element analysis is automated, new design solutions are obtained by finding a compromise between the objective functions related to mass and vibration frequencies. Topologically different design solutions are systematically tested and perfected by sizing and internal parameter optimization in manner to obtain a light and dynamically tailored structure.

Keywords: SAR Plate Assembly, multi objective optimization, genetic algorithms, *Isight*, structural optimization

Sommario

Il progresso nelle tecniche computazionali permette un continuo miglioramento dell'efficienza della fase di design preliminare. Software specifici garantiscono l'integrazione e l'ottimizzazione di un flusso di processo, allo scopo di ridurre tempi e costi ed al contempo di incrementare la prestazione , la qualità e l'affidabilità del prodotto. Questo lavoro di tesi consiste nell'applicazione del software *Isight* per l'automazione e l'ottimizzazione del processo di design strutturale del blocco SAR Plate. Si è affrontato il problema di ottimizzazione multi obiettivo di questo specifico componente elicotteristico attraverso l'utilizzo di 4 differenti algoritmi genetici. Una volta che la procedura di analisi ad elementi finiti è automatizzata, si ottengono nuove soluzioni di design tramite un compromesso tra le funzioni obbiettivo legate alla massa ed alla frequenza propria. Soluzioni topologicamente differenti sono state sistematicamente provate e perfezionate attraverso l'ottimizzazione del dimensionamento e dei parametri interni, al fine di ottenere una struttura leggera e dinamicamente adatta.

Parole chiave: SAR Plate Assembly, ottimizzazione multi obiettivo, algoritmi genetici, *Isight*, ottimizzazione strutturale

Chapter 1

Optimization theory

1.1 General description of an optimization problem

The main scope of an optimization problem is to find an alternative with the most cost effective or highest achievable performance under the given constraints, by maximizing desired factors and minimizing undesired ones. The generality of the given definition confirms that an optimization process comprises a very wide application range including many different fields such as engineering, science, economics, operations research and medicine. Even though all these disciplines have variant objectives, the mathematical tools that are employed in order to achieve any specific objective are universal. Once the optimization problem is mathematically stated, it only becomes a real function to be minimized or maximized in a systematic manner. Consequently, the second fundamental step in an optimization process following the problem statement is the selection of the optimization algorithm, in other words the progress strategy used to achieve the optimal solution. In accordance with this introductory paragraph, this section consists of an overview concerning an optimization problem statement and the choice of a relevant algorithm.

1.1.1 Problem statement

An overview of the basic optimization theory can be beneficial in order to clarify the principal concepts that are going to be used during the rest of this thesis work. As previously mentioned, an optimization problem consists of maximizing or minimizing a constrained function by systematically varying the design variables within an allowed range. The mathematical formulation of this verbal definition is reported from Ref[42]:

$$\textbf{Optimization problem: } \text{Find } X = \begin{Bmatrix} x_1 \\ x_2 \\ \vdots \\ x_n \end{Bmatrix} \quad \text{which minimizes } f(X)$$

$$\text{subject to the constraints:} \quad \begin{aligned} g_j(X) &\leq 0 \quad j = 1, 2, \cdots, m \\ h_j(X) &= 0 \quad j = 1, 2, \cdots, p \end{aligned} \tag{1.1}$$

Considering this notation, $f(X)$ corresponds to the objective function and the vector X to the design variables. The objective function which depends on the design variables can be considered as the criterion with respect to which the design is optimized. The design variables are the set of quantities which are not fixed at the outset of the problem. The collection of these parameters which constitutes the design or problem space $\mathbb{X}$ is used in order to control but especially to improve the system performance. As eq. 1.1 shows the current objective function is subjected to inequality and equality constraints, $g_j(X)$ and $h_j(X)$ respectively. Note that the number of variables or constraints, n, m and p do not need to be related in a way. The constraint functions which specify the requirements to be fulfilled divides the search space into small domains that can be classified as feasible or infeasible. The criterion of feasibility regards the satisfaction of the given constraints.
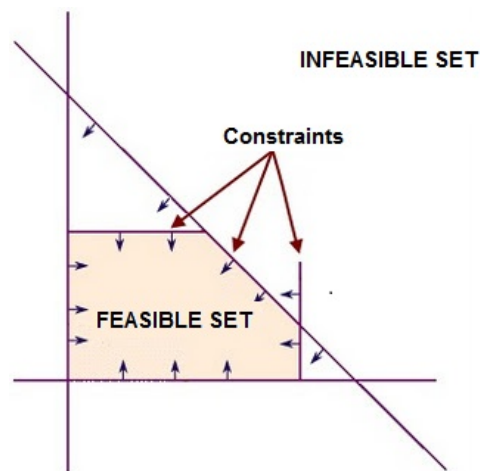
Figure 1.1: Division of the search space

Optimization problems can be classified according to different criteria such as the number of objective functions (mono–objective, multiobjective), its characteristics (linear, convex, differentiable) or the presence of the constraints (constrained, unconstrained). Another type of classification can also be made regarding the type of design variables such as continuous, discrete or a combination of two. These important properties regarding the nature of the objective function and the design variables give important indications about the selection of the adequate optimization algorithm.

1.1.2 Optimization algorithms

Even though trying all possible design variable combinations guarantees to find the best or optimum solution, it might not be applicable due to the presence of elevated number of possible solutions. From this point of view, optimization algorithms can be seen as "smart" techniques that attempt to reduce the total tentative number of experiments in order to reach the optimum solution. According to Ref[43], these algorithms can be divided into 2 main groups: Deterministic and Stochastic. The important difference between the 2 classes depends on the searching techniques for reaching the optimum solution. Deterministic algorithms depart from an initial solution and progress based on the gradient information along the search direction. Whereas a stochastic method adopts the idea of a random search in the design space.

Deterministic algorithms

As previously stated, deterministic optimization methods are based on a variational criteria like gradient information. Even though this type of algorithms is not used in this thesis work, a brief description concerning these methods would provide to the reader a new perspective and a deeper understanding of the optimization problem.

$$\nabla f(X^*) = \begin{pmatrix} \frac{\partial f(X^*)}{\partial x_1} \\[6pt] \frac{\partial f(X^*)}{\partial x_2} \\ \vdots \\ \frac{\partial f(X^*)}{\partial x_n} \end{pmatrix} \quad H(X^*) = \nabla^2 f(X^*) = \begin{pmatrix} \frac{\partial^2 f(X^*)}{\partial x_1^2} & \cdots & \frac{\partial^2 f(X^*)}{\partial x_1 x_n} \\ \vdots & \ddots & \vdots \\ \frac{\partial^2 f(X^*)}{\partial x_n x_1} & \cdots & \frac{\partial^2 f(X^*)}{\partial x_n^2} \end{pmatrix} \quad (1.2)$$

In the case of an unconstrained optimization problem, the local maximum or minimum of an objective function can be found depending on its first and second

derivative with respect to the design variables. According to optimality condi-
tions, the design variable X^* vector that rends null or indefinite the first gradient
of the objective function is called stationary point. The nature of the stationary
point can be determined by considering the information coming from the Hessian
matrix $H(X^*)$ which corresponds to the second derivative of the objective function.
If this matrix is positive definite, the critical point is a local minimum. Instead, if
it is negative definite, the solution is a local maximum and in the case that it is
not definite, a saddle point can be obtained.
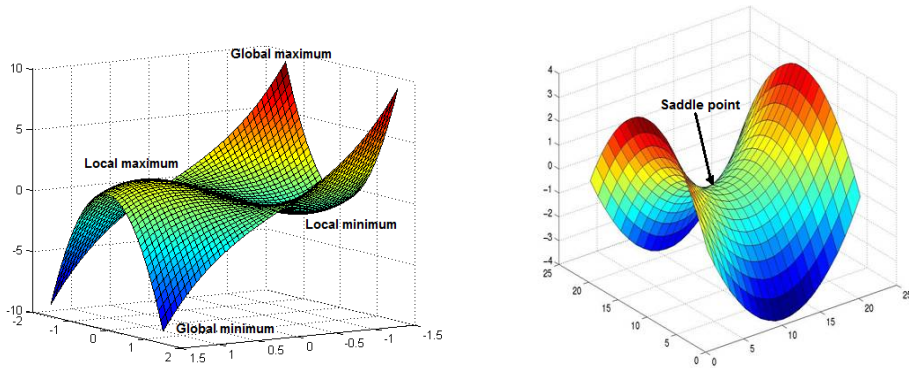
Figure 1.2: Visualization of the stationary points

Note that if an objective function $f(X) : \mathbb{R}^n \to \mathbb{R}$ is to be minimized, its lo-
cal minimum can correspond to the point X^* if there exists an $\varepsilon > 0$ such that
$f(X) \geq f(X^*)$ for all $X \in \mathbb{R}^n$ and $\| X - X^* \| < \varepsilon$.

Even though these conditions of optimality are valid for unconstrained optimiza-
tion problems, there exist various techniques that enable to convert a constrained
problem to a unconstrained one. Principally, these techniques integrate the effects
of the constraints into the objective function. As previously mentioned, the con-
strains can be present in form of an equality or inequality relation. The equality
constraints can be added to the objective function by using the Lagrange multi-
pliers λ and μ. Whereas the inequality constraints are firstly transformed into
an equality relation through slack variables s and then they can be treated as a
usual equality constraint (eq. 1.3).

$$g_j + s_j^2 = 0 \tag{1.3}$$

For the optimization problem stated in eq. 1.1, the corresponding Lagrangian
function $\mathbb{L}$ can be written as in eq. 1.4:

$$\mathbb{L}(X, \lambda, \mu, s) = f(X) + \sum_{j=1}^{p} \lambda_j h_j(X) + \sum_{j=1}^{m} \mu_j [g_j(X) + s_j^2] \qquad (1.4)$$

In order to find the local minimum X^*, Lagrange multipliers rule and the Kuhn–Tucker conditions must be satisfied. The first method can be equivalent to a stationarity condition which sets the gradient of the Lagrangian function to 0.

$$
\begin{cases}
\dfrac{\partial \mathbb{L}}{\partial X_i} = & \dfrac{\partial f(X^*)}{\partial X_i} + \sum_{j=1}^{p} \lambda_j \dfrac{\partial h(X^*)}{\partial X_i} + \sum_{j=1}^{m} \mu_j \dfrac{\partial g(X^*)}{\partial X_i} = 0 & \forall i \in [1, ..n] \\[4mm]
\dfrac{\partial \mathbb{L}}{\partial \lambda_j} = & h_j(X^*) = 0 & \forall j \in [1, ..p] \\[4mm]
\dfrac{\partial \mathbb{L}}{\partial \mu_j} = & g_j(X^*) + s_j^2 = 0 & \forall j \in [1, ..m] \\[4mm]
\dfrac{\partial \mathbb{L}}{\partial s_j} = & 2\mu_j s_j = 0 & \forall j \in [1, ..m]
\end{cases}
$$

The equality given by the derivative of the Lagrangian function with respect to the slack variables is also called complementary slackness condition. If this equation is multiplied by $-s$, the first the Kuhn-Tucker condition in eq. 1.5 can be obtained. Instead, the second equation has a longer demonstration that can be examined by using Ref[44] and that bases on a small perturbation of the inequality.

$$
\begin{cases}
\mu_j g_j(X^*) = 0 & \forall j \in [1, ..m] \\
\mu_j \geq 0 & \forall j \in [1, ..m]
\end{cases}
\qquad (1.5)
$$

To sum up, for deterministic methods that are based on the gradient information, the regularity of the search space is an essential constraint. In other words, the objective and constraint functions should be differentiable respect to the design variables. This limitation does not permit these algorithms to work with discrete design variables. In addition to this, another disadvantage concerns the dependency of the starting solution. This fact increases the risk of remaining trapped near a local minimum or maximum.

A last remark about this type of algorithms regards the number of objective functions that they are able to cope with. Their nature allows them to work with a single objective function only. Similar to the remarks done concerning the constraint handling, there exist some conversion methods that transform a multi objective optimization problem to a single objective one. One of the most diffused techniques attempts to formulate a single objective function $\mathbb{F}$ by assigning a weighting factor w to each objective and then by summing them all (eq. 1.6). At this point the aim becomes to minimize or maximize this unique function. Note that the weighting factors can be selected arbitrarily depending on the importance of the objective function.

$$\mathbb{F} = \sum_{i=1}^{k} w_i f_i(X) \tag{1.6}$$

Stochastic algorithm

Deterministic algorithms are most often used if a clear relation between the characteristics of the possible solutions and their utility for a given problem exists. Instead, if this relation is too complicated or the dimensionality of the search space is very high, it becomes harder to solve the problem deterministically [34]. At this point, the use of stochastic or probabilistic algorithms that can cope with a measurement noise or that implicitly introduce a randomness in the search procedure can be efficient. The reason of their efficiency lays in the fact that they make few or no assumptions about the optimization problem or in other words they consider it as a 'black box'. This approach that is also called *metaheuristic* is adopted by most of the stochastic algorithms. Monte Carlo algorithms which is one of the most fundamental stochastic optimization classes contain several methods with different source of inspiration. To illustrate, evolutionary algorithms are based on the organic evolution whereas simulated annealing is inspired from the cooling process analysed in metallurgy field. As these algorithms do not require any gradient information, their application area becomes wider. For instance, they can efficiently deal with multi objective problems or discrete design variables. On the other hand, this efficiency is generally paid by computational power. Moreover, the accuracy of the optimization results can only be improved by investing more time. In this thesis work, genetic algorithms which make part of the evolutionary algorithms are basically used. Consequently, the following sections of this chapter focus on the details regarding this class of optimization algorithms.

1.2   Evolutionary algorithms

Applicable reference: [34]

Evolutionary algorithms can be defined as population based metaheuristic opti-mization methods that use biology inspired methods in order to improve a set of candidate solutions in an iterative manner. The inspiration point of these algo-rithms is Darwin's biological evolution principles such as natural selection and survival of the fittest. Evolutionary algorithms consider any optimization problem as a "black box" and make few assumptions concerning the underlying objectives. This fact enlarges its application area including diverse fields like engineering, economics, marketing physics, chemistry and politics.

Even though there exist different subgroups of evolutionary algorithms such as Genetic algorithms, Genetic and Evolutionary programming; the driving mecha-nism behind them is unique. The basic cycle that resumes the infrastructure of the evolution algorithms is given in fig. 1.3.
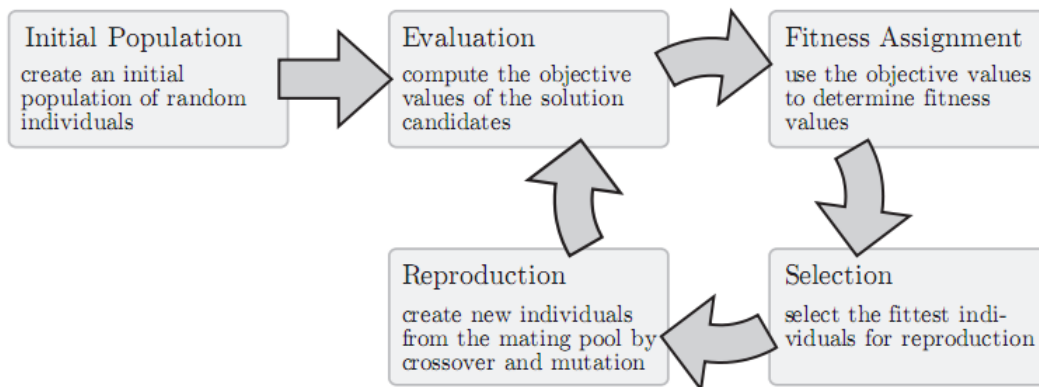
Figure 1.3: Basic cycle of evolutionary algorithms

A brief description of the main steps illustrated in fig. 1.3 can be made in the following manner:

1. **Initialization:** Firstly, an initial population with a predefined number of individuals is created.

2. **Evolution:** For each individual, the values of all objective functions are calculated.

3. **Fitness assignment:** Through special techniques based on the objective function values, a fitness value is assigned to each candidate solution.

4. **Selection:** By taking into account the assigned fitness values, a selection process is applied in order to filter and choose the individuals that are going to be put in the mating pool.

5. **Reproduction:** The selected individuals participate to the reproduction phase in order to create new individuals through genetic operations.

6. **Termination:** The loop continues until the termination criterion is met. This criterion might related to the solution quality or time.

After a general view of the evolutionary algorithms, some of the notions like fitness assignment, selection and reproduction can be examined in details because these elements constitute the keystone of the evolutionary algorithms.

Fitness Assignment In multiobjective optimization problems, each candidate solution is characterized by a vector that contains the objective function values of the corresponding individual. However, many algorithms prefer to transform this vectorial entity to a scalar value that represents the fitness of the solution. Note that this fitness value is equivalent to the quality of the solution within the population so it is a relative entity that depends on the environment. Most of the algorithms calculate this value based on two main concepts:

Pareto Ranking: In order to be able to make a classification based on the quality of the existing solutions, Pareto domination notion is often used. This notion can be seen equivalent to a tradeoff information among conflicting objectives [35].

An element x_1 dominates (is preferred to) an element x_2 ($x_1 \vdash x_2$) if x_1 is better than x_2 in at least one objective function and not worse with respect to all other objectives. Based on the set F of objective functions f, it is possible to write:

$$
\begin{aligned}
\textbf{Pareto} \quad & x_1 \vdash x_2 \; \Leftrightarrow \; \forall i : 0 < i \leq n \; \Rightarrow w_i f_i(x_1) \leq w_i f_i(x_2) \wedge \\
\textbf{Domination} \quad & \exists j : 0 < j \leq n : \; w_j f_j(x_1) < w_j f_j(x_2)
\end{aligned}
$$

where:

$$w_i = \begin{cases} 1 & \text{if } f_i \text{ should be minimized} \\ -1 & \text{if } f_i \text{ should be maximized} \end{cases} \tag{1.7}$$

In light of this definition, there exists a set of solutions that are not dominated by the other ones. These non dominated points form the Pareto front which can be a line or a surface in the presence of 2 and 3 objectives respectively. Note that these points form the external boundaries of the feasible domain as shown in fig. 1.4.
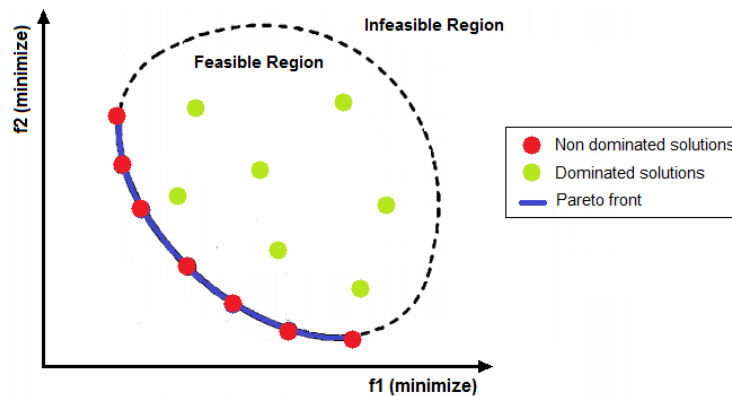
Figure 1.4: Concept of Pareto optimality

Diversity: The disadvantage of Pareto optimality concept is that it promotes the individuals near to to crowded zones of the design space and underrates those in sparsely explored regions. This is a critical point that concerns an exploratory algorithm because in this way the design space can not be efficiently explored. As a result of this, the risk of having a premature con–vergence increases. This concept of considering points that lay in different zones is also called the diversity of the population. In order to preserve a certain diversity among the individuals, new criteria are taken into account while calculating the fitness function. To illustrate, techniques such as shar–ing functions or niche count calculate the distance between the candidate solutions. During the assignment of the fitness values related to the ones in the crowded regions, a penalty function is taken into consideration.

Selection The selection operation corresponds to the act of choosing the indi–viduals that are going to be placed in the mating pool in order to give

birth to next generations. In most of the algorithms, the fitness assignment process is carried out before this step so that the assigned fitness value is considered among the selection criteria. Selection activity constitutes an important characteristic of an evolutionary algorithm because it has a major impact on its overall performance. Some of the existing and widespread selection schemes are:

Truncation selection is a basic and deterministic model that returns the best k individuals of the overall population. These individuals are directly copied in the mating pool until its size limit is reached. Instead the value of k can be arbitrarily chosen like the half or third of the population.

Environmental selection is a negative selection method because instead of deciding which individuals should enter the mating pool, it determines the ones that should die. The metaphor of death is equivalent to the concept of replacement or participation to the following generations.

Fitness Proportionate Selection scheme establishes a proportional relationship between the probability of an individual to enter the mating pool $P(x_1)$ and its fitness value $v(x_1)$. One of the most diffused example of such an approach is the roulette wheel selection where the wheel area dedicated for a candidate solution is proportional to its fitness value compared to the sum of the all fitness values.
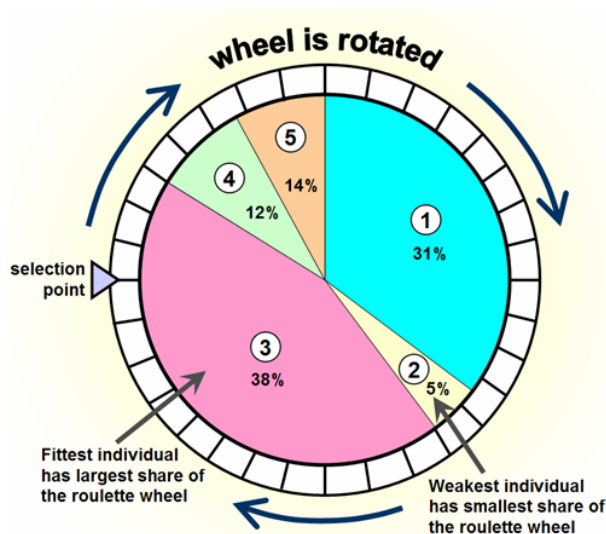
$$P(x_1) = \frac{v(x_1)}{\Sigma_{\forall x_2 \in Pop} \ v(x_2)}$$

Figure 1.5: Roulette wheel selection scheme

The same logic can also be applied in the case of ranking selection where the probability of an individual to be selected is proportional to its position in the sorted list of the all individuals of the population.

Tournament Selection is one of the most efficient and popular methods employed in evolutionary algorithms. This scheme bases on the comparison between predefined k solutions. The winning criterion between 2 individuals is the superiority of their fitness values. Note that a high k increases the selection pressure and promotes the individuals with good fitness values. Consequently, the chance of individuals with bad fitness assignment to produce offspring decreases.

A last remark regarding the selection operations can be made by introducing the concept of *elitism*. This concept ensures that the best individual of the current population is directly propagated to the next generation without being submitted to any selection pressure. In this way, once the global optimum point is found, it would be preserved until the end of the simulations. Elitism concept can be combined by the insertion of an archive where the best solutions are preserved.

Reproduction The term reproduction refers to the creation of a new solution candidate based on the information gathered at step t but which is going to be evaluated at step $t + 1$. To do so, reproduction or search operations that are inspired by the biological procreation mechanisms are utilized. These operations can be divided in 4 different classes:

Creation is an operation which allows the reproduction of a new individual without any ancestors. The natural paragon for this operation might be the occurrence of the first living cell.

Duplication is a similar process to cell division and it enables to obtain two identical individuals based on one parent.

Recombination operation can be compared to the sexual reproduction in nature. In other words, it can be interpreted as the creation of a new individual that possesses certain traits of both parents.

Mutation operation which is exactly like its natural counterpart can be con-sidered equivalent to a small and random variation of an individual's genetics.

The application examples of these search operations are going to be given in the section regarding the genetic algorithms (chap. 1.2.1). Note that the new generations are created after the reproduction phase but the final configu-ration of the following generation depends on the nature of the algorithm. To illustrate, in the case of a *generational* algorithm, the new generations are only constituted of the offspring of the current generation. Whereas ac-cording to a preservative scheme, the next generation is a combination of the offspring and parent individuals and their ratio can be a representative feature of the given algorithm.

Fitness assignment and selection strategies are the most fundamental part of an evolutionary algorithm. In addition to them, another important point concerns the constraint handling. There exist several approaches which uses different methods in order to integrate the effect of the constraints into the progress of the solution [41]. A basic scheme can be the total rejection of the infeasible solutions. How-ever, the majority of these methods propose a penalty function that depends on the degree of violation of the constraints. Then this value is combined with the fitness value to promote feasible solutions. Note that the value of the penalty function depends on different factors and requires special techniques to be computed. An alternative way to the penalty based methods is the modification of the genetics of an infeasible solution by taking into consideration a feasible one. This operation that tends to push an infeasible solution towards the feasible domain is called *repair*.

In addition to these main features, other properties that distinguish an algorithm from another can be gathered in a graph as illustrated in fig. 1.6. These charac-teristic parameters give also an indication about the success of that evolutionary algorithm. One of the most important factors that influence the quality of the results are the tuning or basic parameters such as population size, number of generations and reproduction rates. Moreover, the search space choice and the search operations can be decisive concerning the progress of the solution. Fi-nally, the genotype–phenotype mapping procedure can be an essential element regarding the effectiveness of the algorithm. This notion is clarified in chap. 1.2.1.
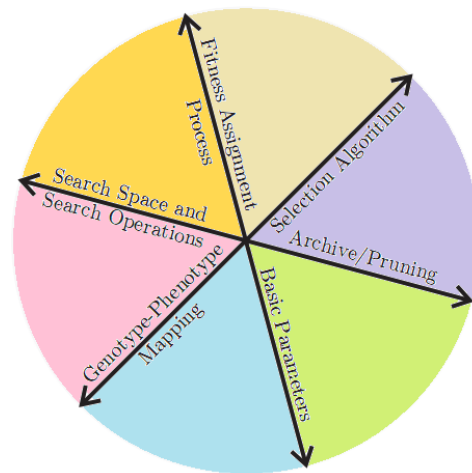
Figure 1.6: Configuration parameters of an evolutionary algorithm

1.2.1   Genetic algorithms

Genetic algorithms which make part of the evolutionary optimization algorithms possess clear advantages over other traditional algorithms in terms of robustness. Even though these advantages are paid with computational cost, continuously developing computer technologies permit to deal with challenging design problems. The complexity of the multi disciplinary problems especially created a growing interest into the use of genetic algorithms [36]. Moreover, academic researches like Ref[37] demonstrate that these type of algorithms has reached a mature state in terms of convergence velocity and reliability. However, the quality of the results always depend on the available computational effort and the effectiveness of the algorithm [38]. Before giving the details about genetic algorithms, it can be useful to see the overall framework by analysing the flowchart given in Ref[40].
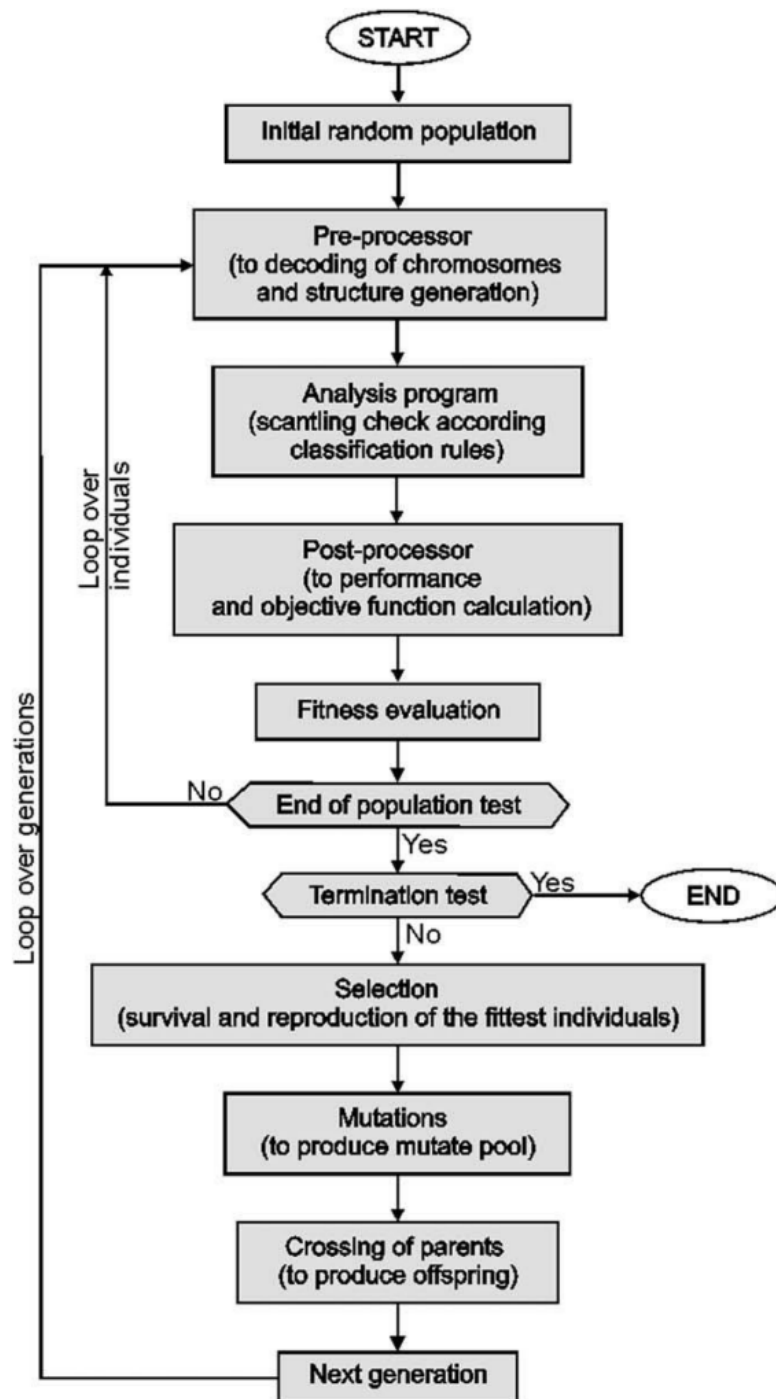
Figure 1.7: Flowchart of a genetic algorithm

The main characteristic of the genetic algorithms is that the elements of the search space are represented through binary strings. This representation method has similarities with the biological encoding mechanisms. Consequently, the terminology

used for these algorithms is borrowed from genetics. It is important to understand these key concepts in order to be able to apprehend the basic mechanism of the algorithm. As previously underlined, all the information regarding an individual or a candidate solution is encoded in binary mode. The whole linear sequence of the encoded information is called a *genome* which is composed of different *genotypes*. This definition can be compared to the chromosomes of any organism where the hereditary information is kept through DNA sequencing. Instead, the *phenotype* is the observable characteristics of an individual that is encoded by a *genotype*. To illustrate, every human being has a special DNA combination which represents its genotype. This encoded information determines all the physical features such as eye color, face shape and blood type. Whereas in the case of a genetic algorithm, the entities that should be encoded are the design variables. Every genetic algorithm possesses a genotype–phenotype mapping procedure which is a fundamental routine during the analysis of a solution.
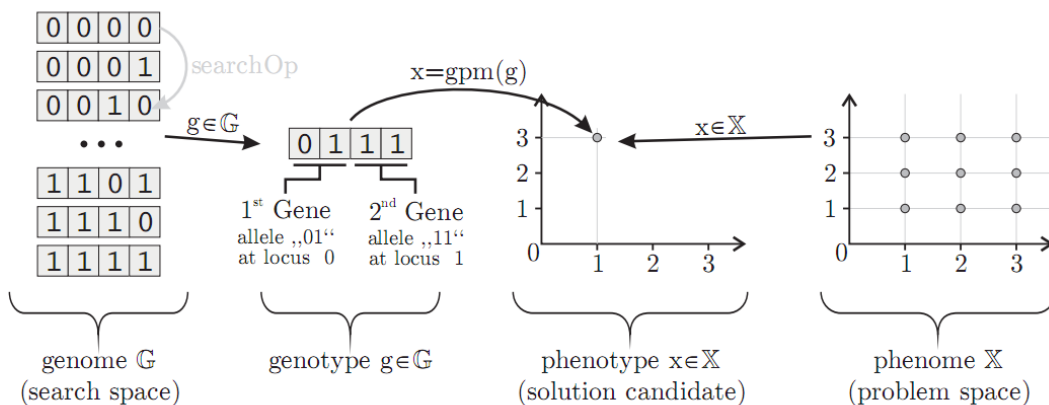
Figure 1.8: Transition between search and problem spaces

Moreover, an *allele* represents the value of a specific gene and its position is called *locus*. As previously highlighted in chap. 1.2, there exist different repro–duction methods to create new individuals. Recombination and mutation can be classified among the most commonly used techniques for the creation of the next generations. Recombination operation which is also called *crossover* is performed by exchanging genotypes between two string chromosomes. Different types of crossover are shown in fig. 1.9. Whereas a mutation that enables to preserve population diversity randomly modifies the allele of a gene from 0 to 1 or vice versa. Similar to the crossover operation, the number of genes that are subjected to a mutation operation can be varying.

(a) Single point crossover   (b) Two point crossover   (c) Multi point crossover
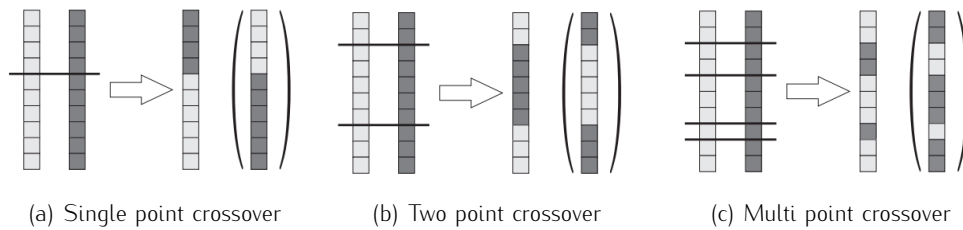
Figure 1.9: Crossover between two string chromosomes

(a) Single gene mutation   (b) Multi gene mutation   (c) Multi gene mutation
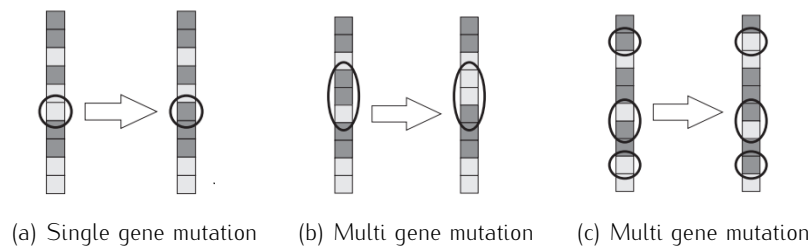
Figure 1.10: Mutation of string chromosomes

Even though by using a special optimization software, it is not necessary to be an expert in programming and numeric methods, a minimum basic theory knowledge is indispensable in order to better understand and interpret the tools that are utilized. Finally, a list regarding the benefits and the drawbacks of the genetic algorithms can be made to give significant indications about their implementation.

- **Advantages:**

  – As they do not put any restrictions on the problem space, they are efficient even for highly nonlinear and non differentiable objective functions. This fact makes them rich in application across a large and growing number of disciplines.

  – The fact that they work with a set of solutions instead of a single one makes them an ideal candidate for handling multiobjective optimization problems.

  – As there is no need to compute partial derivatives, they are able to work with both continuous and discrete design spaces.

  – As the driving force behind them is the exploration of the design space, the quality of the starting point does not affect the rest of the simulation.

  – They can take full advantages of a massively parallel computer architecture.

- Due to their randomness, they are more robust and insensible to an noise or disturbance on the objective function.

- **Disadvantages:**

- Problems with a large number of design variables require large population sizes and many function evaluations in order to achieve a good solution. Thus the computational power is always an important requisition.

- There is no absolute assurance that a genetic algorithm will find a global optimum but it can also converge to a premature solution.

- The tuning of their basic parameters has a significant effect on the quality of the final solution. However, there do not exist universal laws to set these parameters that are problem dependent.

1.3   Presentation of *Isight*

This theoretical background previously given is going to constitute the base of the optimization process that is going to be followed. However, at this point, it is important to underline the fact that the main scope of this thesis work is to optimize a helicopter component by using already existing algorithms. The performed activities do not consist of developing new algorithms or optimization methodologies. As a result of this, this work can be accepted as an industrial application of an optimization process through the use of a specialized software. In order to achieve the main objective of this thesis work, several softwares specialized in structural optimization might be used. To illustrate, Ref[29] proposes a methodology to improve the design of a helicopter empennage by using *SOL 200* which is the optimization tool of *MSC.Nastran*. Alternatively, Ref[30] shows an example of topology optimization of an aircraft wing through the use of *OptiStruct*.

In this thesis work, the optimization tool that is utilized is created by *Dassault Systèmes Simulia Corp* and it is called *Isight*. The purpose of this software can be described as creating flexible simulation process flows to automate the exploration of design alternatives and identification of optimal performance parameters [21]. In fact, the reason to choose this precise software is its ability and ease of process integration and automation. These notions have a leading role in reducing the duration of the preliminary design phase as well as the relevant costs because in this way the loop "design–analysis–new design" can be avoided. Moreover, an

automated process is able to verify numerous new configurations by increasing the probability to obtain one that is closer to an "optimal" design. Any desired automated process flow can be created by choosing and ordering the components proposed by the software. These components may be classified into 2 main groups [15]:

- **Process components** are components that are designed to contain a simulation process flow, which is executed some number of times depending on the component's own specific logic, essentially "driving" the execution of that simulation process flow. Some important process components are:

  Task: This component is a simple process component that always executes a subflow once, unlike other process components that may execute a subflow numerous times.

  DOE: This component is a process component that allows you to use Design of Experiment (DOE) techniques to intelligently sample the design space in order to improve the design.

  Optimization: This component is a process component that provides access to numerous optimization techniques to improve the design.

  Loop: This component is a process component capable of repeatedly executing subflows based on various logical conditions (for, for each, while, do until).

- **Activity components** are components designed to perform some end functionality, sometimes invoking and interacting with an external application that is external to *Isight*. Some important activity components are:

  Excel: This activity component is used for mapping parameters and executing macros using information from an Excel worksheet.

  Calculator: This activity component allows to easily define calculations to compute values of parameters.

Data Exchanger: This activity component permits to move data between *Isight* parameters and text files easily and efficiently.

Script: This activity component serves to execute Java code in a model. It is used to perform calculations that are too complex for the Calculator component, such as those involving loops or conditional statements.

Actually these selected components correspond to the ones that are used during this optimization process. Thus, their description is given in advance so that they are only represented through their icons for the rest of the thesis. In addition to these listed elements, there are other numerous components for different scopes. To illustrate, another important process component which is called *Monte Carlo* allows the user to assess the reliability of the design against randomness. This component or other ones such as *Six Sigma* and *Taguchi RD* permits to obtain a robust design by adopting a stochastic approach. Whereas other activity components permit the direct integration of *Matlab* or *Abaqus* in the subflow. Alternatively, *Simcode* or *OS Command* components serve to execute a command to the operating system, typically to run an executable analysis code. The presence of all these flexible tools facilitates the process integration of a multidisciplinary problem. An industrial instance is specified in chap. 2.3.

1.3.1 Optimization tools

During the structural optimization process, the necessary tools of *Isight* are employed. Actually, the software offers to the user several optimization algorithms that belong to different major classes. These classes and some of the corresponding algorithms can be listed as follows [22]:

1. **Gradient Techniques:**

   – Sequential Quadratic Programming

   – Large Scale Generalized Reduced Gradient

   – Modified Method of Feasible Directions

2. **Direct Methods Techniques:**

   – Hooke–Jeeves Direct Search Method

3. **Exploratory Techniques:**

   – Adaptive Simulated Annealing

   – Genetic Algorithms

As previously mentioned, the nature of the current problem favours the use of the genetic algorithms and *Isight* possesses 4 different genetic algorithms that have different mechanisms. As the user does not have access to the coding part, s/he can not visualize or modify the algorithm but can only deal with the input parameters regarding the selected algorithm. At this point, it would be very significant to highlight a critical notion. Similar to the other specialized softwares like the ones that are used for finite element analysis, *Isight* facilitates the implementation of highly complex problems. Even though it is a great advantage for the user in terms of time and effort, a concious use of these softwares is crucial for the overall control and as well as for the reliability of the results. More specifically for the current case, in order to follow an optimization process, someone should not be an expert in informatics or numerical analysis. However, s/he should be aware of how the selected optimization algorithm functions and how it interacts with the input parameters. Thus, it would be essential to give a brief description of the present genetic algorithms.

- **Neighbourhood Cultivation Genetic Algorithm (NCGA)** [23], [28] is published after NSGA–II by importing its important mechanisms such as management of an archive and assignment of a fitness function. In addition to these, this algorithm introduces a new concept in order to improve the searching performance of a multiobjective genetic algorithm. This new notion consists of "neighbourhood cultivation" where the crossover process is mostly performed between individuals with closer objective values instead of between a randomly chosen individual pair. Such an approach is adopted because a series of numeric research demonstrated that crossover among similar individuals produces better results than that of greatly differing individuals. Another important characteristic of this approach is that it enhances the degree of exploitation (rapid convergence) instead of exploration. The flow chart of NCGA can be summarized as follows:

1. **Initialization:** Generate an initial population Q_0 of Population size N. Set t=0. Calculate fitness values of initial individuals in Q_0. Copy Q_0 into archive P_0 whose size is also N.

2. Start new generation: set t=t+1.

3. Generate new search population: $Q_t = P_{t-1}$.

4. **Sorting:** Individuals of Q_t are sorted with along to the values of focused objective and the focused objective is changed at every generation.

5. **Grouping:** Q_t is divided into groups which consists of two individuals. These two individuals are chosen from the top to the down of the sorted individuals.

6. **Crossover and Mutation:** In a group, crossover and mutation operations are performed. From two parent individuals, two child individuals are generated and the parent individuals are eliminated.

7. **Evaluation:** All of the objectives of individuals are derived.

8. **Assembling:** The all individuals are assembled into one group and this becomes new Q_t.

9. **Renewing archives:** Assemble Q_t and P_{t-1} together. Then individuals are chosen from 2N individuals through the environment selection scheme.

10. **Termination:** Check the terminal condition. If it is satisfied, the simulation is terminated. If it is not satisfied, the simulation returns to Step 2.

Note that in this algorithm, the new generation is a copy of the archive that corresponds to the previous iteration. Whereas in NSGA–II, binary tournament selection scheme is applied. This selection pressure on the elites can be a disadvantage by resulting in diversity loss and danger of being trapped in a local minimum. In fact, numerous test functions show that NCGA gives better results with respect to NSGA–II when the objective functions have a multiple peak landscape. Lastly, it is possible to list population size and number of generations as the most significant tuning parameters of the current algorithm.

- **Non–dominated Sorting Genetic Algorithm (NSGA–II)** [23], [27] is an im–
  proved version of the NSGA due to the reduction of the computational com–
  plexity, introduction of the elitism concept and preservation of the diversity.
  Elitism is included in NSGA–II through the use of an Pareto archive P_t that
  consist of the best non dominated solutions until t^{th} iteration. Following the
  t^{th} iteration, the Pareto archive is updated as P_{t+1} by considering P_t and
  the searching population Q_t. Then finally, the searching population Q_{t+1} is
  acquired by taking into account P_{t+1}. This sequence is represented in fig.
  1.11. Note that the genetic variation operators are applied to the searching
  population Q_t and its size is kept equal to the one corresponding to the
  Pareto archive P_t.
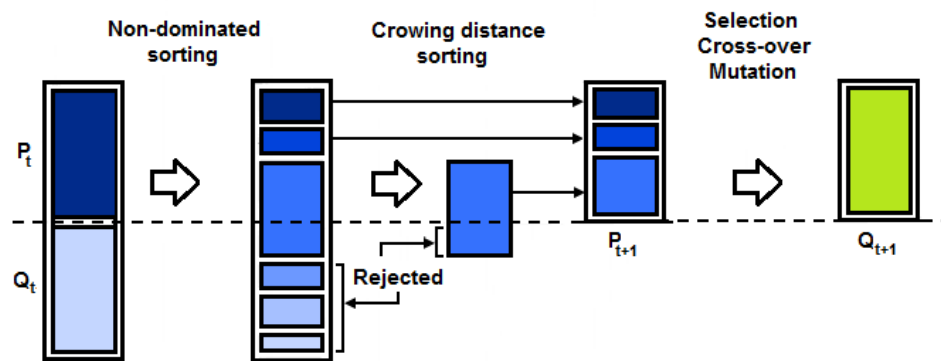
Figure 1.11: Non–dominated Sorting Genetic Algorithm procedure

As fig. 1.11 shows, there exist 2 selection mechanisms that constitute the
backbone of the algorithm: Non–dominated and crowding distance sorting.
These two concepts help to guide the selection towards a better and uni–
formly spread–out Pareto–optimal front. Moreover, in order to cope with
constrained multi objective problems, a constrained–domination principle is
applied with the tournament selection scheme. This principle favours the non
dominated feasible solutions with smaller overall constraint violation. Fi–
nally, the most important tuning parameters of this algorithm can be listed
as population size and number of generations.

- **Archive–Based Micro Genetic Algorithm (AMGA)** [24], [23] is an evolution–
  ary algorithm that relies on previously explained genetic variation operators
  for creating new solutions. As the name indicates, the algorithm functions
  with a very small population size and it maintains an external archive of

good solutions obtained. This external archive that also provides information about the search history is updated at each iteration. The selection bases on this archive (elite population) and the concepts of binary tournament and Pareto domination. Such an approach attempts to minimize the number of function evaluations required to achieve the desired convergence. Consequently, the most important input parameters are constituted of the initial population size, archive size, parent population size and number of function evaluations. A pseudo-code that can resume the algorithm is as follows:

---

1. Generate the initial population

2. Evaluate the initial population

3. Update the archive (using the initial population)

4. Repeat the following steps...

    a) Create parent population from the archive

    b) Create mating pool from the parent population

    c) Create off-spring population from the mating pool

    d) Evaluate the off-spring population

    e) Update the archive (using the off-spring population)

5. ... until termination is reached

6. Report desired number of solutions from the archive

Note that the strategy to update the elite population relies on the domination level and diversity of the solution. This approach allows to obtain a large number of non dominated solutions at the end of the simulation. As a final note, it is important to mention that AMGA borrows several concepts from existing algorithms such as NSGA-II. However, a comparison between the two algorithms demonstrated that AMGA has a superior performance respect to NSGA-II for multi objective optimization problems and this fact is also verified during this thesis work.

- **Multi-Island Genetic Algorithm (MIGA)** [23], [25], [26] divides the population into several sub-populations called "islands". All the traditional genetic operations are separately performed on each island. Then some individuals

are selected and migrated to different islands periodically. Such a mechanism searches many designs and multiple locations of the design space in order to avoid converging partial optimum. The total number of function evaluations are based on sub-population size, number of islands and number of generations. In addition to these parameters, the migration rate and interval are present among the tuning parameters.
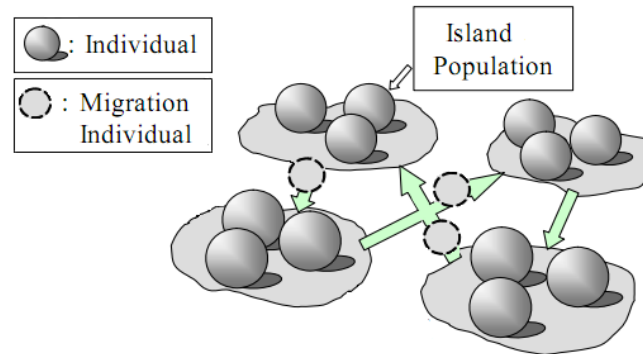
Figure 1.12: Representation of the Multi-Island Genetic Algorithm

MIGA assigns to each individual a fitness function that is a measure of the quality of the design point. This fitness function is calculated by combining the objective and penalty functions. In order to create the child generations, tournament selection technique is adopted. The relative tournament size gives an indication about the randomness regarding the selection of the child generations. In the case the maximum tournament size is equal to the size of the sub-populations, the child generations will only consist of the duplicates of the best individuals. This elitist scheme guarantees that the best genetic material is carried over to the child generation.

1.4   Overview of structural optimization

Structural optimization aims to obtain a set of "optimal" design solutions from which a designer or a decision maker can derive maximum benefit by using the available resources [33]. These benefits may vary depending on the application field. To illustrate, weight reduction is one of the most critical aspects in aeronautical field whereas the main focus can be on strength or stiffness in a civil engineering example. Instead for a helicopter component, improving the dynamic

behaviour can be essential besides the weight minimization. Cost reduction or manufacturing issues can also be considered as common points for any type of structural optimization problem.

Before proceeding with the optimization process regarding this specific case, it would be also beneficial to understand the chronological order that the structural optimization followed together with the optimization algorithms. These two notions have always had a close interaction with each other [32].

Even though the first structural optimization activities date to the work of Maxwell (1896) and Mitchell (1904), the pioneer work in this field has been proposed by Schmit in 1960. This time period also corresponds to the development of gradient based optimization algorithms such as Sequential Linear Programming, Sequential Unconstrained Minimization techniques and Feasible Directions Methods. In these years, significant research activities are performed concerning trusses, shell and frame structures. Gallatly, Berke and Gibson called this era as the "period of triumph and tragedy" because despite all these research activities, the numerical methods and the computational resources were not sufficient enough to solve sophisticated problems with large numbers of design variables.

The 1970's offered a solution to the previous problem through the introduction of optimality criteria methods. Kuhn-Tucker optimality conditions improved the efficiency and the robustness of the optimization process. Instead the structural engineering field started to emphasise on creating approximative models to reduce the number of design variables.

The 1980's were the time interval that correspond to the birth of the commercial structural optimization softwares. Besides the increasing computational power, a renewed interest in stochastic methods raised. These methods include Genetic Search, Simulated Annealing and other techniques that attempt to mimic natural or evolutionary processes.

From 1990's until recent years, the researches consolidated the efficiency of the genetic algorithms and this fact also promoted the idea of integrating these methods in the commercial softwares. These improvements allowed to deal with engineering problems that have higher complexity levels. Regarding the structural field, the new trend is the topology optimization which is also explained during the fol-

lowing paragraph. Before discussing this new approach and the other structural optimization types, it would be interesting to report a statistic concerning the size of an optimization problem over time.
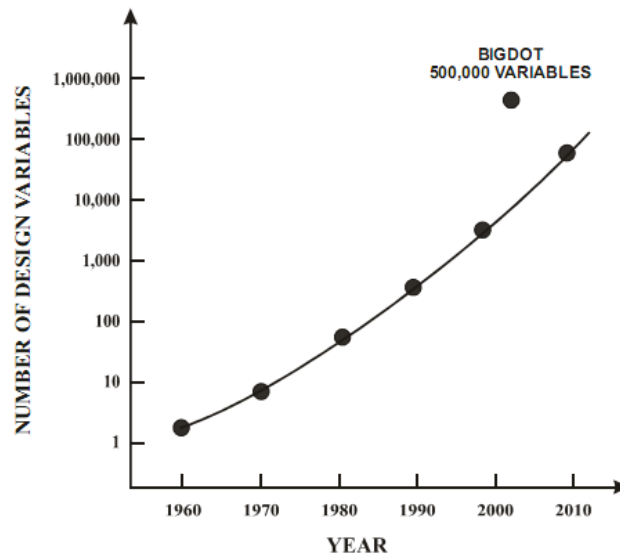
Figure 1.13: Growth in optimization problem size

According to the nature of a structural problem, the optimization activity can be classified into 4 main groups [31]:

Topology optimization is employed during the conceptual design phase in order to obtain the first rough shape that respects the geometric space limitations, boundary and load conditions. This new topology is obtained by redistributing the material in the allowed design space, which was initially homogeneous.

Shape optimization aims to improve the structural performance of the object by changing its boundaries. To illustrate, in the case that a finite element approach is adopted, the position of the nodes on the external boundary can be changed in order to obtain a desired load distribution within the structure.
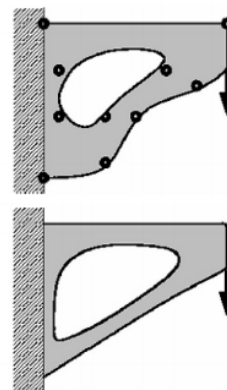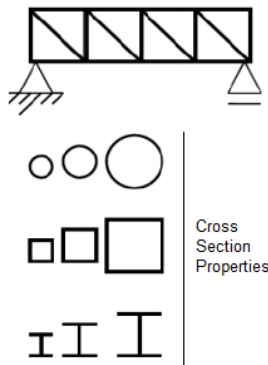
Sizing optimization is applied following topology and shape optimization processes. This sizing procedure may concern the geometrical properties of a cross section such as its dimensions, area or moment of inertia.

Internal parameter optimization is utilized when the object in investigation has an anisotropic behaviour like in the case of composite structures. For such instances, the mechanical properties highly depend on the orientation angles of the layers that constitute the laminate. Consequently, this element can be considered as a parameter that may allow to obtain some desired global structural behaviour.
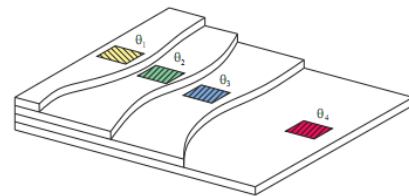
The flowchart in fig. 1.14 shows the process sequence that should be followed during a structural optimization process [14].
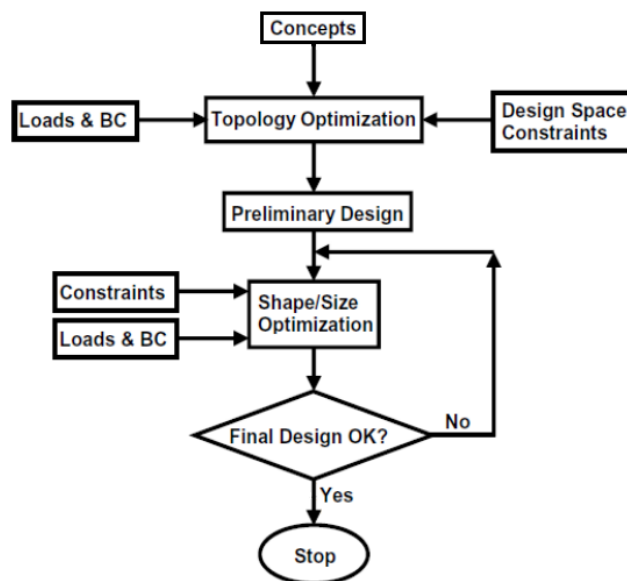
Figure 1.14: Structural optimization flowchart

Note that the first step always concerns the selection of the topology which gives the best mass distribution of a structure under the given boundary and load conditions. After this step, the preliminary design is refined through a shape and sizing optimization until it satisfies the necessary requirements. After this step, the optimization process terminates and a detailed analysis is performed in order to certificate the final design.

It is possible to see in the following chapters that all of these 4 structural optimization strategies are utilized during this current optimization problem. First of all, a topology selection is made between a sandwich and a reinforced laminate model. Once the structural topology is determined, geometrical entities are modified in order to improve the design. To illustrate, the thickness and the cross sectional properties related to specific components are changed. These changes can be considered as examples of shape and sizing optimization respectively. In addition to these, the use of composite materials introduced some applications regarding internal parameter optimization. In this early stage, it would be useful to emphasize that topologically different design solutions are not obtained as result of an conventional optimization process but they are gradually determined by the "decision maker".

Chapter 2

Optimization problem

Once the theoretical research part is completed and the basic concepts concerning the multi objective optimization by genetic algorithms are clarified, the theory is applied to redesign a helicopter component. Before entering into details of the optimization problem, it is important to highlight the main objective of this study. First of all, the design and the required analysis for the certification of the SAR Plate Assembly are already completed and it is currently in the construction phase. Consequently, all the activities covered in this thesis do not have an intention to redesign an object to be constructed but proposes an alternative design at academic level. In other words, the most significant aspect is not to optimize a component that is going to be manufactured but to follow an optimization process. At this point, the content of this thesis can be considered as another investigation into the benefit of optimization by *Agusta Westland* to inform decisions about future approaches. This innovative method would be introduced through a specialized software, *Isight* which is developed by *Dassault Systèmes Simulia Corp.* Thus, this thesis also includes an evaluation about the possible use of this software for future applications.

2.1   Object of optimization

Applicable references: [7]

The helicopter component that constitutes the main focus of the optimization process is basically a rectangular plate which is typically used for "Search and Rescue (SAR)" operations. The main function of the SAR Plate Assembly is to carry the necessary auxiliary equipments such as oxygen bottles or any other item required for the specific task.

2.1.1   Structural description

The SAR Plate Assembly is placed vertically in the helicopter cabin in a manner that it is fixed to the floor and to the upper deck by its shorter edges via standard attachments. The precise dimension values regarding the SAR plate can be found in app. D.
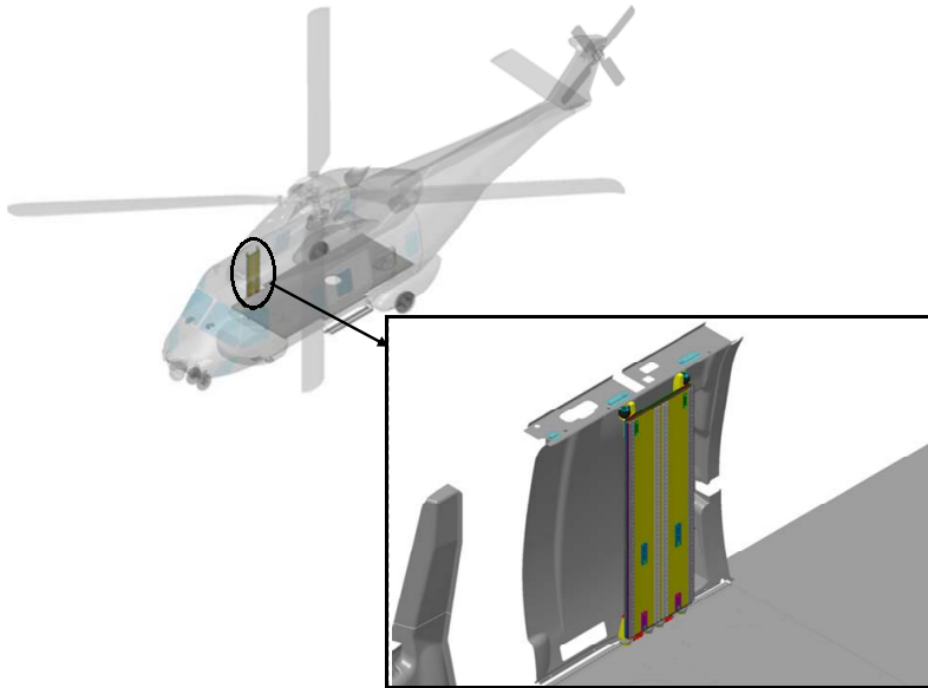
Figure 2.1: Position of the SAR Plate Assembly in the helicopter

Actually there exists a practical reason under the fact that SAR Plate is attached in this way; indeed when necessary, it can be replaced by any seat that can be installed on the side walls. This means that the dimensions of the plate are consciously determined in order to allow a possible change due to different configurations. This approach is very commonly used for aeronautical structures because it permits to exploit in a more efficient way the available space. In the meanwhile it also facilitates and accelerates the operations required to switch between interchangeable configurations. This flexibility can be seen equivalent to cost and time reduction.

The main structure of the SAR Plate is composed of a metallic sandwich whose skins and honeycomb core are made of aluminium. A layout of a typical sandwich structure is shown in fig. 2.2. The details about the dimensions of the principal

elements of the SAR Plate Assembly and the properties of their corresponding materials are given in chap. 3.
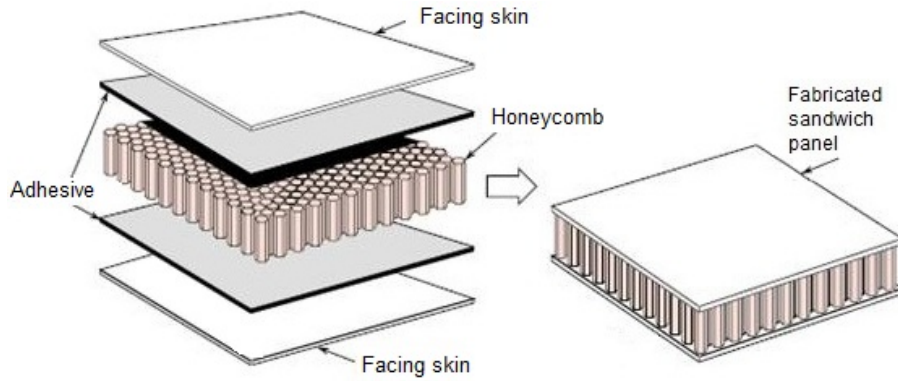
Figure 2.2: Layers of a metallic sandwich

In addition to the metallic sandwich, there exist other subcomponents for varying structural reasons such as fixing, dynamic and static aspects:

- **Upper interface fittings**
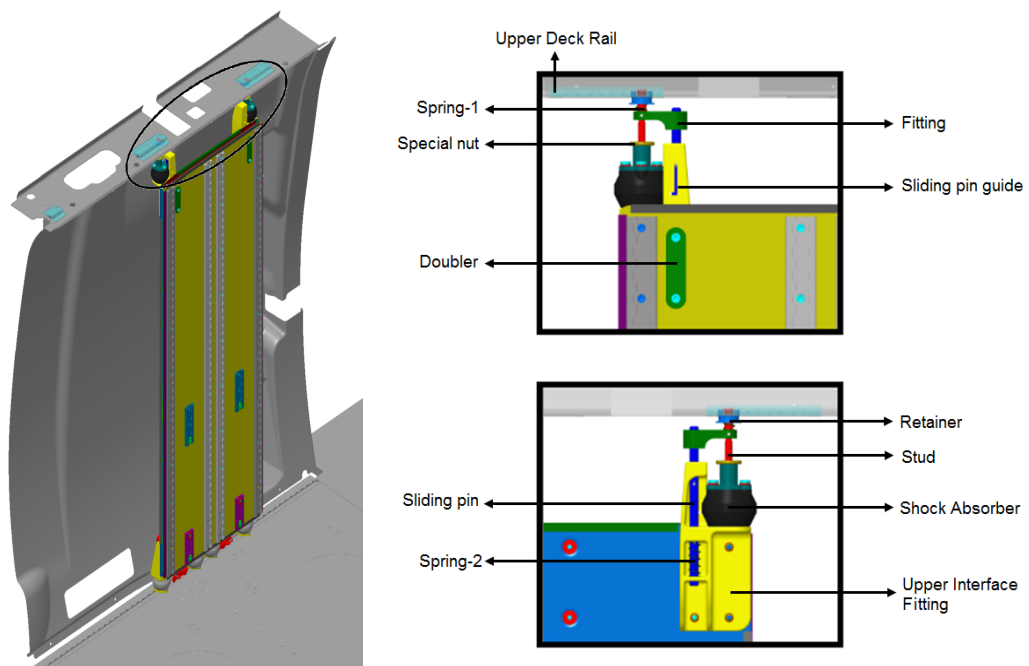
Figure 2.3: Front and rear view of the upper interface fitting

According to the information given by the supplier, the allowable load limit of the upper interface is quite low with respect to the floor deck. Consequently,

the upper interface fitting of the SAR Plate has a special mechanism that is explicitly designed in order to avoid transferring vertical loads to the upper deck rail.

As it appears in fig. 2.3, the SAR Plate is not rigidly connected to the upper deck. In addition to the shock absorbers, the adoption of a vertical sliding mechanism prevents the load transfer along this direction. Actually, there are two possible scenarios: the first concerns the operational load cases and the second one the crash load cases. These two main load conditions are going to be examined in more details subsequently. However, for each of these cases the load paths are distinct because of the sliding mechanism. During the operational load cases, the magnitude of the force is reduced by the shock absorber and transferred to the upper deck. Instead in the crash cases, the forces are so high that the shock absorbers are supposed to be ineffective. At this point, the plate which is rigidly connected to the upper interface fitting tends to slide over it. This move prevents a catastrophic failure and also serves to satisfy the certification requirements. These two load paths can be easily understood by examining fig. 2.4.
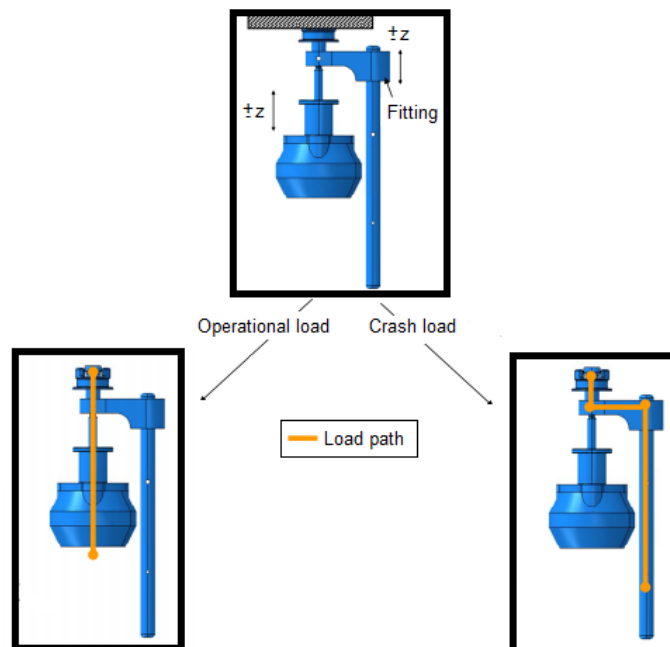
Figure 2.4: Upper interface load paths

- **Lower interface fittings and cable assy**

After analysing the upper interface fittings and their functioning mechanism, the lower interface fittings are considered. The lower interface fittings are similarly connected to the floor by the means of the shock absorbers.
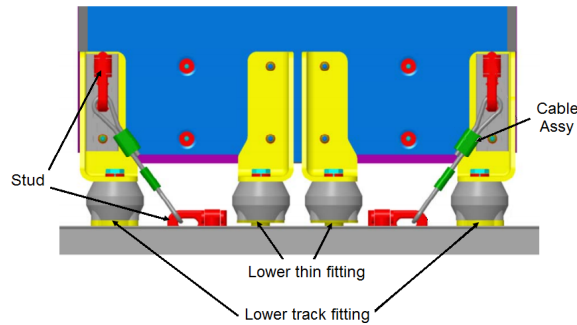
Figure 2.5: Lower interface fittings

The SAR Plate contains 4 lower interface fittings and two cable assy that connect the fitting to the floor by a stud as illustrated in fig. 2.5. As in the previous case, the choice of such attachment configuration is closely related to the load conditions. Note that there is a slight difference between the fittings that are placed externally with respect to the internal ones. The external shock absorbers are simply supported by the floor rail whereas the internal ones do not have a physical contact with the floor. In the case of necessity, they only serve to redistribute the force in order to avoid the overloading of the two external attachment points.
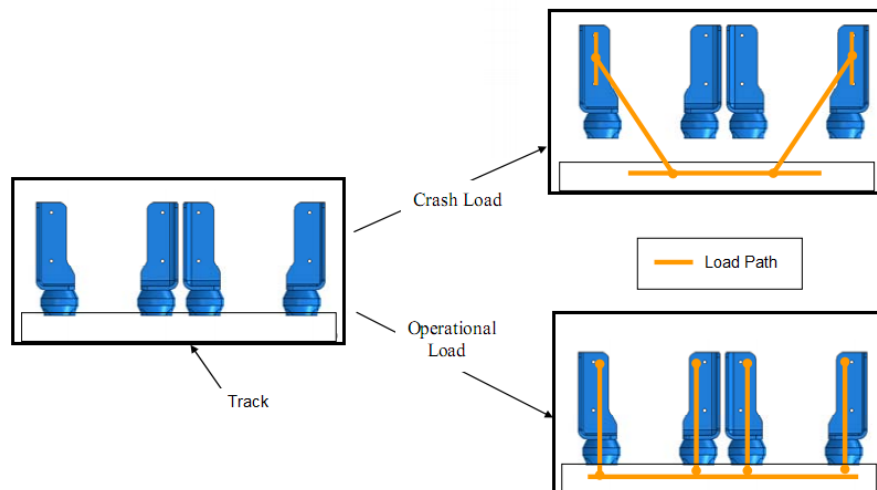
Figure 2.6: Lower interface load paths

Furthermore, in addition to the fittings there exists also a couple of cable

assy as a precaution for a catastrophic failure due to crash. Previously, the sliding mechanism of the upper part was highlighted. Actually, the cable assy are additional elements that complete the crash load path. In case of an upward force, the plate would tend to move vertically along the force direction and slide over the hole present in the fitting. At this moment, the cable assy would retain the plate and inhibit its movement.

- **Shock absorbers** Due to dynamic requirements, 6 shock absorbers are put between the interface fittings and the attachment points on the floor or upper deck rails. The reason for such a configuration is explained in details in chap. 2.1.5.

- **Tracks and bottle retainers** As mentioned before, the component under investigation is designed to be used for "Search and Rescue" purposes.

Figure 2.7: AgustaWestland CH-149 Cormorant during a SAR training
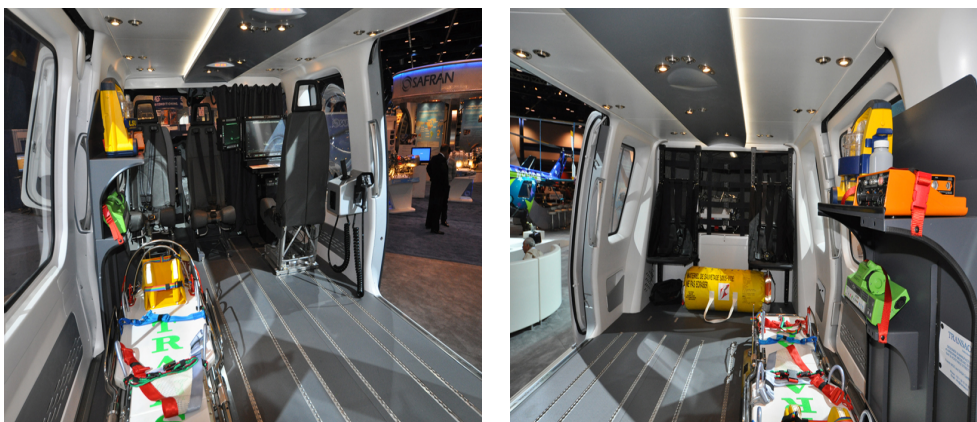
Figure 2.8: Cabin of an helicopter fitted for SAR operations

54

This kind of missions may require some special equipment such as rescue litter, oxygen bottles and medical kits. In order to be able to carry the necessary equipment, vertical tracks that have the same shape as the upper deck and floor rails are fixed on the plate as shown in fig. 2.9.
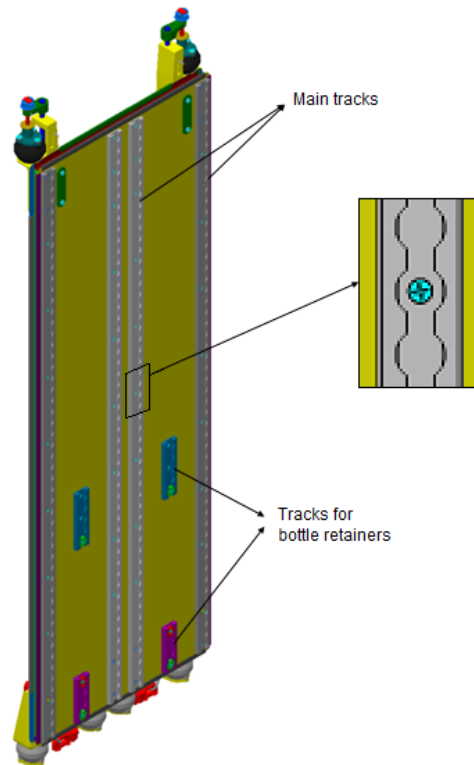
Figure 2.9: Position of the tracks

The continuous use of standard elements facilitates also the attachment of the masses on the plate. According to the object that has to be hanged, a relevant attachment can be selected and the object can be fixed on the plate.
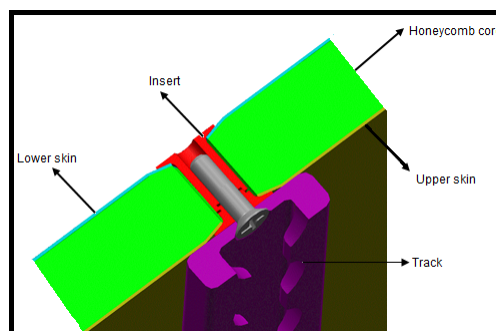
Figure 2.10: Cross section view of the SAR Plate inserts

These metallic tracks are installed on the plate by the use of screws and inserts that penetrate along the honeycomb core and compress the upper and lower skins. A schema of the junction type between the plate and the tracks is given in fig. 2.10.

During the SAR missions, there might be the need to carry oxygen bottles. So the plate is designed in a manner that these bottles can be fixed on the lower part of the plate with the help of bottle retainers as shown in fig. 2.11.
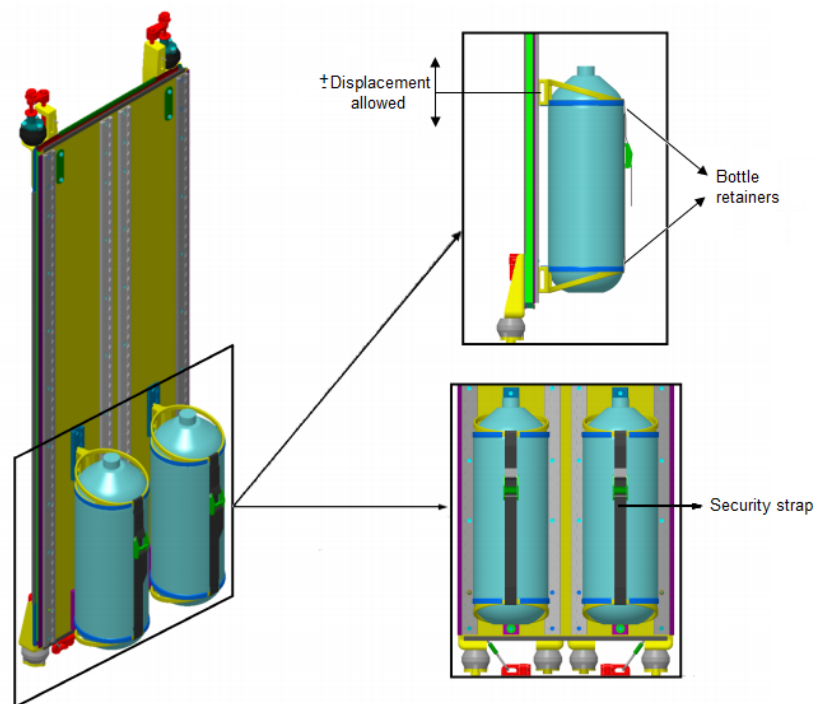
Figure 2.11: Installation of the oxygen bottles

The bottle retainer tracks that are present on the centre line between the main tracks permit the installation of the bottles only on the lower part of the SAR Plate. Each oxygen bottle is fixed by a couple of bottle retainers; the one on the lower part is fixed whereas the upper one can move vertically along the rail line of the track. This degree of freedom provides the flexibility to install all the bottles having different manufacturing tolerances regarding its height. The ability to move vertically is blocked by the help of the security straps. Once the finite element model is prepared, the tension loads on the security straps are calculated and applied in order to verify the resistance of the mechanism.

- **Lateral reinforcements**

  As a last structural element, the lateral reinforcements that form a frame around SAR Plate can be analysed. These reinforcements have a "C" shape cross section and they are made of steel. The purpose of using such com-ponents involves two different aspects: stiffness and protection. The main function of these reinforcements is introducing stiffness to the system that might be considered positive in terms of static and dynamic robustness. In addition to this, these laterally fixed reinforcements also help to protect and isolate the honeycomb core from external factors.
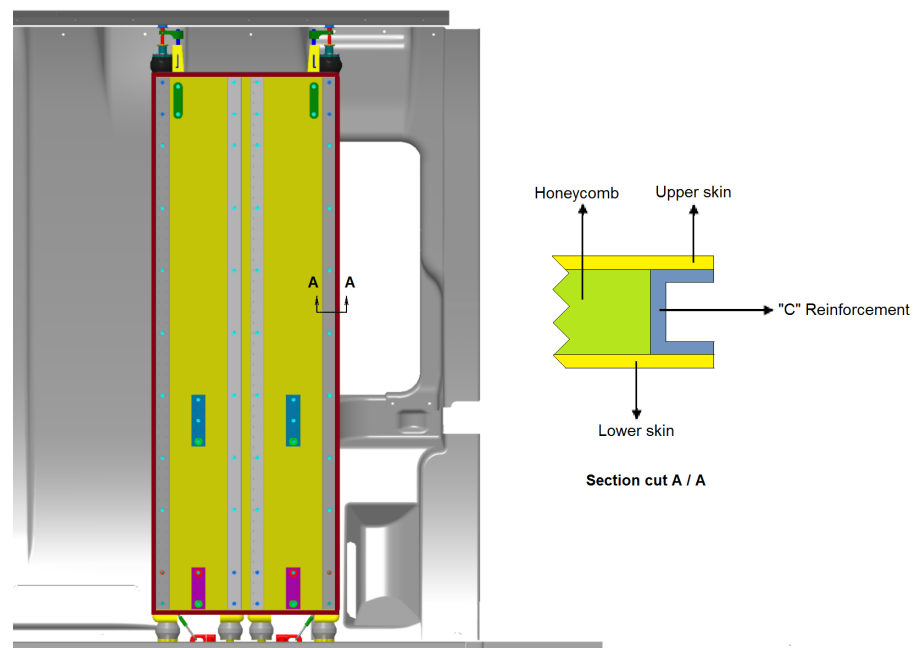
Figure 2.12: Position of lateral reinforcements and cross section of SAR Plate

2.1.2   Mass properties

As it is going to be explained in 2.2, the main purpose of the optimization process is to minimise the mass of the SAR Plate Assembly. This notion increases the importance of the mass distribution within the plate. Once the function of each item is well understood, the user can decide whether it would be useful for the new design or it can be removed. To illustrate, the additional elements like shock absorbers and their subcomponents might be ignored in the new design. At this point, a detailed list that shows the mass distribution regarding the SAR Plate Assembly is given in tab. 2.1.

Id	Description	Mass/Piece [kg]	Quantity	Total mass [kg]
N251G2060101	SAR PLATE ASSY			
/8655	Adhesive,Epoxy,Ty Il,Cl	0.00000	AR	0.00000
/8703	Adhesive,Rbr,Ty I,Cl 2	0.00000	AR	0.00000
A019B101A	Shock Absorber	0.10600	6	0.63600
A921A24A0950EB1	Security strap	0.02850	2	0.05700
EN2139-05010	Washer	0.00043	16	0.00688
EN2139-05016	Washer	0.00069	4	0.00276
EN2367-07006	Cotter pin	0.00002	4	0.00008
EN2549-100008F	Bolt	0.01429	6	0.08574
EN3037-050030RF	Bolt	0.00404	4	0.01616
EN3381-050010RF	Bolt	0.00200	36	0.07200
EN3381-050018RF	Bolt	0.00250	6	0.01500
EN3381-050028RF	Bolt	0.00339	8	0.02712
EN3381-050032RF	Bolt	0.00374	4	0.01496
EN3536-050	Self-locking nut, Esagon	0.00105	16	0.01680
EN3759-060012R	Screw	0.00502	6	0.03012
LN29787-06008	Screw	0.00100	6	0.00600
LN29787-06012	Screw	0.00200	6	0.01200
MS171464	Pin	0.01600	2	0.03200
MS171468	Pin	0.00057	2	0.00114
MS171621	Pin	0.00300	2	0.00600
MS24585C331	Spring	0.00100	2	0.00200
MS24585C379	Spring	0.00100	2	0.00200
MS24585C387	Spring	0.00100	2	0.00200
MS35338-44	Washer lock	0.00108	6	0.00648
A169AP05D1	Insert/cap	0.00200	16	0.03200
A169AS05D12	Insert/Sleeve	0.00600	16	0.09600
MS35338-47	Washer lock	0.00108	6	0.00648
A193AP05D1	Insert/Sleeve	0.00200	42	0.08400
A193AS05D12	Insert/Sleeve	0.00600	42	0.25200
N251G2063201	Skin	1.06600	2	2.13200
N251G2064201	Core	1.34000	1	1.34000
N251G2087201	Upper/lower stiffener	0.07000	2	0.14000
N251G2089201	Lateral stiffener	0.21200	2	0.42400
N251G2065201	Long track	0.73100	2	1.46200

continues on the next page…

Id	Description	Mass/Piece [kg]	Quantity	Total mass [kg]
N251G2066201	Upper track	0.07100	2	0.14200
N251G2067201	Lower track	0.05700	2	0.11400
N251G2068201	Spacer track	0.00500	2	0.01000
N251G2069201	Spacer	0.00400	4	0.01600
N251G2072201	Lower LH interface fitting	0.16900	1	0.16900
N251G2074201	Lower RH interface fitting	0.16900	1	0.16900
N251G2076201	Upper LH interface fitting	0.40300	1	0.40300
N251G2078201	Upper RH Interface fitting	0.40300	1	0.40300
N251G2080201	Stud	0.04300	2	0.08600
N251G2081201	Retainer	0.02600	2	0.05200
N251G2084101	Bottle retainer assy	0.25000	4	1.00000
N251G2090201	Lateral long track	0.73100	2	1.46200
N251G2091201	Lower Track Fitting	0.03600	2	0.07200
N251G2092201	Track	0.05700	2	0.11400
N251G2093101	Cable assy	0.24900	2	0.49800
N251G2096201	Lower central LH	0.15800	1	0.15800
N251G2097201	Lower central RH	0.15800	1	0.15800
N251G2098201	Lower thin track fitting	0.03600	2	0.07200
N251G2099201	Sliding pin	0.10400	2	0.20800
N251G2100201	Handling pin	0.00300	2	0.00600
N251G2101201	Fitting	0.08900	2	0.17800
N251G2102201	Adapter	0.09400	2	0.18800
N251G2103201	Special Nut	0.01500	2	0.03000
N251G2104201	Upper/Lower front	0.00900	2	0.01800
N251G2105201	Upper aft protection	0.00600	1	0.00600
N251G2106201	Lateral front protection	0.02700	2	0.05400
N251G2107201	Lateral aft protection	0.02300	2	0.04600
N251G2108201	Lower aft protection	0.00200	2	0.00400
N251G2109201	Doubler	0.01600	2	0.03200

Table 2.1: Masses corresponding to each component of the SAR Plate Assembly

🟩	Main SAR Plate elements	🟦	Standard fixing elements
🟪	Special SAR elements	🟥	Optional fixing elements

Table 2.2: Color legend for tab. 2.1

	Mass $[kg]$
Main SAR Plate elements:	7.216
Standard fixing elements:	2.759
Optional fixing elements:	1.854
Special SAR elements :	1.057
Total	12.886

Table 2.3: Summary of the mass distribution within the SAR Plate Assembly

Note that the components are divided into several groups and the shock absorbers and their subcomponents are gathered together under the group of *"Optional fixing elements"*. The removal of these elements is going to be the starting point of the mass minimization process. Another group, *"Special SAR elements"*, contains the items related to the oxygen bottles. These items are not directly going to participate to the mass reduction process but their effect is going to be included by considering a loading configuration with the oxygen bottles.

The mass target that is going to be a reference value during the optimization process can be determined according to this classification. As the *"Optional fixing elements"* will not make part of the new design, this mass difference can be spent for other structural elements. Thus, the minimum mass of the new design can be obtained as a sum of *"Main SAR Plate elements"* and *"Optional fixing elements"*. Note that this minimum mass threshold is equal to **9.07** kg. Furthermore, since *"Standard fixing elements"* make part of both original and new design, their presence is ignored during the optimization process. However, the overall plate mass should be calculated by adding their contribution to the mass value which is found by the optimizer.

2.1.3   Different loading configurations

Once the major components that constitute SAR Plate are presented, another crucial point can be examined: possible loading configurations. After the installation of the plate, the user should follow specific rules during the loading operation. In other words, the masses or the items that should be carried by the plate can not be randomly distributed. These regulations are determined by taking into account the static and dynamic analysis performed to certificate the component. In an extreme case, the entire load can be disposed towards the upper part and

this may cause the failure of the attachment between the plate and the upper deck. This was an instance regarding the static aspect. However, the dynamic aspects can also be very important because the maximum load quantity that can be supported by the plate is much higher than its own mass. This fact proves that the modal behaviour of the plate is dominated by the introduced masses. All these analysis cases led the manufacturer to define some limits and guidelines for loading the SAR Plate. These guidelines that result in diverse configurations may be listed as follows:

1. SAR Plate is divided into six loading areas or boxes (fig. 2.13)

2. Maximum CoG distance out of plane is $150mm$ (fig. 2.13)

3. Vertical distance between two connection points on the track is equal to $25.4mm$ (fig. 3.5)

4. CoG of the disposed masses should coincide with the defined CoG lines (fig. 2.14)

5. When the oxygen bottles are not installed:

   a) Maximum allowed equipment mass is $55kg$

   b) Maximum allowed mass on each upper (#5 & #6) box is $4kg$

   c) Maximum allowed mass on each intermediate (#3 & #4) and lower (#1 & #2) box is $15kg$

6. When the oxygen bottles are installed:

   a) Maximum allowed equipment mass is $55kg$ (including the oxygen bottles)

   b) Average mass of each oxygen bottle is $6kg$

   c) Oxygen bottles must be disposed on lower(#1 & #2) boxes

   d) Maximum allowed mass on each upper (#5 & #6) box is $4kg$

   e) Maximum allowed mass on each intermediate (#3 & #4) box is $17.5kg$
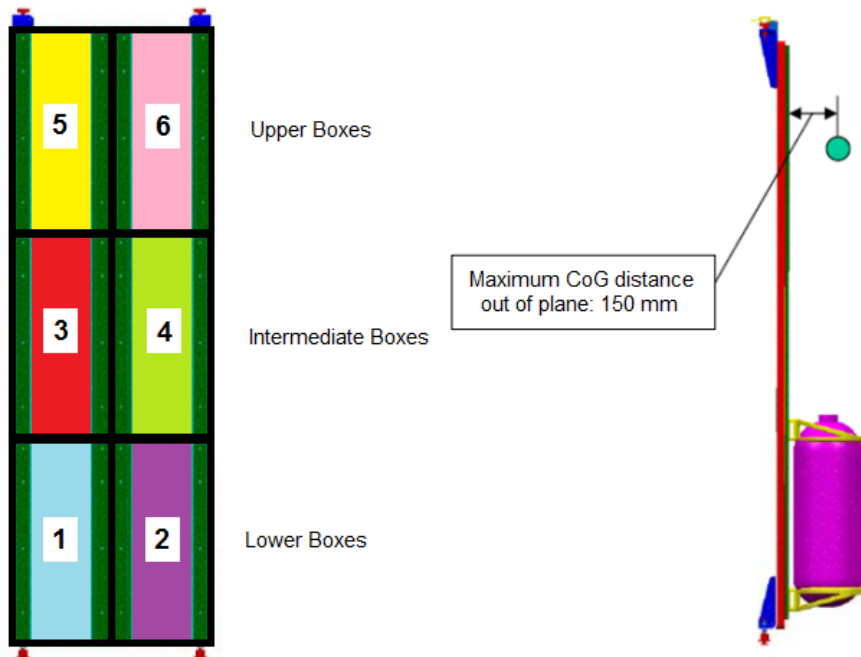
Figure 2.13: Definition of the boxes and the loading principals
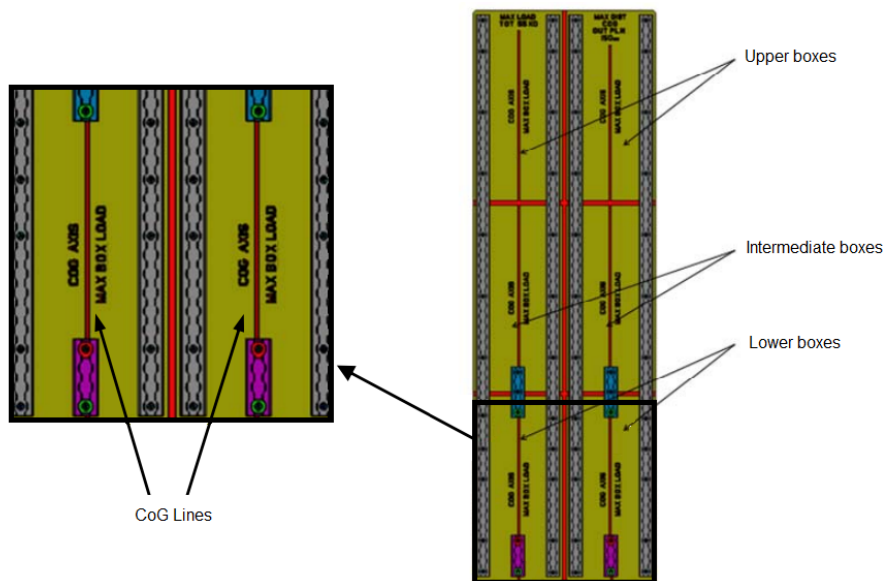
Figure 2.14: Definition of the CoG lines

Once these loading instructions are followed, there appear 4 main loading con‐
figurations that represent the expected worst case scenarios:

- Up (101)

- Middle (102)

- Down (103)

- Bottle (104)

(a) Up (101)

(b) Middle (102)

(c) Down (103)

(d) Bottle (104)
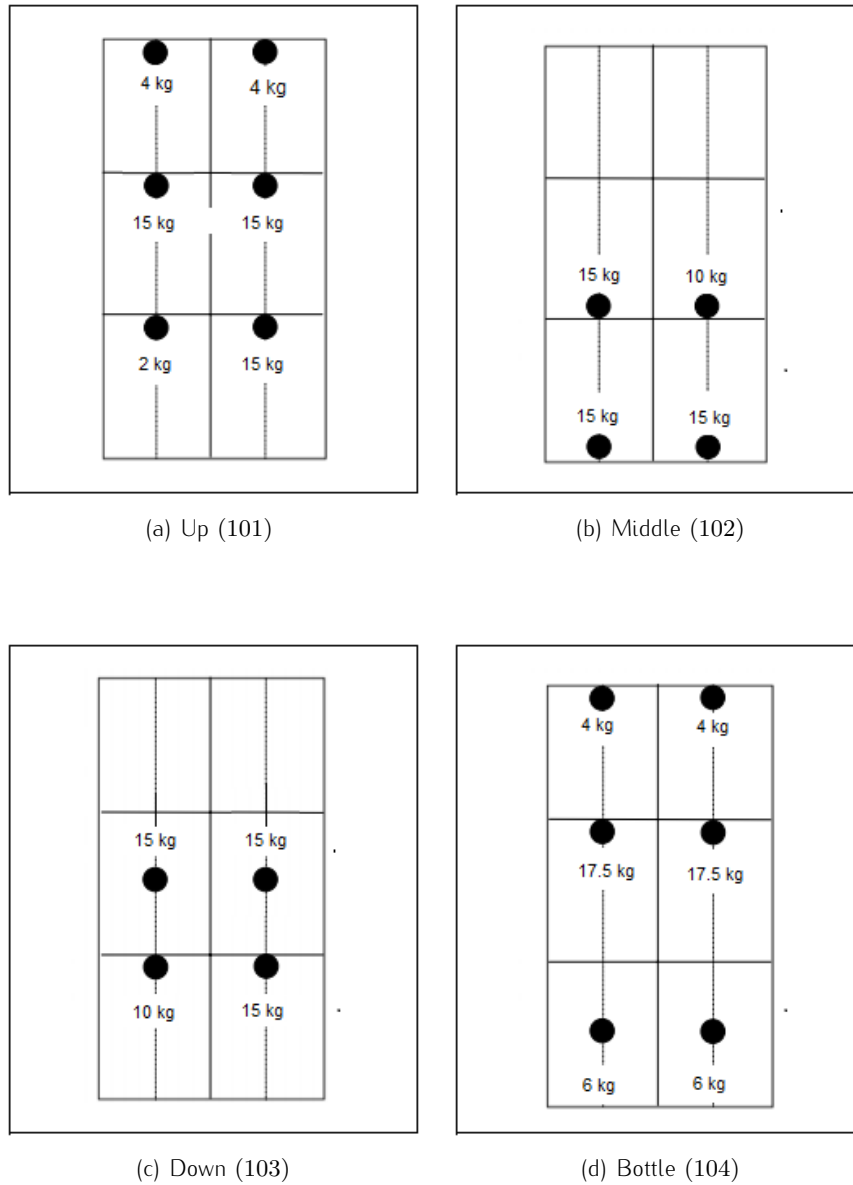
Figure 2.15: Critical loading configurations

These configurations tend to concentrate the disposed masses towards a specific zone such as upper deck, floor and middle of the plate. In addition to these, there is always the configuration that is equipped by the oxygen bottles. During the following parts of the thesis, these 4 configurations are going to be considered

as a fix constraint and it is going to be assured that the new design satisfies the necessary requirements for all of these 4 cases.

2.1.4   Load conditions

As previously mentioned during the explanation regarding the functioning mechanism of the interface fittings, there exist several load conditions. These load conditions can be divided into 3 groups:

- Normal flight conditions (tab. 2.4)

- Hard landing conditions (tab. 2.5)

- Crash conditions (tab. 2.6)

All the load conditions are described as acceleration vectors that have varying magnitudes and directions. The reference frame used to define these directions is given in fig. 2.16. For each major load condition, there exist 6 subcases that comprehend loads along the 3 principal axis X, Y and Z with both positive and negative directions.

Note that all these load conditions exist for any type of loading configuration and consequently the total number of possible load scenarios that should be verified becomes the combination of all these subcases.
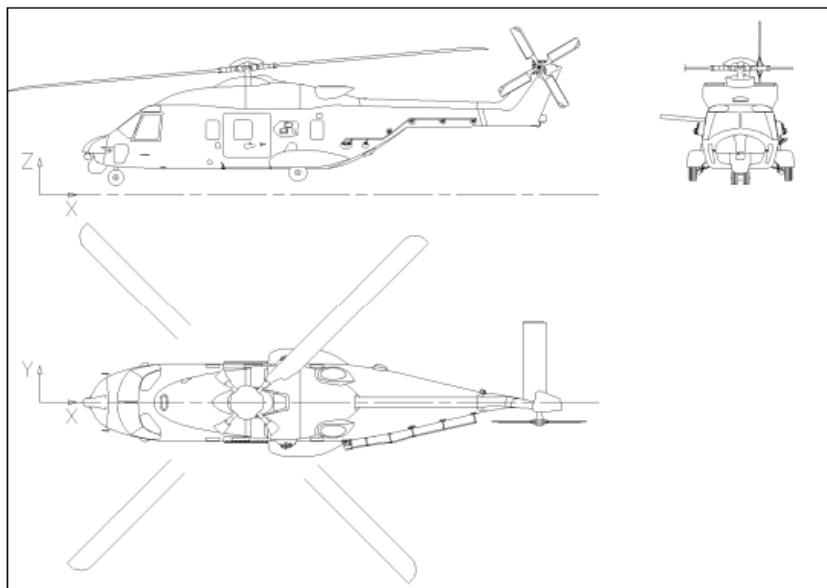
Figure 2.16: Main reference frame

	X	Y	Z
Sideward LH	–	$-1g$	–
Sideward RH	–	$+1g$	–
Forward	$-1g$	–	–
Rearward	$+1g$	–	–
Downward	–	–	$-3.5g$
Upward	–	–	$+1g$

Table 2.4: Normal flight conditions

	X	Y	Z
Sideward LH	–	$-3g$	–
Sideward RH	–	$+3g$	–
Forward	$-6g$	–	–
Rearward	$+1.5g$	–	–
Downward	–	–	$-6g$
Upward	–	–	$+3g$

Table 2.5: Hard landing conditions

	X	Y	Z
Sideward LH	–	$-16g$	–
Sideward RH	–	$+16g$	–
Forward	$-20g$	–	–
Rearward	$+20g$	–	–
Downward	–	–	$-20g$
Upward	–	–	$+10g$

Table 2.6: Crash conditions

2.1.5   Modal behaviour

Once the structural design elements are fixed, dynamic aspects of the object are analysed in order to be sure to avoid undesired vibrations due to resonance peaks. For a helicopter component, one of the most significant aspects is to avoid that the natural frequencies that are related to the global mode shapes of the structure do not coincide with the forcing frequencies introduced by the rotor rotation. For this specific case, the frequencies that should be avoided correspond to 4 and 8 times the main rotor frequency, including a tolerance band of $\pm 10\%$.

During the project design phase, the dynamic behaviour of the structure is anal–ysed through modal analysis performed by a finite element solver. However, it is

observed that the natural frequency of the SAR Plate Assembly was not out of the previously mentioned avoid bands around $17.1Hz$ and $34.2Hz$. In order to resolve this problem, 6 shock absorbers are strategically placed in correspondence to the fixing points with the helicopter cabin. Consequently, 4 shock absorbers are put near to the bottom and 2 near to the top as illustrated in fig. 2.17.
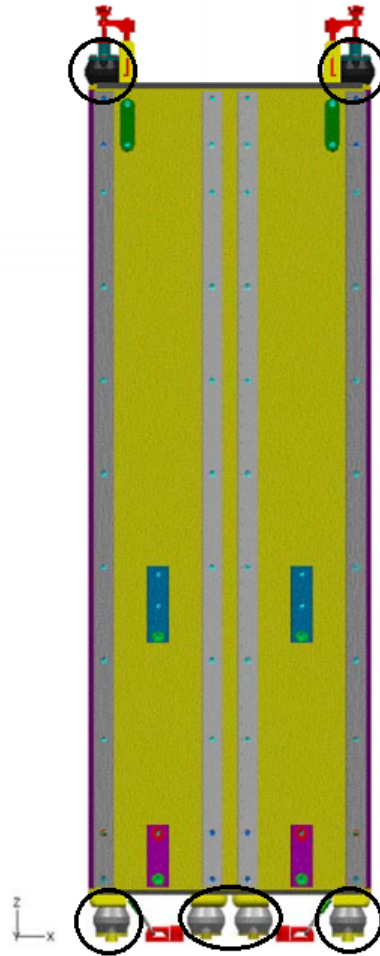
Figure 2.17: Position of the shock absorbers

The relevant shock absorbers are selected from the catalogue [8] based on the operational range of the plate determined by the load conditions. Actually the number of the placed shock absorbers depends on the force distribution on each of these suspension elements. By having this configuration, it is confirmed that the operational range of each damper is limited between 160–600N. This essen-tial information is used in order to determine the dimensions of the shock absorber:

Dimensions $[mm]$	
$\oslash$ A	60
B	40
$\oslash$ C	M10
$\oslash$ C_2	25
C_3	25
$\oslash$ T	M6
$\oslash$ W	40
P	6
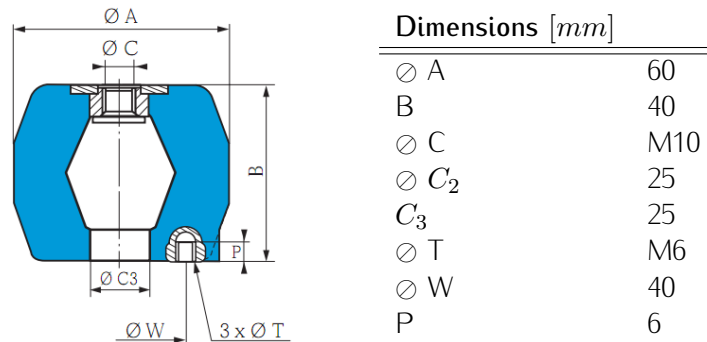
Figure 2.18 & Table 2.7: Geometrical properties of the appropriate shock absorber

Once the type and quantity of the shock absorbers are chosen, the verification concerning the attenuation of the desired frequencies is done using the analytical relations. In the case that a shock absorber is subjected to a vertically forced vibration that excites the structure by an alternating sinusoidal signal having a frequency of w and a magnitude of F_m, the elastic suspension system transmits to the structure a force with the same frequency but a different magnitude F'_m. Consequently, the rate of transmission λ for a specific shock absorber, can be defined as the ratio between the magnitude of the excitation force and the transmitted force.
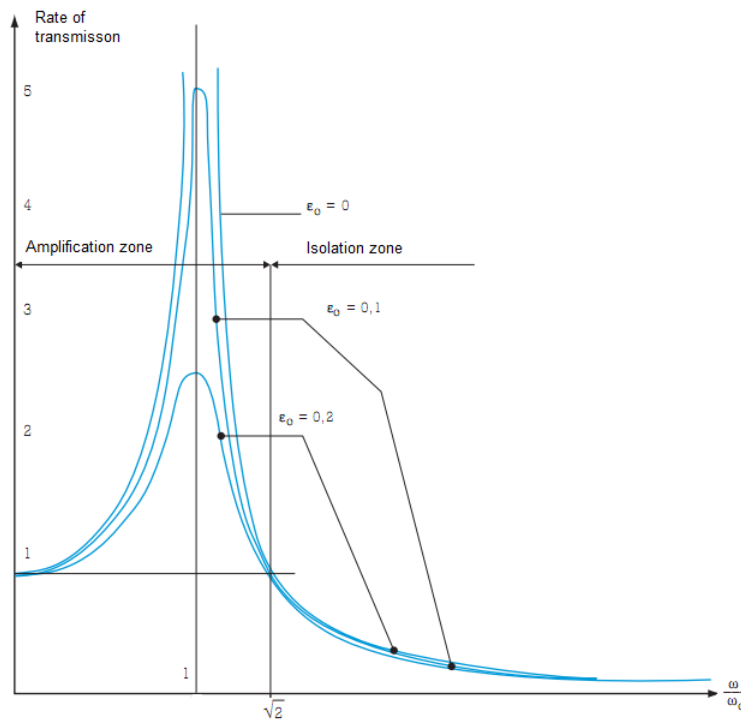
Figure 2.19: Attenuation of the vibrations near resonance

67

$$\lambda = \frac{F'_m}{F_m} = \sqrt{\frac{1 + 4\epsilon_0^2}{(1 - \frac{w^2}{w_0^2}) + 4\epsilon_0^2}} \tag{2.1}$$

The fig. 2.19 demonstrates that it is more convenient to have a higher ratio of w/w_0 in order to obtain a better damping rate. Consequently, the natural frequency of the damper, w_0 should be chosen as low as possible with respect to the operational frequency range. Note that in the isolation zone where w/w_0 is greater than $\sqrt{2}$, the influence of ϵ_0 is weak and in the meanwhile having a λ inferior to unity assures an attenuation of the transmitted force amplitude. Whereas in the amplification zone where w/w_0 is inferior to $\sqrt{2}$, the amplitude of the signal is amplified and its maximum is reached at resonance. This maximum value can be controlled by increasing the ϵ_0 at disposition.

For a rigid suspension mechanism, λ is equal to unity, which is equivalent to mention that the excitation force is equally transmitted to the structure. Instead for an elastic suspension system made of elastomer, λ is calculated with respect to the eq. 2.1. According to this formula, the rate of transmission depends on w_0 that corresponds to the natural frequency of the shock absorber and ϵ_0 to the characteristic damping rate. The value of ϵ_0 might vary based on the material of the shock absorber. To illustrate, for a shock absorber made of rubber, $4\epsilon_0^2$ is a negligible term and as a result of this the equation that expresses the the attenuation rate in percentage becomes:

$$\boxed{E\% = 100 \left(1 - \frac{1}{\left(\frac{w}{w_0}\right)^2 - 1} \right)} \tag{2.2}$$

In the specific case of the SAR Plate Assembly, the shock absorber adopted has a natural frequency that changes between 2.5 and $7Hz$ and the rotor natural frequency that should be avoided are 17.1 and $34.2Hz$. When these values are placed in the eq. 2.2, the attenuation of the vibrations varies between 79% and 99%. The problem regarding the dynamic analysis can be concluded considering the fact that using 6 suspension elements are enough to cope with the vibration amplification due to the induced periodic rotor forces.

A last point that can be taken into account about the shock absorbers is their

modelling during a finite element analysis. Actually for a given shock absorber, the producer company provides to the customer a data sheet that includes a force–displacement curve. This curve may be obtained also experimentally by measuring the displacement of the rubber for predefined axial compression or shear forces. The behaviour of a damping element is quite complex to model. In this case, they are modelled by the means of *GAP* elements. This type of elements is able to simulate the non linear behaviour of the damper, once the law of motion is introduced through the force–displacement values.

2.2 Formulation

As previously mentioned, the SAR Plate Assembly has a quite simple geometry and this fact makes it a good candidate for the optimization process because a simplified finite element model that run in short time allows to mostly focus on the optimization iterations and judge the abilities of the software in a short time in comparison with a complex model. As all other optimization problems require, the main aspects such as objectives, constraints and the variables should be determined. All these important properties regarding the optimization problem of the SAR Plate can be listed as in tab. 2.8:

Objectives:	Minimize the mass of the SAR Plate
	Find an alternative design by removing the shock absorbers
	Shift the operational frequency band outside of the avoid band
Constraints:	Geometrical boundaries
	Interface load limits
	Strength limits of the material
	Ability to carry upto 55 kg
	Presence of the frequency bands to be avoided
	Verification of the all load conditions for all configurations
Design variables:	Topological changes
	Geometrical entities
	Materials

Table 2.8: Definition of the optimization problem

Once the outline of the optimization problem is determined, all of its components can be examined in details by considering each statement separately.

2.2.1   Objectives

- **Minimization of mass**: For any vertical take–off and landing aircraft, one of the most crucial design criteria is the weight to power ratio. More specifi-cally in the case of an helicopter, this ratio might be considered at hovering condition. In order to derive a first order estimate of the power required to hover, the induced velocity at the rotor should be determined. There exist several aerodynamic theories that can be used to obtain this induced ve-locity value. The complexity of the formulation varies based on the desired accuracy of the model. One of simplest methods is the one dimensional ax-ial momentum theory which supposes to have a stream tube with a vertical axis through the rotor centre [9]. According to this formulation, the induced velocity and then the ideal power required to hover can be calculated as in eq. 2.3 and eq. 2.4:

$$V_i = \sqrt{\frac{T}{2\rho_{air}A_d}} \tag{2.3}$$

$$P_{ideal} = TV_i = T\sqrt{\frac{T}{2\rho_{air}A_d}} \tag{2.4}$$

Note that at hovering conditions, the weight W is equal to the thrust T produced by the rotor. As a result of this, the term that represents thrust in eq. 2.3 and eq. 2.4 can be replaced by the weight. This equivalence leads to an interesting relation between hover lift efficiency ($\frac{W}{P_{ideal}}$) and the disc loading ($\frac{T}{A_d}$). These two concepts might be used in order to classify aircraft with different flight principals as illustrated in fig. 2.20.

$$\boxed{\frac{W}{P_{ideal}} = \sqrt{2\rho_{air}}\sqrt{\frac{A_d}{T}}} \tag{2.5}$$
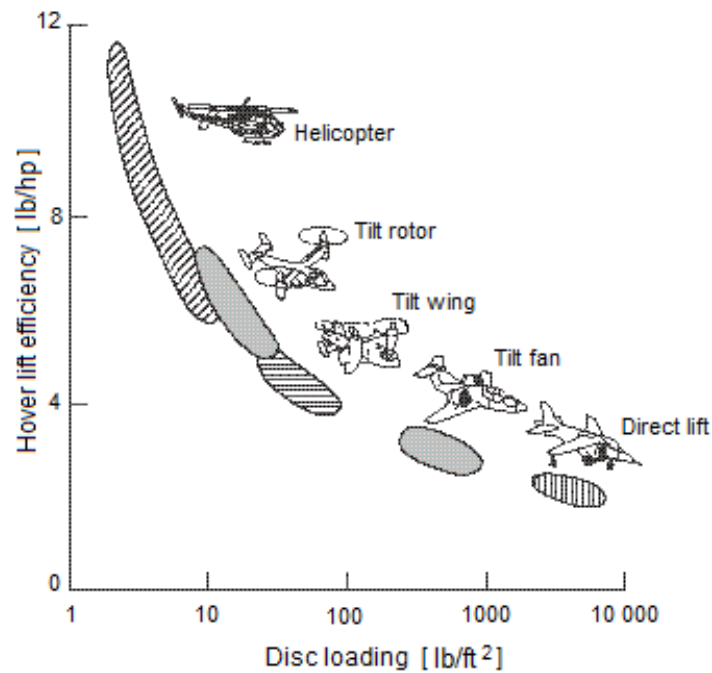
Figure 2.20: Variation of weight to power ratio with disc loading

All this basic but fundamental background is given in order to highlight the influence of the weight for an helicopter design. The fig. 2.20 shows that a slight increase in weight causes an important rise of thrust if the power and rotor area are kept constant. This additional power need is much more for an helicopter because it is placed towards the left extreme of the graph respect to the other aircraft. This fact makes the mass reduction of any component that should be mounted on the helicopter very critical. Even a few mass re-duction of any element might be equivalent to the possibility of transporting more payload or having a longer range with less fuel consumption. After all the information given about some key concepts regarding helicopter design, the conclusion is that the main objective of this optimization problem con-cerning SAR Plate Assembly is to minimize its mass.

• **Exclusion of the shock absorbers**: As previously mentioned, the main ob-jective of this optimization activity is to find an alternative structural design solution which weights less compared to the original design but which also satisfies the given constraints. The first step to reach this objective is the removal of the 6 shock absorbers which fundamentally work as a filter. There

are various reasons to validate this purpose: First of all, all these additional suspension elements introduce weight to the system even if they do not really make part of the structure. Second reason is that they increase the overall cost of production and force the designer to make a market survey to find the accurate component that might really supply the specific need. In the meanwhile, introducing an extra element obligates the analysts to perform additional controls by taking into account any type of condition that may cause an inconvenience. Furthermore, these suspension mechanisms are so hard to model in an accurate manner and so the predictions about the overall comportment of the system might not reflect the real one. Lastly, while modelling these parts in any finite element program, there can also be the necessity to posses extra information respect to those that the supplier may provide. In other words, some specific experiments can be required and this can be seen as an increase in cost but also time.

- **Shift of the operational frequency bands**: Another critical point about structural design for a helicopter component concerns the dynamic interactions with the rotor rotation. Actually the detailed explanation about the modal behaviour of the SAR Plate is reported in 2.1.5. This critical issue can be handled from two different perspectives. The presence of the avoid bands can be introduced into the optimization problem as an objective and constraint at the same time or only as a constraint. The difference between these two approaches is that when it also makes part of the objective function, the optimizer chooses the following design variables by measuring how far are the current values from the frequency objective. Instead in the other case, the optimizer independently proceeds with a new iteration and considers the frequency constraints as a simple check to decide whether the current design is feasible or not. In this thesis, the first approach is adopted due to the significance of the dynamic effects.

After this decision, the alternative scenarios are proposed and examined in order to be able to orient the optimization problem towards the desired direction. First of all, the complete frequency range is divided into 3 main zones where the frequency of the input does not cause amplification problems due to resonance.
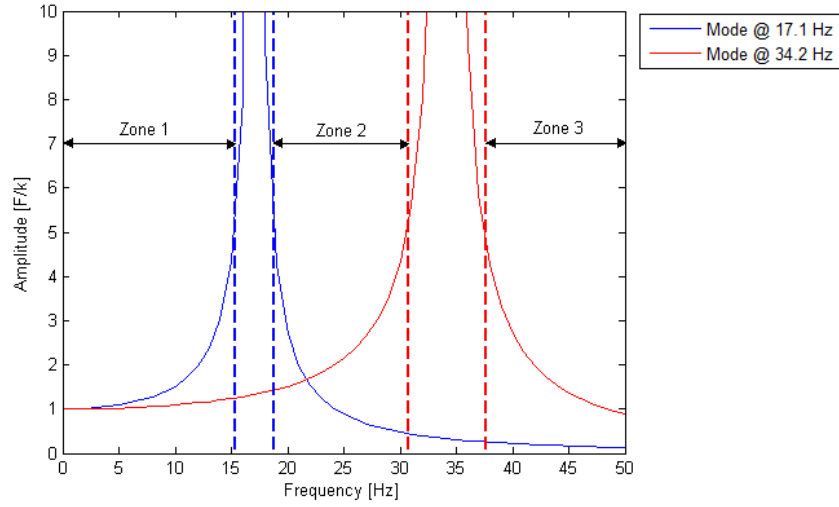
Figure 2.21: Limits of the acceptable frequency zones

These zones are determined by excluding the rotor vibration modes present at $17.1Hz$ and $34.2Hz$ with a tolerance band of $\pm 10\%$. Consequently, 3 main hypothesis can be made: All the global modes of the SAR Plate should be inferior to $15Hz$ or squeezed between $19Hz$ and $30Hz$ or superior to $38Hz$. The first case is critical because such low natural frequencies may cause robustness problems at static analysis level. The second case can be acceptable but even a little perturbation of the system may cause to interfere with the avoid bands. As a result of this, the third alternative is accepted by being conscious of the fact that higher natural frequencies can be reached by higher inertia values. The elements that might introduce inertia can cause a rise in weight so the optimization problem is going to be a compromise between two conflicting objectives: minimization of the weight and the maximization of the frequency.

A last but important note is about the definition of the operational range of the SAR Plate. During the paragraph 2.1.3, diverse loading configurations are presented. This point of view regarding the frequency issue should be valid for all the possible configurations: $(up, down, middle, bottle)$. This statement is equivalent to say that there exist an operational frequency range between the unloaded plate and the worst case among $(up, down, middle, bottle)$. Knowing that the natural frequency is proportional with $\sqrt{\frac{k}{m}}$, the configuration with the maximum payload would constitute the lower frequency bound and the unloaded plate the upper one. Consequently, any payload up to

the maximum acceptable threshold would be between these limits. As it is going to be possible to observe in the following part of the thesis, this concept would be the most challenging part of the optimization process.

Based on the overall situation, it can be deduced that the optimization problem at hands has more than one objective and this fact prevents the use of traditional gradient based or single objective methods. Consequently, during the optimization process, the genetic algorithms that are adequate for multi objective problems will be adopted.

2.2.2   Constraints

- **Geometrical boundaries**: One of the purely geometrical constraint states that the boundaries defined in the xz plane for the SAR Plate are fixed. Instead the limit along the y axis is determined by the form of the fuselage that supports the SAR Plate Assembly and the availability of the internal space depending on the given mission.

- **Interface load limits**: In the section 2.1.1, the details about the structure and functioning principles of the interface fittings are given. As previously mentioned, the lower and upper attachment points have different allowable interface load values. These values that constrained the designers to create an unusual fixing mechanism are illustrated in fig. 2.22(a) and fig. 2.22(b).

It is possible to observe that the allowable load value for the upper deck rail along z axis is quite low and this is the reason laying under the sliding mechanism of the upper interface. Note that after each iteration, the resulting force values along each direction is read and compared to the allowable ones.
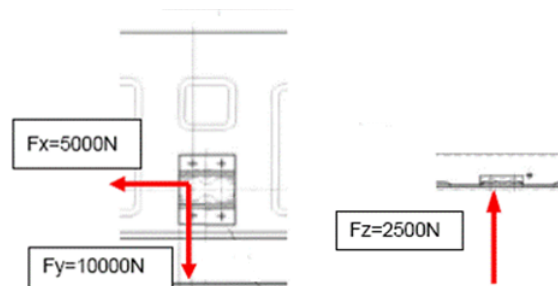
(a) Upper attachment points (section cut A/A in fig. D.2)
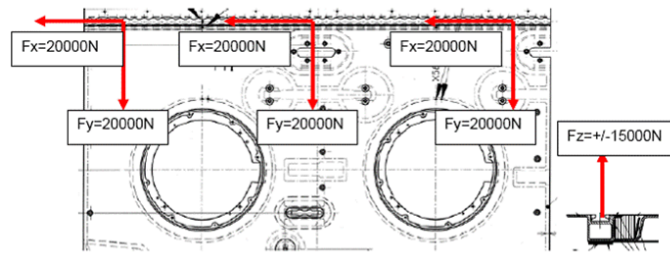
(b) Lower attachment points (section cut B/B in fig. D.2)

Figure 2.22: Interface limit loads

- **Strength limits of the material**: In addition to the dynamic aspects, static analysis is done and the stress levels are checked to ensure that there is not any value that goes beyond the allowable stress limits. In addition to this, for composite solutions, the failure index of each ply is also verified and the approach of "First Ply Failure" (app. B) is adopted. For the honeycomb core, the transverse shear stress is considered and compared with its upper limits.

- **Maximum payload limit**: The SAR Plate should be able to carry equipment upto $55kg$ by respecting the predefined loading indications. Note that any mass value between 0 and $55kg$ defines a possible loading configuration and at the same time the operational band of the plate.

- **Frequency avoid bands**: This aspect is covered while analysing the objectives of the optimization problem. Moreover, all the critical points concerning the dynamical properties are discussed within that section.

- **Verification**: The importance of the presence of diverse loading configurations and load conditions is continuously highlighted. The last constraint of the optimization problem would be a repetition of this concept. However, it is very significant that the alternative design proposed by the optimizer should be valid for all possible cases that make part of the operational range.

All these constraints can not be directly implemented in the optimization software and so the user should find implicit paths that ensure the implementation of all

of these factors.

2.2.3   Design variables

- **Topological changes**: A topological optimization helps to prepare the main ingredients to be tuned by a size optimization. In the case of the SAR Plate, two principal alternatives are going to be considered: the first one is a sandwich structure (metallic and composite) similar to the original design and the second one is a composite laminate that is reinforced by stiffeners. All these alternatives are going to be divided into subcases and discussed separately.
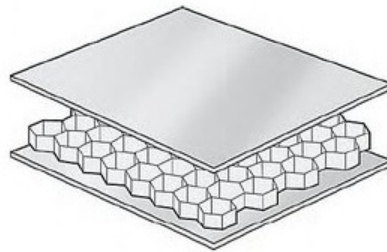
(a) Sandwich panel
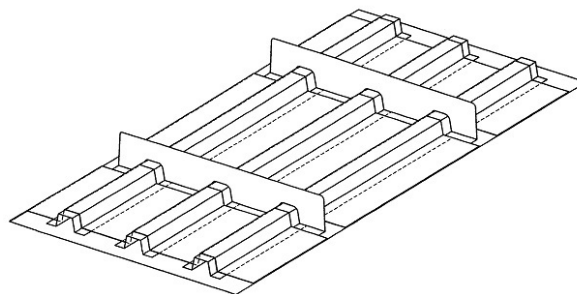
(b) Reinforced composite laminate

Figure 2.23: Different topological solutions for the SAR Plate

Note that in this thesis work, a conventional topological optimization activ-ity which determines the best material distribution within the structure is not performed. Instead, the passages between topologically different design solutions are decided by the user.

- **Geometrical entities**: For most of the structural optimization cases, the ge-ometrical entities are the most significant design variables. In this case,

even though the external borders are kept as a fixed constraint, the third dimension along the thickness provides a degree of freedom to the optimizer. Thus, honeycomb or skins thicknesses can be considered as fundamental elements that may change the response of the plate. For different types of variables, the acceptable range can be continuous or discrete. For instance, the thickness of an honeycomb core can be classified as continuous because even though it is costly, it is possible to obtain the desired precise thickness through a milling operation. Whereas the thickness values for a metallic skin are discrete because there exist predefined thicknesses that are listed in the catalogues.

- **Materials**: Another factor that is fundamental for a structural optimization is the possibility to select different materials. Especially, the use of composite materials is a very important tool because of the variability concerning its thickness, type and orientation angles. A "smart" combination of these elements permits the user to obtain a "tailored" component.

During the optimization process regarding topologically different solutions, the design variables are also going to be varied. While analysing each optimization case, all the possible variables will be listed and elaborated.

2.3   Implementation

Before analysing the optimization process, it would be useful to give some basic information about the use of the software. As previously mentioned, the optimization process is realized through the software *Isight*. First of all, in order to implement an optimization problem, the main logic regarding the schematization of the whole process should be determined. In other words, the user should decide about the principal steps required to represent the conceptual flow of the physical process. This concept of creating and ordering activities might also be called as *Sim-flow* or *Work flow*. To illustrate, a complex multidisciplinary optimization problem from aerospace industry can be considered. The problem consists of the optimization of the geometry of a hypersonic vehicle [10]. In an aerospace application, several disciplines that interacts with each other should be taken into consideration as shown in fig. 2.24
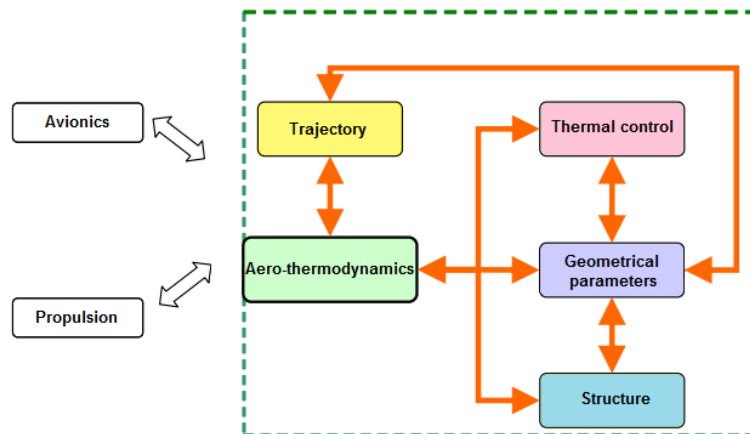
Figure 2.24: Interaction of the various disciplines for an aerospace problem

All these disciplines can be considered as *black boxes* that have inputs and outputs so the critical point is to organize the *work flow* in an intelligent manner so that the input–output relationship between various boxes is respected. The proposed solution is shown in fig. 2.25.
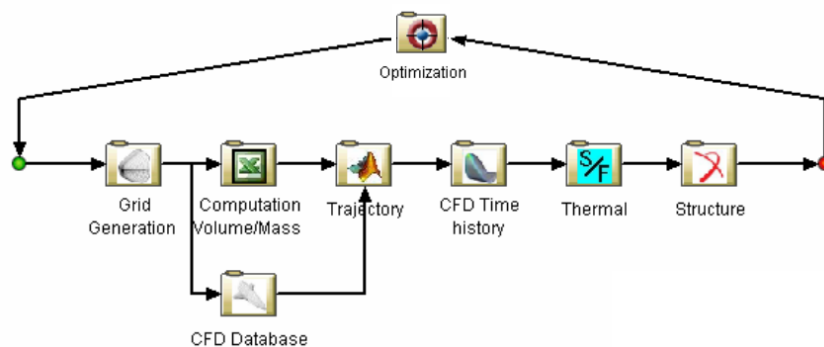
Figure 2.25: Schematization of the *Work flow* in *Isight*

This *Sim-flow* is equivalent to say that once the geometrical entities are determined by the optimizer, the finite element model is formed according to the three-dimensional geometry. The mass and the volume of the vehicle that has the predefined geometrical properties are calculated. Then by combining the computational fluid mechanics data base and the mass of the system, the information about Mach and altitude corresponding to the desired trajectory is obtained. This information serves to calculate the pressure distribution and the aerothermal fluxes through the "*CFD Time History*" block. As a next step, the temperature distribution on the desired surfaces is calculated by taking into account the aerothermal

fluxes and the geometry. Lastly, a structural analysis is performed in order to see the maximum displacement and the stress of the vehicle. In order to realize this last step, a thermo–elastic approach is used by considering the temperature and the pressure distribution that are calculated by the previous blocks. Then the optimizer changes the geometrical entities based on the given objectives and constraints and the loop restarts. Note that in order to do all the described tasks, the necessary operations are done within each *black box*. The main purpose to introduce such a complex problem is not to focus on how each block functions but rather on how to implement a process flow logic by respecting the interactions between different blocks.

To summarize all the information given until this point about the implementation of the problem, the concept of *work flow* is highlighted as the starting point. Once the work flow is established and modelled in the software, the process can be considered automatized because the same loop is going to be run for a predefined number of iterations. The key element in order to decide about the order of the *work flow* is to perfectly understand the process. In order words, it is critical to decide which *black box* is necessary in order to perform the desired analysis and the input–output relationship between each box. After this step, these elements are going to be translated in a language that the software understands. For *Isight*, it would be to choose the adequate component, place it on the *Sim-flow* and define the *Data flow*.
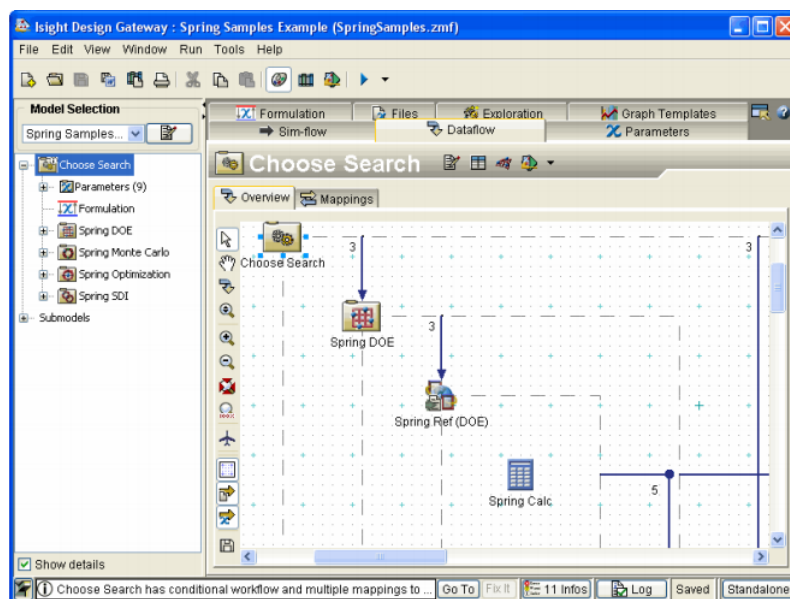
Figure 2.26: *Data flow* scheme between components

In *Isight*, each component or block possesses its own variables and these variables can be defined by filling the necessary information about them. To illustrate, the user should define for each variable its mode (input or output), its type (real, integer, string or boolean), its structure (scalar, array or aggregate), its name and its values. Note that even a file can be a variable. Once the variables of each block are defined, the relevant ones corresponding to different blocks are mapped among them in a manner to satisfy the input–output relationship between the blocks.
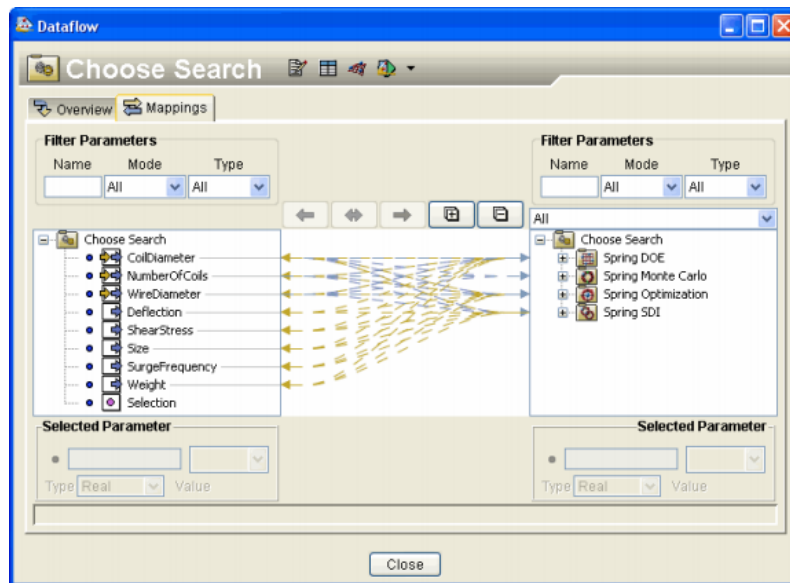
Figure 2.27: Mapping of the variables that belong to different components

Even though this thesis does not have an objective such as to furnish instructions about how to use *Isight*, some introductory information about *Sim-flow*, variables and *Data flow* is given. The reason for that is to inform the reader about the fundamentals of the software and to embody its interface. Note that there exist 2 main interfaces: the first one is the *Design Gateway* where the model is prepared and the second is *Runtime Gateway* where the model runs and the results are accessible.

2.3.1 Additional component for structural analysis

In the chap. 1, the main components of *Isight* are listed and their functions are clearly explained. In order to perform a structural analysis by adapting a finite element approach, a pre–processor is needed in order to implement the geometry and divide it into elements. In addition to this, a solver is required in order to

obtain the response of the structure. In this thesis, *Patran* is chosen as the pre–processor and *Nastran* as solver. Actually, the pre–processor prepares *.bdf* file that is given to the solver as input. After the execution of the solver, the results can be directly read from the *.f06* file. In order to automate this process in *Isight*, a unique *Simcode* component or 3 separate components can be used:

- **Data Exchanger 1**: This component takes the *.bdf* file and changes it by writing the value of a variable on the corresponding position.

- **OS–Command**: From the command line, this component executes *Nastran* by introducing the *.bdf* file as an input.

- **Data Exchanger 2**: This component takes the *.f06* file, reads and attributes the desired output information to a given variable.
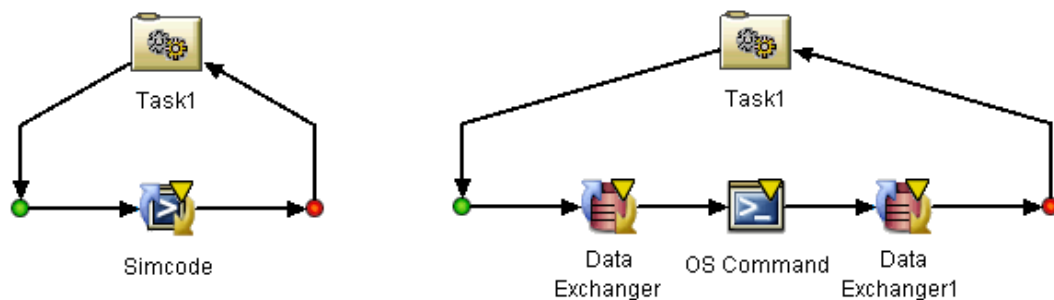
Figure 2.28: Automation of the structural analysis loop

In this thesis work, instead of these two solutions, a special plug–in component developed by *Exemplar srl* is used. This additional component called *Exe4Nastran* aims to facilitate data exchange with *Nastran* technology within the working framework offered by *Isight*. Moreover, this component is composed of 5 major sections:

1. **Configurations**: In this section, a special input file is loaded by the component. This configuration file has a special format that permits to identify the entries of the input and output files of *Nastran*. In other words, the specifications that should be written in *.bdf* file or read from *.f*06 file. Each row corresponds to the definition of a *Nastran* card. To illustrate, in fig. 2.29, when the *Nastran* input file is parsed and there exist a bar property (*PBAR*), the component assigns the numbers corresponding to different

columns of this line as area, area moments of inertia and torsional constant respectively. The same logic applies also for the output file parsing.
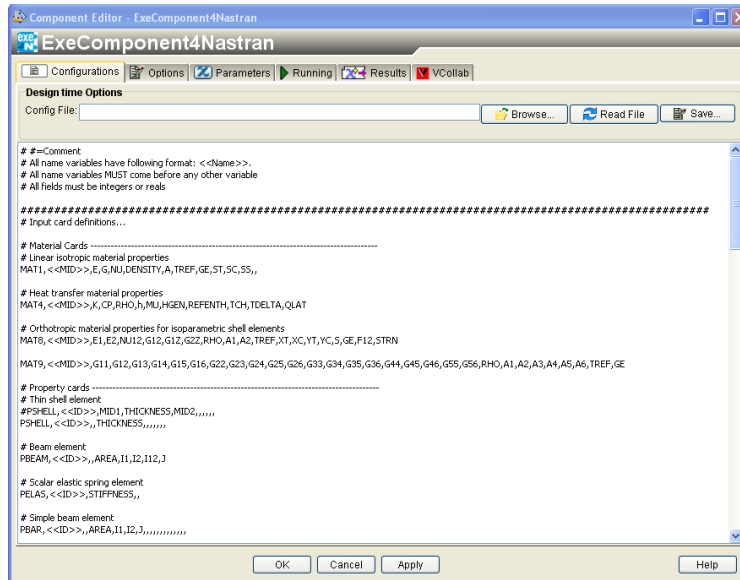
Figure 2.29: Component GUI: Configurations

2. **Options**: At this point, the input file for *Nastran* is loaded as a root file and it is parsed by the component. In this way, the component identifies all the variables that are defined in the previous configuration file.
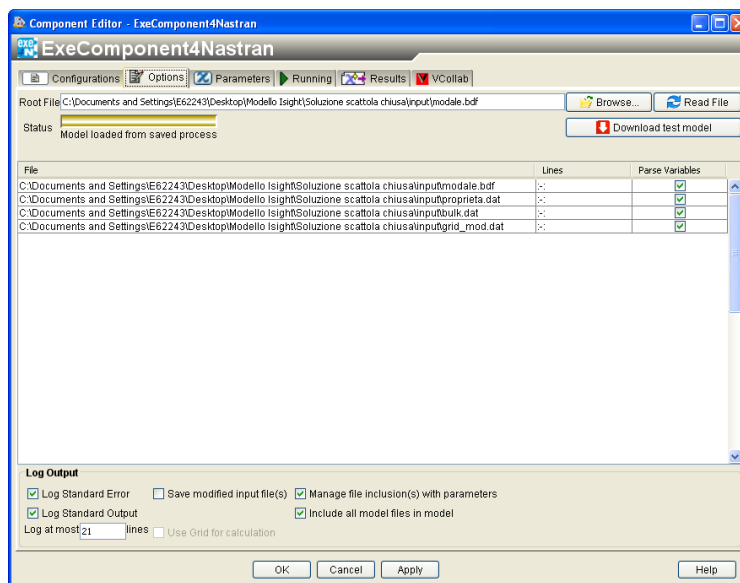
Figure 2.30: Component GUI: Options

3. **Parameters**: Once a variable is identified, it is listed as a parameter on the left column as illustrated in fig. 2.31. Consequently, the user may select the desired parameters by adding them as a variable of the component.
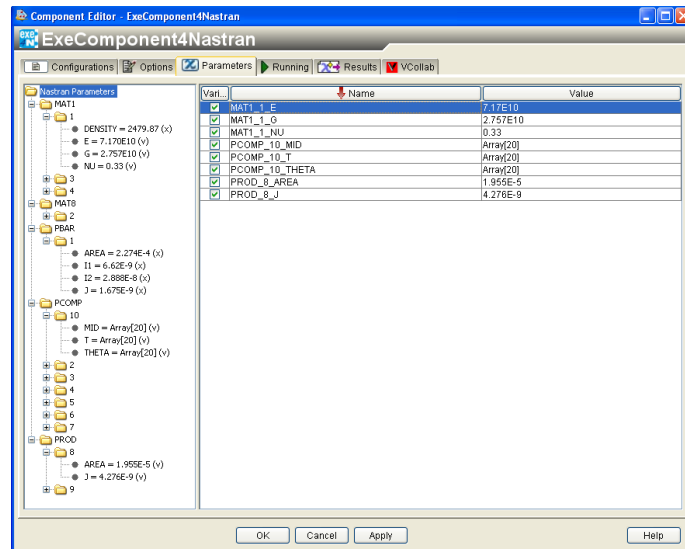
Figure 2.31: Component GUI: Parameters

4. **Running**: This section serves to set all the parameters for running *Nastran* such as introduction of the input file, selection of the directory regarding the executable *Nastran* link and definition of the memory options.
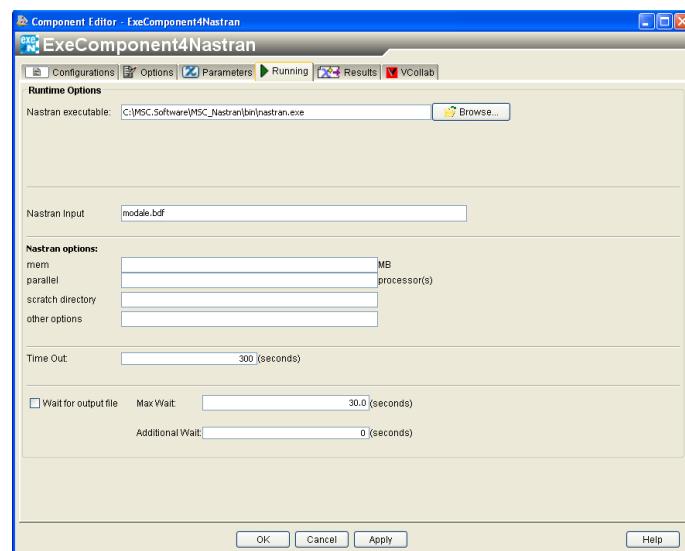
Figure 2.32: Component GUI: Running

5. **Results**: In this last section, the .*f*06 file is parsed and the defined output

variables are read. As in the case of the input variables, the user may select the desired outputs among the listed parameters.
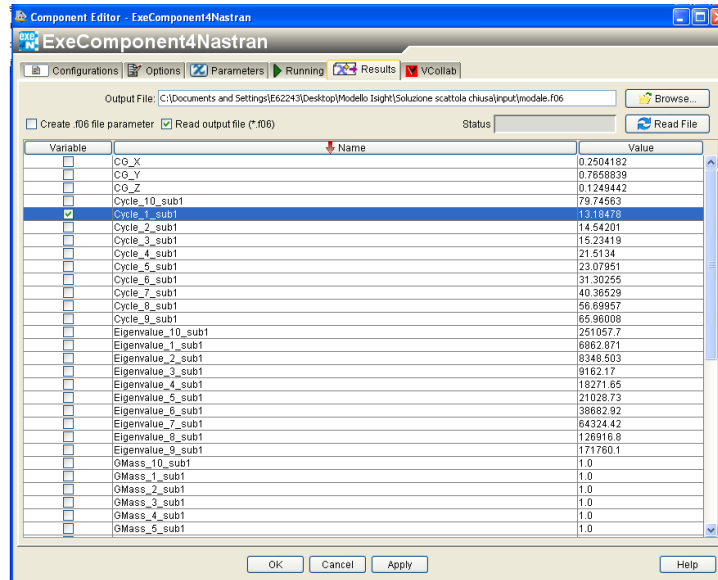
Figure 2.33: Component GUI: Results

In addition to these sections, other specific features regarding some utilities about composite materials or output management can be included into the component by choosing the relevant license. This component is especially presented in details because it is not a default component of *Isight* but most importantly it is the most essential element of this structural optimization process. Furthermore, this new block shows that the user is not obligated to use the default components present in the software but a desired component can be created through *application pro– gramming interface*. This component written in any programming language can be published in the *Isight* library and used in the *Sim–flow* by combining with the other default components without any problem.

Chapter 3

Optimization process

Once the fundamental elements of the optimization problem regarding the SAR Plate Assembly are defined, the optimization process is implemented through *Isight*. This thesis work principally comprehends the construction of an adequate finite element model of the plate and its integration into the *Work flow* regarding the optimization process. After these two main steps that automates the process, simulations are run for a predefined number of iterations and then the results are examined and interpreted.

The whole work of optimization can be divided into 4 main groups which represent topologically different structures. The steps described in the previous paragraph are followed by each of these groups. Actually the formation of the groups was not known a priori but they are gradually formed depending on the results of the previous ones. These 4 groups that correspond to different configurations can be summarized as follows:

1. Metallic sandwich model

2. Composite sandwich model

3. Reinforced laminate model

4. Reinforced closed box model

A brief description of the listed configurations can be given as an introduction. The starting point so the first configuration is a metallic sandwich structure which possesses skins and the honeycomb made of metallic materials. Instead the second configuration is composed of skins made of composite layers and a non metallic core is selected for the honeycomb. The choice of composite materials is also valid

for the third configuration which has a unique skin. In the mean while, the honey–comb part is totally removed and replaced by stiffeners that serve to reinforce the structure. Finally, the fourth and the last configuration is analysed. This latter solution can be considered as an extension of the third configuration because the presence of the unique skin and the stiffeners are preserved whereas a second skin is attached at the extremity of the stiffeners. In order to better visualize, a sandwich structure can be conceived by substituting the honeycomb core by stiffeners. These major models are constructed by following the given order and each one is examined in this chapter under separate sections. Furthermore, each section includes the details concerning the finite element modelling, optimization process and the corresponding results.

3.1 Configuration 1: Metallic sandwich model

The starting point in order to select the structure regarding the first configuration has been the original design of the SAR Plate Assembly. Consequently, a metallic sandwich model is adopted in order to initiate the optimization process.

3.1.1 Finite element model

In most of the cases, the *FEM* of a component is made based on its already exist–ing *CAD* model (*.iges*) prepared by a designer. The analyst decides the strategy of modelling in a manner to represent the component as accurate as possible. Actually, the certification of the SAR Plate Assembly is based on finite element analysis and other specific manual calculations. This *FEM* includes quite com–plicated elements in order to obtain a realistic representation. To illustrate, the shock absorbers are modelled by the use of non linear elements. The honeycomb and the tracks are represented through solid and planar elements respectively. Furthermore, spring elements are inserted in order to model the stiffness of the upper interface zone. Even though these factors help to obtain a better approx–imation of the real model, they introduce additional difficulties for modelling. In addition to this, the complexity of the model increases the time required for the solver. Supposing that the optimization process is constituted of a continuous run–ning of the Work flow, the necessary time for a unique run has significant effects on the total optimization time. As a result of this, the *FEM* that is going to be used during the process would be a compromise between the total optimization

time and the complexity regarding the modelling.

One of the most critical aspects of this *FEM* concerns the formulation of the honeycomb core. Actually, there exist two different approaches for honeycomb modelling: the first one uses the three dimensional solid elements whereas the second one planar shell elements. As previously mentioned, during the finite element analysis of the original SAR Plate Assembly, the first approach is chosen by the analyst. Even though the solid elements give more accurate results, in this thesis the second approach is adopted due to 2 main reasons:

- **The nature of a sandwich panel**: In general terms, the shear forces normal to the plane are carried by the honeycomb core. Instead the bending moment or the in-plane forces on the sandwich structure act as membrane forces in the facing skins. This fact highlights that the in-plane stiffness of the honeycomb core is negligible compared to that of the facing skins.

- **The need for reducing simulation time**: The time required to solve a model composed of solid elements are much higher respect to shell elements.
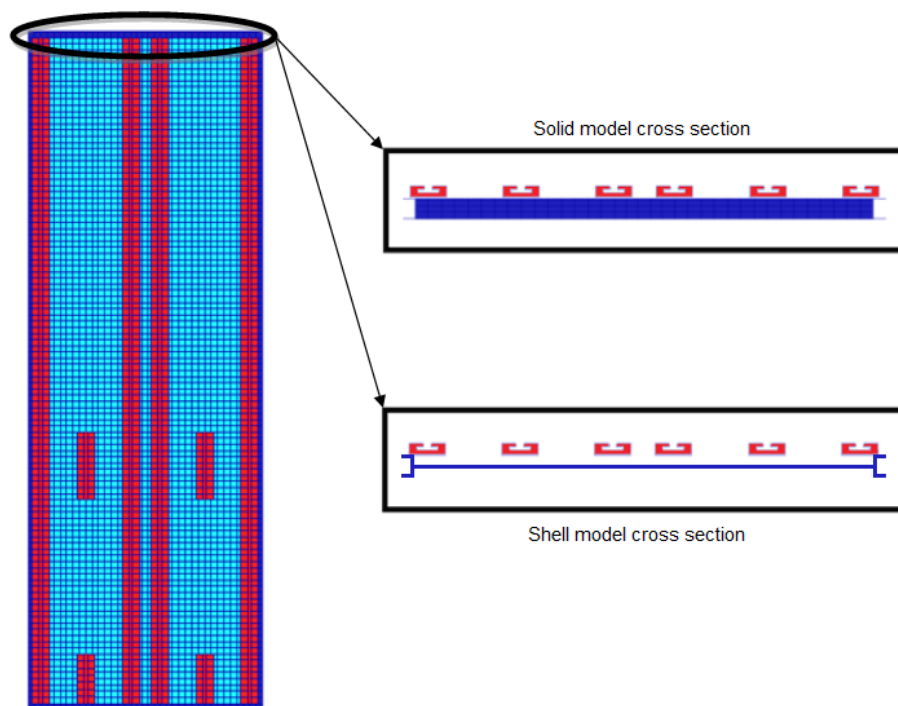
Figure 3.1: *FEM* with solid and shell elements

However this important choice is justified by constructing both models using shell and solid elements and comparing the results. In both of the cases, the facing skins are modelled with planar elements due to the existing proportion between thickness and its other dimensions. In order to avoid complexity at this prelim- inary design phase, the tracks are modelled by using beam elements and their corresponding cross section is assigned to these elements. Another fundamental element which is the reinforcement in form of "C" around the plate is also included in *FEM*. In the shell model, they are modelled through beam elements whereas in the solid one through shell elements. Both of the models are illustrated in fig. 3.1.

As one of the most critical points of the optimization problem concerns the modal behaviour of the plate, the natural frequencies and the mode shapes corresponding to the principal modes should be as close as possible for these 2 modelling approaches. In order to make a comparison, the first two global modes are selected.

(a) Bending out of plane   (b) Torsion
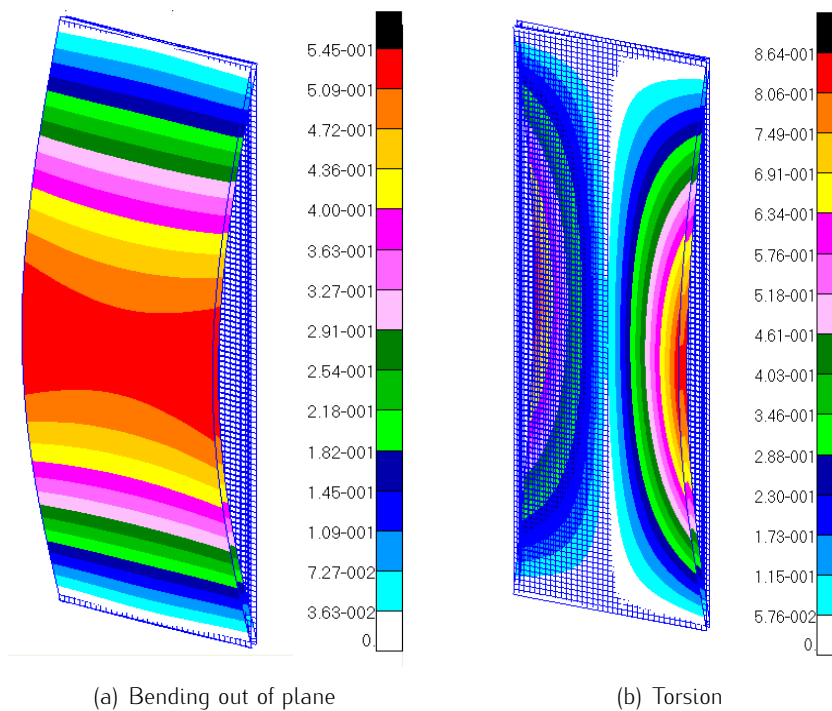
Figure 3.2: The first 2 natural frequencies of the empty plate

As the tab. 3.1 shows, the difference between the frequency values of the two models does not exceed 5%. Consequently, the choice of representing the SAR Plate by the use of shell elements is justified. Once the final *FEM* is obtained, a further verification at static level is going to be made respect to the original

SAR Plate model. In this manner, the *FEM* that is used during the optimization process would be verified in both dynamic and static terms.

Mode description	Mode Frequency [Hz]		Difference (%)
	Solid	Shell	
Bending out of plane	35.7	34.9	2.24
Torsion	98.3	94.7	3.70

Table 3.1: Comparison of the vibration modes regarding the solid and shell models

After this significant modelling choice, the remaining details about the *FEM* can be given. At the end, the whole plate is represented by a plane with the accurate dimensions and properties. In order to model the effect of the superposition of the skins and the honeycomb part, a property of *PCOMP* is assigned to the planar elements. In general terms, this *PCOMP* card is utilized to model layered composite materials by specifying the properties of each layer. Similarly, in this case the sandwich structure can be idealized as a composite structure that has 3 main layers: upper skin, honeycomb core and lower skin respectively. The complete input set can be listed as in tab. 3.2.

Layer no	Description	Thickness [mm]	Material	Angle
1	Upper skin	0.64	Al 2024	0
2	Honeycomb	19.05	Al 5056	0
3	Lower skin	0.64	Al 2024	0

Table 3.2: Definition of the *PCOMP* card for the metallic sandwich structure

An important note about the use of *PCOMP* in this thesis should be underlined: for each *PCOMP* property, there exists an offset value that stands for the distance from the reference plane to the bottom surface. This value is set to 0 instead of its default value which corresponds to the half of the element thickness. The reason for such a choice is to ensure the continuity of the external surfaces.

Note that in order to define a *PCOMP* card, it is necessary to define a material orientation angle respect to the local coordinate system. This fact serves to consider the differences regarding the mechanical properties of orthotropic materials. In this case, it is enough to assign an isotropic material to the skins (*MAT1*) be-

cause of the fact that their mechanical properties do not depend on the direction. However, this situation is not valid for the honeycomb core which is represented by an orthotropic material model valid for planar elements (*MAT8*).

Al 2024

E_{xx}	$[MPa]$	72395	ρ	$[kg/m^3]$	2768
G_{xy}	$[MPa]$	27579	σ_{tu}	$[MPa]$	441
υ		0.33	σ_{ty}	$[MPa]$	324

Table 3.3: Mechanical properties of the skin material
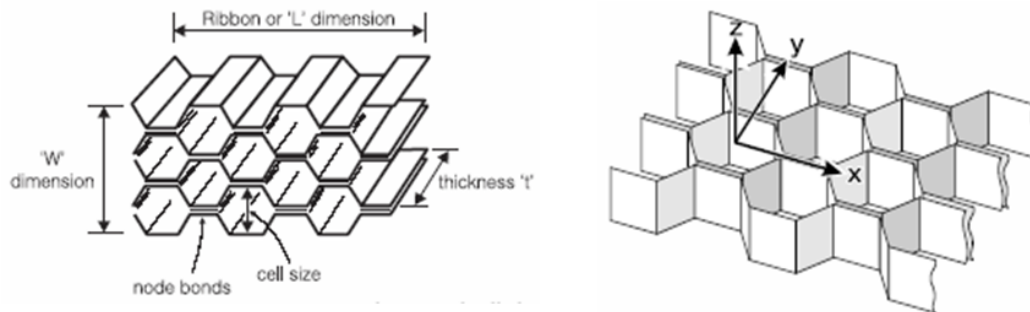
Figure 3.3: Local coordinate system of a honeycomb core

Al 5056

E_{xx}	$[MPa]$	≈ 0	G_{xz}	$[MPa]$	985.95
E_{yy}	$[MPa]$	≈ 0	G_{yz}	$[MPa]$	351.63
v_{xy}		≈ 0	ρ	$[kg/m^3]$	128.5
G_{xy}	$[MPa]$	≈ 0	Cell size	$[mm]$	3.2

Table 3.4: Mechanical properties of the metallic honeycomb material

Note that in order to define the directional properties of a honeycomb, an additional local coordinate system should be created. This coordinate system has the ribbon or "L" direction parallel to the z axis whereas "W" direction to x axis of the global reference system.

The tracks and the "C" reinforcement sections are modelled through beam elements and their corresponding cross section properties are assigned by the use of a *PBAR* card. Indeed, this choice facilitated the optimization process. The tracks have standard and constant forms whereas the dimensions of the reinforcement

elements can be considered as one of the design variables of the optimization problem. Consequently, the ability and the ease of changing them have a great importance. Obviously, this target of modifying the dimensions of a section is easier for beam elements with respect to those that have shell formulation. For the beam case, it is enough to calculate the new section properties such as area, moment of inertia and torsional constant, then insert them into the *PBAR* card. Instead for the shell case; in order to be able to change the form of a section, the position of the relevant nodes should be changed. This operation is surely much more onerous respect to the previous one. In addition to the geometrical entities, an isotropic material input is necessary in order to be able to define a *PBAR* property. Material properties for the tracks and the "C" reinforcement elements are listed in tab. 3.5 and tab. 3.6.

Al 7075

E_{xx}	$[MPa]$	71016	ρ	$[kg/m^3]$	2796
G_{xy}	$[MPa]$	26890	σ_{tu}	$[MPa]$	448
v		0.33	σ_{ty}	$[MPa]$	345

Table 3.5: Mechanical properties of the track and interface fitting material

Steel AISI 4140 (Tempered and quenched)

E_{xx}	$[MPa]$	200000	ρ	$[kg/m^3]$	7833
G_{xy}	$[MPa]$	75800	σ_{tu}	$[MPa]$	1516
v		0.32	σ_{ty}	$[MPa]$	1275

Table 3.6: Mechanical properties of the "C" reinforcement material

As fig. 2.12 shows, there exist zones at the extremity of the plate where the skin and the flange of the reinforcement elements are overlapped. Moreover, the material corresponding to the skins is aluminium whereas the reinforcement parts are made of steel. In order to be able to simulate this overlapping, an equivalent thickness of the skin is calculated by considering the proportion between the elastic moduli of these two materials and this value is added to the original flange thickness.

$$t_{tot} = t_{flange} + t_{steel}\frac{E_{Al}}{E_{steel}} \tag{3.1}$$

Another important aspect concerns the modelling of the interface fittings. During the finite element analysis of the original SAR Plate, these elements are modelled with solid elements once their exact geometry is exported from any *CAD* software

(fig. 3.4). As the *FEM* that is going to be used during the optimization process should be a simplified model, the idea of utilizing three dimensional elements is rejected. Alternatively, they are included in the model as an additional layer to the sandwich structure. In other words, the interface fittings are projected on plate surface and the corresponding elements are gathered together in order to form a different group. A special *PCOMP* property that has 4 layers is created and assigned to the elements that constitute this group. The key point is to be able to introduce in an accurate manner the mass and the inertia properties of these structural elements. To realize this, the real thickness of the interface fittings are given as an input to the *Nastran* card and in this way the inertia properties are conserved with respect to its original values. Instead, the mass difference is compensated by creating an isotropic dummy material that has the same prop–erties of Al 7075 except the density. The density value is separately calculated in a manner to obtain the same interface fitting mass value that is listed in tab. 2.1.
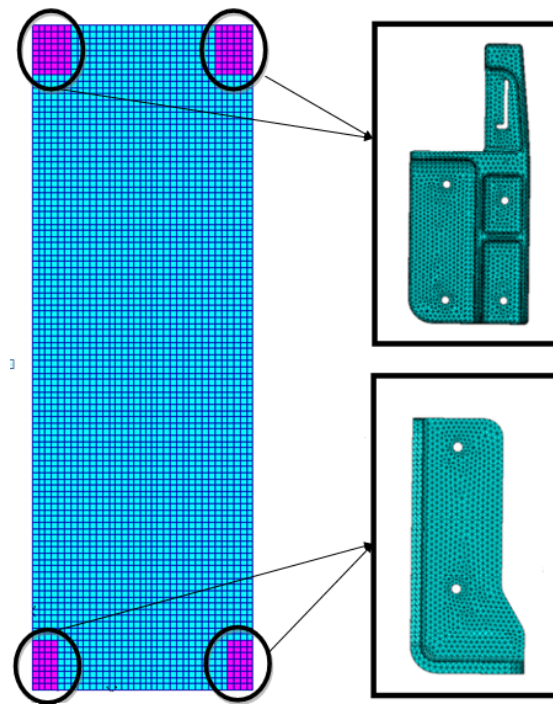
Figure 3.4: Projection of the fittings on the plate

One of the significant particularities concerning the *FEM* is the introduction of the loads. In chap. 2.1.3, the guidelines for loading the plate and the existence of 4 different extreme load configurations are explained in details. The new design

of the SAR Plate should satisfy the given constraints for all of these different configurations ($empty, up, down, middle, bottle$). Moreover, a smart modelling technique is used in order to provide to the optimizer the flexibility to switch between different configurations. First of all, the positions of the masses are determined by considering the maximum CoG distance out of plane. Instead of constructing 5 separate models, a unique one is prepared and point elements are placed in correspondence to the real position of the all possible masses. These point elements are connected to the plate respecting the given vertical distance between two connection points on the track. In order to simulate the physicality of these connections, *RBE3* elements are explicitly selected due to the fact that they distribute the given load on the independent nodes.
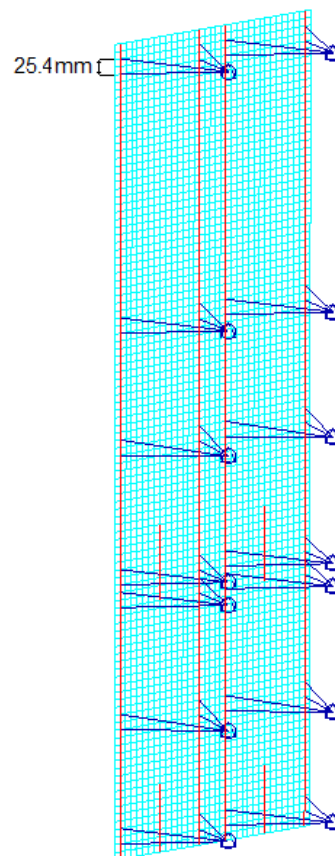
Figure 3.5: Load introduction to the plate in correspondence to the tracks

In this way, the desired load configuration can be obtained by assigning to the desired point elements the corresponding mass by the use of *CONM2* elements. Instead a null mass value is assigned to the remaining point elements. Obviously, assigning null mass value to all of the elements allows to obtain the empty plate

configuration. As the *RBE3* elements do not introduce any additional stiffness to the system, connecting a point element with null mass to the plate through these elements create the effect that this connection does not really exist. In this way, the optimizer can use a unique *Nastran* input file and change only the mass values in order to obtain any of these 5 configurations.

The last modelling remarks would be about the load conditions and constraints. During the optimization process, the worst load conditions (crash) are considered. As listed in tab. 2.6, for the static case, 6 different subcases are created in order to cover the loads conditions along all directions. Note that the loads are defined as accelerations and consequently they are simulated by the *GRAV* card.

(a) Upper interface zone   (b) Lower interface zone
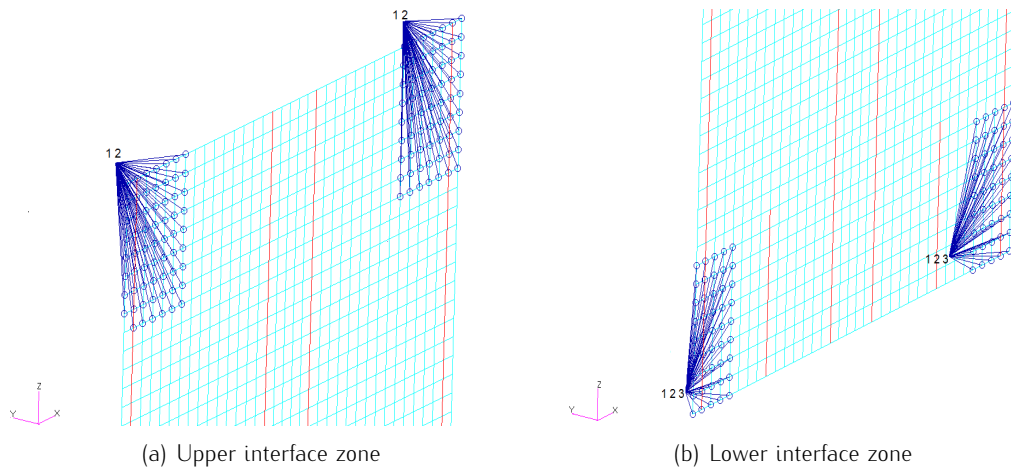
Figure 3.6: Modelling of the interface connections

The constraints or the boundary conditions are defined in a manner to reproduce the functioning mechanism of the original SAR Plate. Thus, all the translational degrees of freedom of the nodes that simulate the lower attachment points are fixed. Instead the vertical movement of the upper attachment points is kept free but the translational degrees of freedom along the track surface are fixed. The correct position of the attachment points are determined by taking into account the hole on the interface fittings. As the aim of the new design is to remove the shock absorbers, the lower connection points in correspondence to the lower thin fittings are neglected and the plate is constrained through 4 points. Furthermore, in order to model the effect of the stiffness regarding the interface fittings, the constrained nodes are connected to the elements that correspond to the projection of the real fittings by the use of *RBE2* elements.

Once all these elements are included in the *FEM*, the overall mass balance is done in a manner to verify that each modelled component weights equal to its predicted value listed in tab. 2.1. In the case of discrepancies, the density values are slightly changed in order to ensure the equality. As a last step, a verification at static level is performed by comparing the interface loads at the constrained nodes. The reference point for such a comparison has been the original SAR Plate model and in order to guarantee equivalent conditions, the non linear and the spring elements that simulate the shock absorbers and the interface stiffness respectively are removed. A random configuration is considered and the interface loads are compared in order to be sure that the simplified model gives reliable results also statically. Due to the presence of various modelling differences, a complete overlapping is not expected but mostly the order of magnitude and the sign of the forces are verified.

Until this point, a detailed description of the *FEM* that is employed during the optimization process regarding the metallic sandwich model is given. Note that the *FEM* corresponding to the following configurations are based on this model so the new models are obtained by introducing the relevant modifications to this present model.

3.1.2   Optimization model

Once the preparation of the *FEM* of the plate is terminated, the optimization model is constructed. First of all, the objectives, constraints and design variables of the optimization problem are clarified. Note that the main objective of the whole optimization process is the minimization of the mass. In addition to this, a criterion about the frequency issue is determined as a secondary objective. However, there exist several formulation options concerning this frequency objective. As a result of this, an intermediate analysis is done in order to choose the most convenient one.

Selection of the frequency objective

Modal behaviour of the plate is previously explained and in the chap. 2.2.1, it is deduced that 2 alternative solutions exist in order to avoid the forcing frequency bands. Note that the third solution which would make use of the frequency band between 0 and $15Hz$ is completely neglected due to the lack of robustness

during static analysis. Among the remaining two alternative solutions, the one which tries to squeeze the operational frequency band between $19Hz$ and $30Hz$ is implemented. Note that this operational frequency band of the plate has its lower limit when the plate is fully loaded and its upper limit when the plate is empty. After defining the objectives and the constraints, the design variables can be listed. For this configuration, the existing variables depend on the geometrical entities such as the honeycomb and skins thicknesses. In the meanwhile material properties such as honeycomb core density are also taken into account. Moreover, these values would be changing departing from their values corresponding to the original design of the SAR Plate Assembly.

- **Case 1: Operational frequency band between 19 and 30 Hz**

  Objectives: Minimize M_e
  Maximize f_l^1
  Minimize f_e^1

  Constraints: $f_{1_{loaded}} > 19Hz$
  $f_{1_{empty}} < 30Hz$

  Design variables:

Honeycomb thickness	tab. 3.8
Upper skin thickness	tab. 3.7
Lower skin thickness	tab. 3.7
Honeycomb density	30–150 kg/m^3
Web thickness of the "C" reinforcement	0.2–2 mm
Flange thickness of the "C" reinforcement	0.2–2 mm

The design variables can be classified under two major groups: continuous and discrete. The first 4 variables belong to the second group whereas the properties of the "C" reinforcement elements can be considered continuous within the defined range. However, the honeycomb thickness and its density are introduced into the model as continuous variables even though their existence is discrete. One of the reasons to adopt such an approach is based on the possibility to change the thickness of a honeycomb by a milling operation departing from an already existing core block. A similar logic is also valid for the honeycomb density because a desired density value can be approximately obtained by changing the cell shape or size. Instead, this flexibility can not be applied for the facing skins and the only available values are the ones that are present in the market. In order to give

an idea about the existing metallic honeycomb and skin thickness, some values
are imported from the catalogues [11],[12]:

Facing skin thickness [mm]					
0.2	0.3	0.51	1.02	2.03	4.06
0.22	0.35	0.64	1.27	2.54	4.83
0.25	0.41	0.81	1.6	3.18	

Table 3.7: Preferred thickness values for aluminium alloy skins

Honeycomb thickness [mm]		
6.35	12.7	25.4
9.53	19.05	38.10

Table 3.8: Preferred thickness values for metallic honeycomb core

Once the critical concepts of the optimization problem are established, the *Work
flow* sequence in *Isight* is constructed as shown in fig. 3.7.
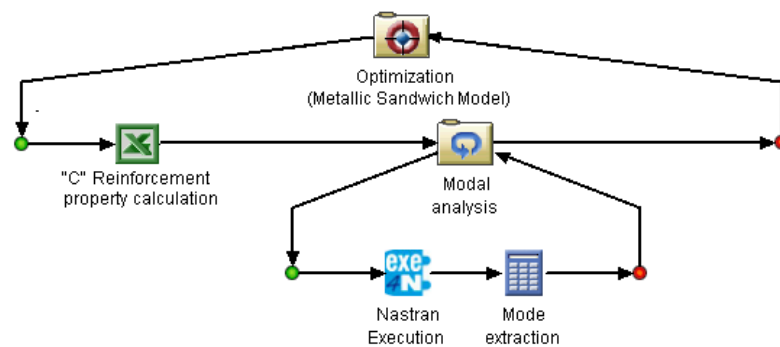
Figure 3.7: *Sim flow* scheme for comparing the frequency objectives

As previously underlined, this sequence is determined due to the input–output
relationship between the blocks. In the *Sim-flow* present in fig. 3.7, the *Opti-
mization* block decides how to change the variables respecting the given initial
conditions. Then the geometrical properties of the "C" reinforcement such as area,
moment of inertia and torsional stiffness constant are calculated under the *Excel*
block. Once these values are combined with the other geometrical entities com-
ing from the *Optimization* block, they are passed to the *Exe4Nastran* component
under the loop. At this intermediate step, only modal analysis is performed in
order to save time. The iteration criteria of the loop covers all the possible load-
ing configurations ($up, down, middle, bottle$) and the empty plate as previously

described. The *Exe4Nastran* component changes the *.bdf* file accordingly, runs *Nastran* with *SOL 103* command and reads the desired outputs from the *.f*06 file. The *Calculator* block calculates the lowest so the most critical natural frequency between the possible loading configurations.

The graph reported in fig. 3.8 shows that there exist a linear relationship between f_e^1 and f_l^1. This means that while trying to maximize f_l^1 increases also f_e^1 and the present design variables can not enable the operational frequency band to fit into the desired interval. It is also visible that the new solutions gradually get concentrated in an area which tries to minimize the distance defined respect to the boundaries of the feasible zone. However, the current design space does not permit feasible solutions.
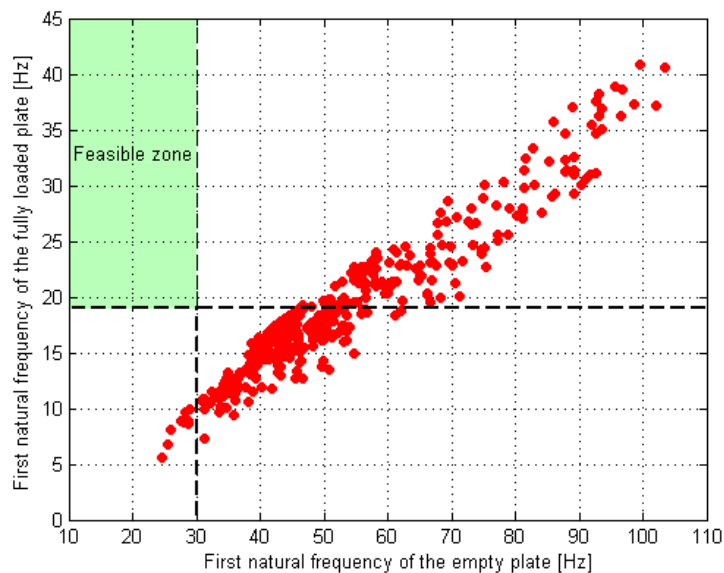
Figure 3.8: Correlation between the frequency of the empty and loaded plate

The obtained results confirm that the objective that tends to fit the operational frequency band between 19 and 30 Hz is not applicable for this component. Consequently, shifting the entire frequency band beyond 38 Hz is going to be the unique frequency objective for the rest of the optimization process. As previously mentioned, this new option is less sensitive to any kind of perturbation respect to the previous one. Thus, it also allows a better solution in terms of dynamic robustness.

Main model

The frequency criteria is stabilized in a manner to move the lower bound of the operational frequency band beyond $38Hz$ so that the any possible load combination would not cause a problem. Then the main optimization problem regarding the metallic sandwich model is set by adding the static analysis to the previously prepared model. Consequently, additional constraints related to the static analysis are considered even though the objectives remained the same. The general optimization problem is formulated in the following manner:

- **Case 2: Optimization of the metallic sandwich model**

  Objectives: Minimize M_e
                        Maximize f_l^1

  Constraints: $f_{1_{loaded}} > 38Hz$
                        $R_{x_{down}} < 20000N$ $R_{x_{up}} < 5000N$
                        $R_{y_{down}} < 20000N$ $R_{y_{up}} < 10000N$
                        $R_{z_{down}} < 15000N$

  Design variables: Honeycomb thickness   tab. 3.8
                        Upper skin thickness   tab. 3.7
                        Lower skin thickness   tab. 3.7
                        Honeycomb density [1:6] $30\text{–}150kg/m^3$
                        Web thickness of the "C" reinforcement $0.2\text{–}2mm$
                        Flange thickness of the "C" reinforcement $0.2\text{–}2mm$

There also exists a slight difference regarding the design variables with respect to the previous case. This difference concerns the honeycomb density. The number of the design variables is incremented by considering the fact that the current ones can not create significant effects on the modal behaviour of the plate. In order to do this, the plate is divided into 6 boxes (fig. 2.13) where the honeycomb density varies for each zone but its thickness remains uniform. The scope of such a move is to enlarge the boundaries of the design space in order to obtain more feasible solutions. In the meanwhile, this division would also be an indication about the local effects on the global modal behaviour.

Once all the necessary elements are defined, the optimization model in *Isight* is constructed:
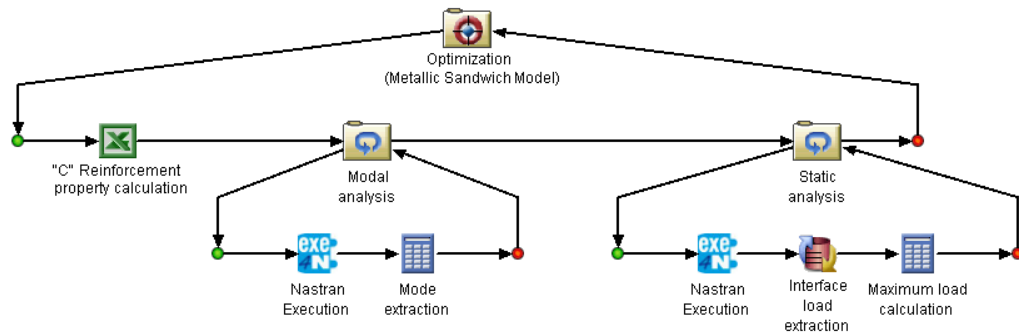
Figure 3.9: Optimization *Work flow* scheme for the metallic sandwich model

As previously mentioned, the main model is obtained by developing the one used in order to determine the frequency criterion. The improvements comprehend the inclusion of a second loop for static analysis. The iteration criterion and the formulation of the *Exe4Nastran* component for the new loop is the same as the other one. The only difference is that the *.bdf* input file is configured for a static analysis so it includes *SOL 101* instead of *SOL 103*. As the default *Exe4Nastran* is not equipped to read constraint forces, a *Data Exchanger* block is inserted. This block reads the reaction forces on the constraints and then passes them to the *Calculator* in order to obtain their maximum values. Note that all the load conditions with different accelerations are covered at each iteration by defining 6 different subcases in the input file. After this step, the loop closes and the *Optimization* component changes the variables based on the evaluation of its objective and penalty functions. Note that the mass of the SAR Plate is calculated under the modal analysis loop.

3.1.3   Results

After the preparation of the *Work flow*, the parameters inside the optimization block should be defined. In chap. 1, the genetic algorithms present in *Isight* are clearly explained. For different applications, any of these 4 algorithms can be the most suitable one. As a single iteration lasts more or less a couple of minutes, all the algorithms are tested in order to find the best one for this application. In order to be able to compare different algorithms, approximately equivalent conditions are created. This means that the total iteration number is kept equal for each algorithm. In addition to this, the population size and the number of generation are selected in a coherent way for each of them. Even though this is a very basic and insufficient manner of comparing different algorithms, it gives an idea

about the quality of the results for this application. As this aspect is not among the purposes of this thesis work, relevant scientific articles such as [19] can be examined for a more detailed analysis.
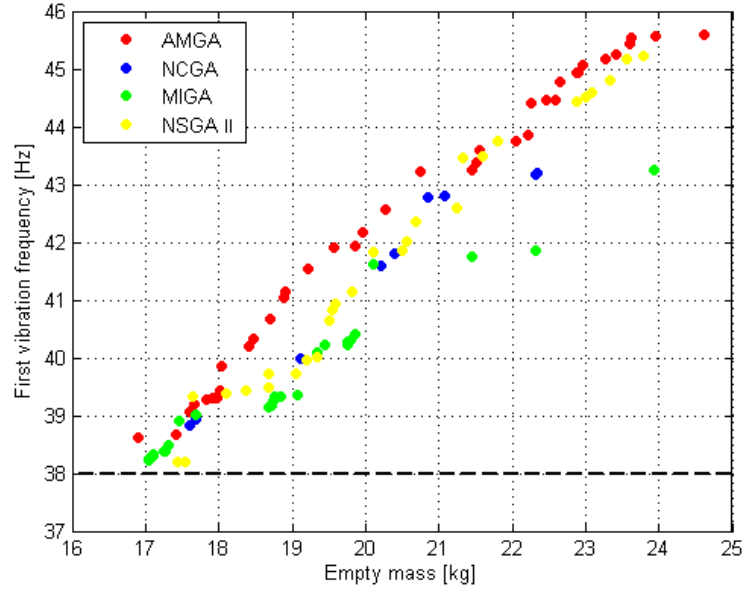
Figure 3.10: Comparison of the Pareto front of different algorithms

Algorithm	Mass $[kg]$	Frequency $[Hz]$
AMGA	16.90	38.6
NCGA	17.60	38.8
MIGA	17.04	38.2
NSGA II	17.44	38.2

Table 3.9: Comparison of the best solutions of different algorithms

The fig. 3.10 demonstrates the *AMGA* and *NSGA II* permit to obtain a clearer Pareto front with respect to the other ones. However, the best solution is obtained for *AMGA* according to tab. 3.9. In accordance with another thesis work that bases on structural optimization using the genetic algorithms present in *Isight* [14], *AMGA* appears as the most suitable algorithm for such an application. The efficiency of this algorithm is also verified by the optimization processes regarding the other configurations. At this point, the solution proposed by *AMGA* can be analysed in details. As it can be observed in fig. 3.11, the optimization process begins with exploration of the design space and then concentrates more on the feasible solutions in a manner to gradually form the Pareto front.
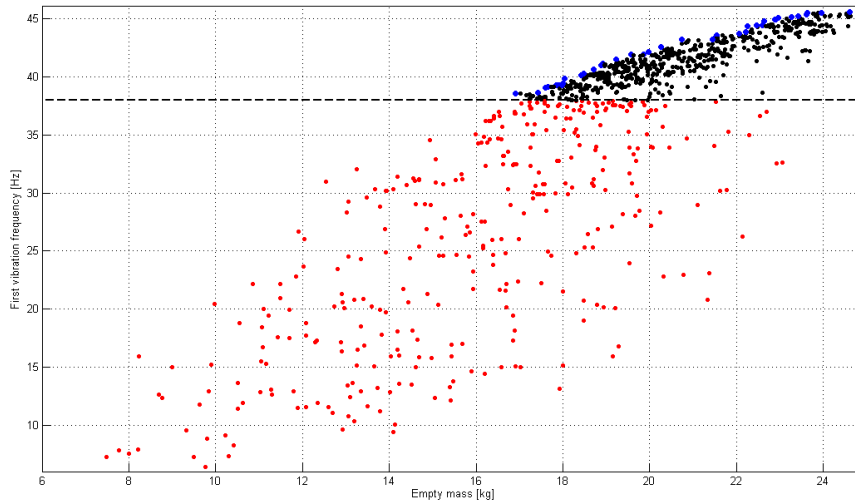
Figure 3.11: Optimization of the metallic sandwich model

The best solution proposed by the optimizer has the following properties:

Design variable evaluation

Honeycomb density[1]	31.98	kg/m^3	Honeycomb thickness	37.98	mm
Honeycomb density[2]	93.97	kg/m^3	"C" Flange thickness	1.18	mm
Honeycomb density[3]	39.39	kg/m^3	"C" Web thickness	1.46	mm
Honeycomb density[4]	52.81	kg/m^3	Lower skin thickness	4.83	mm
Honeycomb density[5]	31.98	kg/m^3	Upper skin thickness	1.6	mm
Honeycomb density[6]	45.90	kg/m^3			

Table 3.10: Best solution proposed for metallic sandwich model
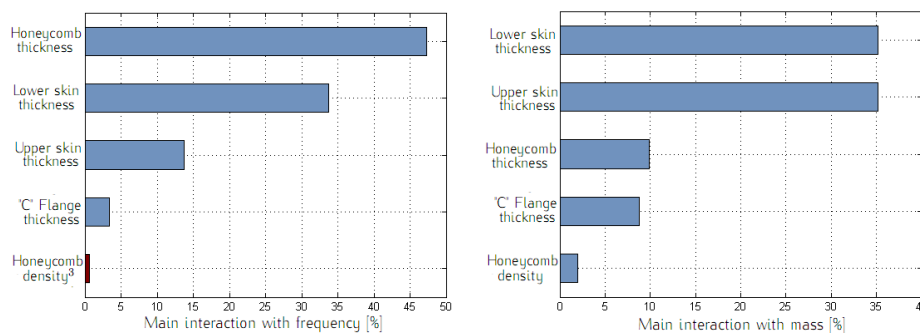
Figure 3.12: Interactions between variables and objectives

As a last result, the design variables that have major impact on each objective are presented. The fig. 3.12 shows that the honeycomb thickness has an important effect on the frequency and the optimizer tends to increase it until its upper limit.

A honeycomb core that has a very low density introduces an important inertia or stiffness to the system. Consequently, it is able to raise the frequency significantly. In addition to this, the lower facing skin also has an important contribution to the frequency because as it is more distant from the centre of gravity of the system, its effects are more significant due to the presence of the transport moment. The interaction graph for the mass also gives results that are coherent to the predicted ones. By considering its density and area, the facing skins have the major effect on the total plate mass.

Finally, the graph present in fig. 3.13 is plotted to demonstrate how the local modifications of the honeycomb density influence the global frequency. It appears that different material distributions within the plate can only create slight differences concerning the global frequency. Thus, it can be deduced once again that the mass of the honeycomb is not as effective as its thickness with regards to increasing the first bending frequency. However, if the division criterion is taken into account, modifications around the central zone have major effects with respect to the ones near to the plate ends. Indeed, this statement is also confirmed during the optimization process related to the following configuration where local changes are introduced in order to obtain the desired modal behaviour.
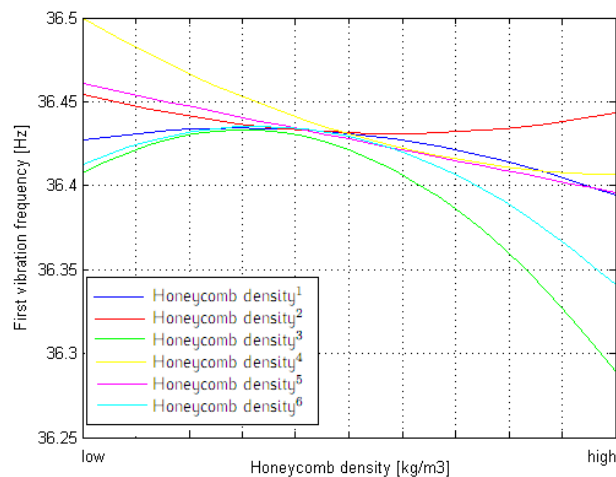
Figure 3.13: Interaction between honeycomb density and frequency

The most important result that is obtained after all these optimization steps is that the mass values of the feasible solutions are much higher than the target mass defined in 2.1.2. As a result of this, this configuration with a metallic sandwich structure is discarded without performing further static analysis and a new optimization process is initiated by considering another configuration.

3.2   Configuration 2: Composite sandwich model

The results obtained for the metallic sandwich model showed that the considered design variables are not able to change the modal behaviour of the plate in a drastic manner. The idea of using a sandwich structure is kept whereas the material choice is changed by switching from metal to composite. The main reason of taking such a decision relies on the fact that composite materials permit to obtain "tailored" material behaviour by combining different factors. These factors principally depend on the material properties such as lamina or ply type, thickness and orientation angle. Consequently, the use of composite materials enables the user to have more design variables to vary so more design flexibility.

3.2.1   Finite element model

The main structure of the *FEM* of the composite sandwich model has the same formulation as the previous case. The difference is that the metallic honeycomb is replaced by a core block made of nomex and the metallic facing skins by composite laminates. Actually, the use of *PCOMP* property is still valid for this model but the number of layers is going to be much higher respect to the previous one.
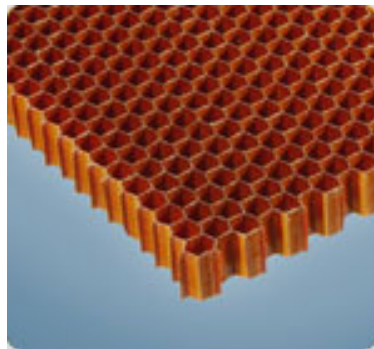
(a) Nomex honeycomb   (b) Aluminium honeycomb

Figure 3.14: Metallic and non metallic core materials

Nomex Grade I Class II Type I Hexagonal Cell

E_{xx}	$[MPa]$	≈ 0	G_{xz}	$[MPa]$	53.78
E_{yy}	$[MPa]$	≈ 0	G_{yz}	$[MPa]$	32.41
v_{xy}		≈ 0	ρ	$[kg/m^3]$	64
G_{xy}	$[MPa]$	≈ 0	Cell size	$[mm]$	4.8

Table 3.11: Mechanical properties of the non metallic honeycomb material

Honeycomb thickness [mm]				
3.18	6.35	12.7	19.05	38.10
4.0	9.53	15.0	25.4	50.8
4.78	10.0	15.88	31.75	

Table 3.12: Preferred thickness values for non metallic honeycomb core

The use of composite skins offers to the user two different options regarding the choice of lamina reinforcement type: unidirectional and fabric. A unidirectional lamina possesses continuous fibres that are aligned along a unique direction. Such a lamina type is typically used to sustain loads that are parallel to its fibre grain direction. However, it is too weak against transverse loads since the entire load should be carried by the matrix. Whereas a fabric or woven lamina contains continuous fibres oriented on at least two axes. In this specific case, the fibres run along two main directions i.e. 0° and 90°. This fact removes the evident difference regarding the resistance along longitudinal and transverse directions as in a unidirectional lamina. A compromise between the two can be found by setting the ratio of the fibre quantity along the given directions. The values that are used during the modelling phase are listed in tab. 3.13 and tab. 3.14.

Vicotex 6376 Fabric

E_{xx}	$[MPa]$	62350	X_t	$[MPa]$	472
E_{yy}	$[MPa]$	59150	X_c	$[MPa]$	502
G_{xy}	$[MPa]$	4140	Y_t	$[MPa]$	499
ρ	$[kg/m^3]$	1530	Y_c	$[MPa]$	440
ν_{xy}		0.04	S_{12}	$[MPa]$	100
t_{FEM}	$[mm]$	0.310			

Table 3.13: Mechanical properties of a fabric ply [4]

Vicotex 6376 Unidirectional

E_{xx}	$[MPa]$	132000	X_t	$[MPa]$	1635
E_{yy}	$[MPa]$	8350	X_c	$[MPa]$	997
G_{xy}	$[MPa]$	4100	Y_t	$[MPa]$	39
ρ	$[kg/m^3]$	1550	Y_c	$[MPa]$	145
ν_{xy}		0.31	S_{12}	$[MPa]$	81
t_{FEM}	$[mm]$	0.135			

Table 3.14: Mechanical properties of a unidirectional ply [4]

Note that the reported values are valid for H.T.W. (hot and wet) conditions and the ultimate strength values are inserted in the *FEM* by using a division factor that is equal to 1.15.

The remaining details of the model are similar to the previous case except one aspect. The decision of switching to a composite structure influences the material choice related to the "C" reinforcement elements. These elements that are made of steel should be converted to composite in order to avoid a possible thermal incompatibility during the polymerization phase. This requirement creates also an inconvenience concerning the modelling. Until this point, the reinforcements are modelled by beam elements which necessitate an isotropic material input. Instead, in order to be able to simulate the effect created by the superposition of different plies, a *PCOMP* card with an orthotropic material input should be used. In order to resolve this discrepancy, the mechanical properties of an equivalent laminate are calculated through the implementation of the analytical relations. The idea is to depart from the properties of a single lamina then integrate the effects of the additional layers and at the end to obtain the properties of the entire laminate. In other words, an equivalent section is created by passing from ply(local) to laminate(global) level. All the steps in order to achieve such an objective are explained in details in app. A.1.

3.2.2   Optimization model

The final version of the optimization model regarding the composite sandwich model is obtained by following a gradual sequence. Considering the results of the each intermediate step allowed to justify the decisions taken in order to perfection the model.

In chap. 3.2.1, the problem regarding the modelling of the reinforcement elements is highlighted. At this point, in order to simplify the initial steps, the "C" reinforcement part is not included in the *FEM* so that the effect of using a composite structure as core and skin material can be more clearly observed.

Selection of the lamina type

First of all, the duality due to the composite material selection is considered. As previously mentioned, there exist 2 main material choices for the facing skins: fabric and unidirectional. These two materials can also be used together in the case of a hybrid composite structure but in this thesis, such a hybrid model is not taken into consideration. Moreover, a unique lamina type is selected after comparing these two possibilities. In order to do this, a simple optimization model is constructed as illustrated in fig. 3.15.
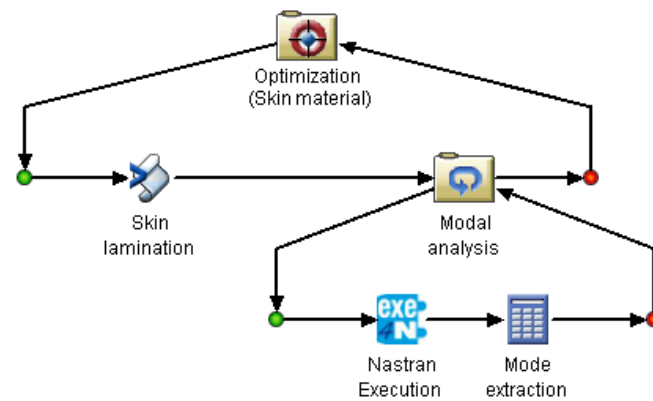
Figure 3.15: Optimization *Work flow* scheme for the skin material

At this level, only dynamic analysis is performed in order to verify the capabilities of the composite materials. In other words, a general sensitivity analysis is made in order to have a rough idea about how mass–frequency relationship is affected from the new material choice. While constructing this basic model, a fundamental block that is going to be developed and used in the final model is created: *Skin lamination*. By the use of a *Script* component, this block principally calculates the *PCOMP* properties such as material type, thickness and orientation angle of a laminate. The programming language is chosen as dynamic java and a special code routine that enables to construct a symmetric laminate is written. So the design variables would be limited for a unique skin, then the other one is obtained in a manner to ensure the global symmetry.

In order to proceed with the analysis, there exists an important question to be answered about the total ply number. This is a significant variable that should be determined because consequently, that much command line should be written

while defining the *PCOMP* property. Even though it is not the most efficient manner, a temporary method is implemented in order to estimate the necessary ply number that permits to reach $38Hz$. Each skin is supposed to have 6 layers and a new design variable that defines the number of ply per layer is created. Actually this variable can vary between 1 and n and it assigns to each layer different number of plies under the *Skin lamination* component. In other words, it is an alternative way of defining a composite structure having in total 6n layers but its corresponding *PCOMP* card is defined by only 6 command lines instead of 6n. This approach is not neither realistic nor efficient for an optimization process because it keeps the same orientation angle for each block of n plies. However, in order to obtain a first estimation, it is a quite practical and fast method.

Once the significant aspects of the optimization model are described, the optimization problem can be defined as follows:

- **Case 1: Unidirectional ply**

  Objectives: Minimize M_e
                         Maximize f_l^1

  Constraints: $f_{1_{loaded}} > 38Hz$

  Design variables: Ply angles   [0 45 -45 90]
                         Ply number per layer [1 2 3 4 5 6]

- **Case 2: Fabric ply**

  Objectives: M_e
                         Maximize f_l^1

  Constraints: $f_{1_{loaded}} > 38Hz$

  Design variables: Ply angles   [0 45]
                         Ply number per layer [1 2 3]

This optimization run aims to compare the 2 types of lamina. As previously mentioned, any composite structure has 3 main parameters to be determined: thickness, material and orientation angle. In fact, the 2 design variables serve to define the orientation angle and the thickness whereas for each case the material type is considered constant. Note that the unidirectional plies can be positioned along the 4 principal angles whereas the fabric plies can only be placed at 0° and 45° because of its nature 0° is equivalent to 90° and 45° to −45°. Furthermore, the variable that determines the ply number per layer is chosen in order to be able to span the interested mass zone. As the thickness of a fabric ply is approximately double of a unidirectional one, the ply numbers are set by considering this ratio so that the mass intervals overlap. Note that the honeycomb thickness is kept constant in order to be able to observe the effects of the material choice only.
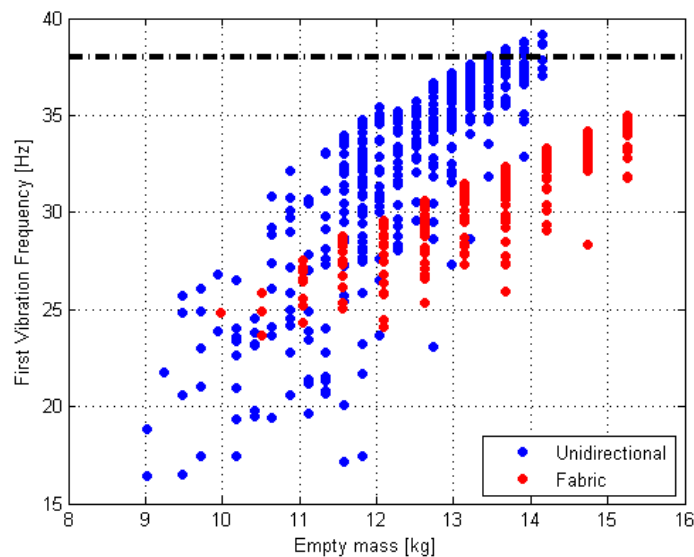
Figure 3.16: Comparison between the unidirectional and fabric ply types

While comparing these ply types, same optimization algorithm (*AMGA*) with same parameters are used. As fig. 3.16 shows unidirectional material is more convenient than the fabric because for the same mass value, higher frequency values can be reached by the use of unidirectional material. Moreover, the slope that indicates the trend line of the points is higher for the unidirectional material with respect to the fabric. This is equivalent to mention that unidirectional plies are more efficient to rise the frequency for a same amount of mass increase. After this justification, the ply type is not going to be considered any more as a variable and the unique ply type that is going to be used during the rest of the optimization

process is going to be unidirectional.

Even though the introduction of the "C" reinforcement elements would help to increase the stiffness as well as the natural frequency of the plate, the previously obtained results demonstrate that the lower frequency bound constraint is satisfied with corresponding mass values higher than the expected. The tendency in the optimization process of the metallic sandwich has been to increase the honeycomb thickness until its maximum value. At this point, in order to have a prediction about the future of the model, the maximum limit listed in tab. 3.12 is considered and the correlation between honeycomb thickness and frequency is once again verified. The fig. 3.17 shows that an increase of the honeycomb thickness introduces a vertical shift of the point cloud so it allows to reach higher frequency values for the same masses.
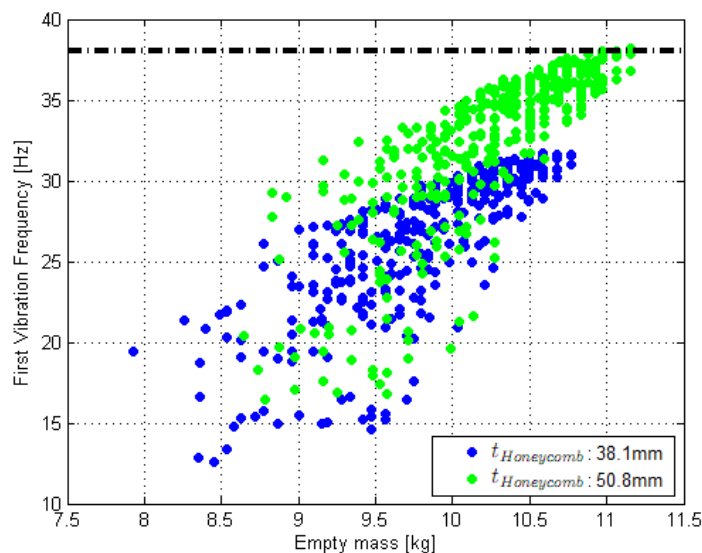
Figure 3.17: Comparison between the unidirectional and fabric ply types

Selection of the local reinforcement type

The results regarding the optimization process of the metallic sandwich model showed that better solutions can be obtained by changing the material density distribution along the plate. This idea is also implemented in the composite sandwich model but with a different logic. Instead of changing the honeycomb density of different zones, local reinforcement areas are created. In other words, the skin thickness is not any more kept constant but predefined zones are reinforced

by the insertion of additional plies. Considering the nature of the plate, 2 main areas are determined: the first one contains the zones near the extremities of the plate whereas the second one is concentrated on the central part (fig. 3.18).
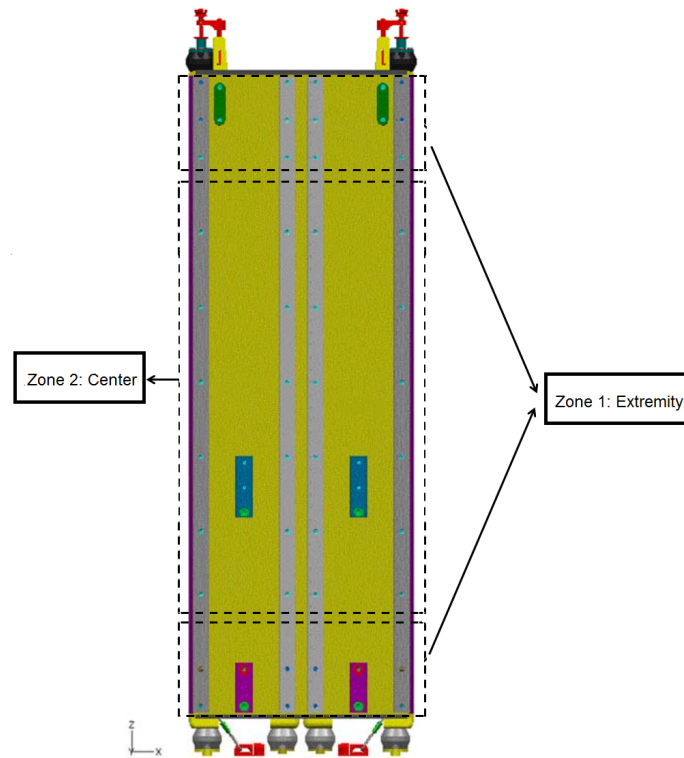
Figure 3.18: Local reinforcement zones

In order to reinforce a desired zone, it is enough to place additional skin pieces with the corresponding dimensions. Then they are going to be compacted with the rest of the structure during the polymerization process. However, there exists a significant point about the SAR Plate: the external skin surfaces should be flat due to the attachment lines with the tracks. This constraint can be respected by following a typical manufacturing process regarding the milling of the honeycomb. In order words, the thickness of the honeycomb corresponding to the local reinforcement zones should be reduced by considering the desired number of reinforcement lamina. During this milling process, sudden thickness changes are not preferred so the reduction operation should be gradual. To illustrate, this reduction rate can be approximately accepted as $0.25 inch/lamina$. The fig. 3.19 shows a possible reinforcement example regarding the central part and the extremities respectively.

(a) Center   (b) Extremity
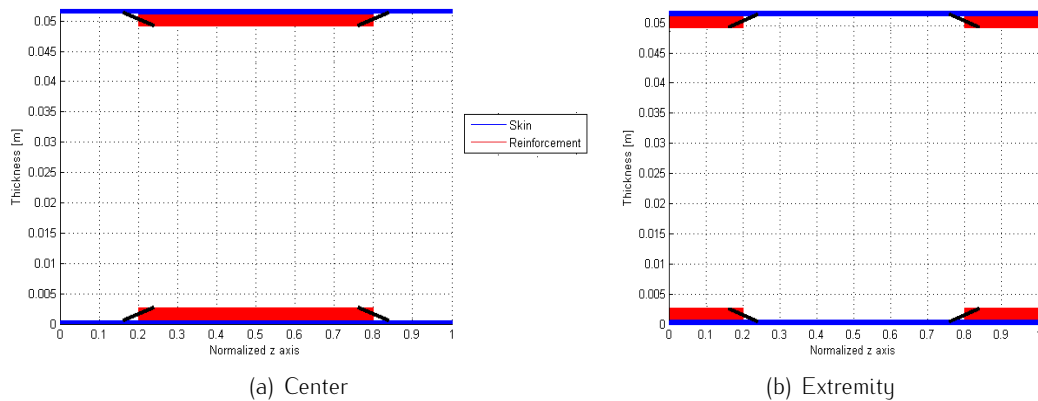
Figure 3.19: Plate cross section with a local reinforcement at 20% ($t_{Honeycomb}$): $50.8mm$

The next step would be to construct another simple optimization loop (fig. 3.20) with the scope of deciding which zone is more convenient to be reinforced. As shown in fig. 3.19, the limits of the extremity zones are temporarily fixed to 20% of the total plate height. In order to speed–up the simulations, a comparison between the loading configurations is done and the configuration which gives the lowest frequency value is determined. Consequently, only the worst case (*bottle*) is considered during the simulations and in this way an important amount of time is saved.

- **Case 3: Reinforcement type**

Objectives:	Minimize M_e
	Maximize f_l^1
Constraints:	$f1_{loaded} > 38Hz$

Design variables:	Ply angles (skin layers)	[0 45 –45 90]
	Ply number per layer (skin layers)	[1 2 3 4 5]
	Ply angles (reinforcement layers)	[0 45 –45 90]
	Ply number per layer (reinforcement layers)	[1 2 3 4 5]
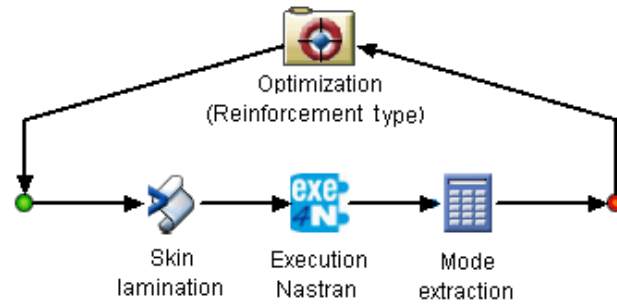
Figure 3.20: Optimization *Work flow* scheme for the reinforcement type

The *Optimization* block decides the ply number used for the base skin and the amount of the additional reinforcement layers to be inserted. The same simulation loop is run for 2 different *.bdf* inputs that enable to obtain different local rein-forcement types. The mass-frequency relation is plotted for each of the 2 cases and the curves related to the non dominated design points are compared in order to decide the most efficient local reinforcement type.
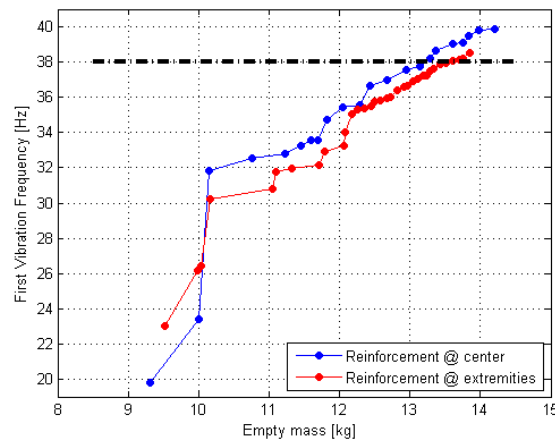
Figure 3.21: Comparison between different types of reinforcement

The fig. 3.21 shows that the local reinforcement concentrated on the central part permits to reach higher frequency levels for the same mass value. As the main scope is to suppress the bending out of plane, adding material or inertia to the central part of the plate helps to diminish the maximum displacement out of plane. However, before deciding the final local reinforcement type, a further analysis is done by also considering the limits of the zones along the vertical direction. Different *.bdf* files are prepared in order to represent different reinforcement levels for both reinforcement types. Furthermore, the base values for the design variables

are taken from the previous optimization process. The comparison is done after automating the system by the use of a *Task* activity as illustrated in fig. 3.22.
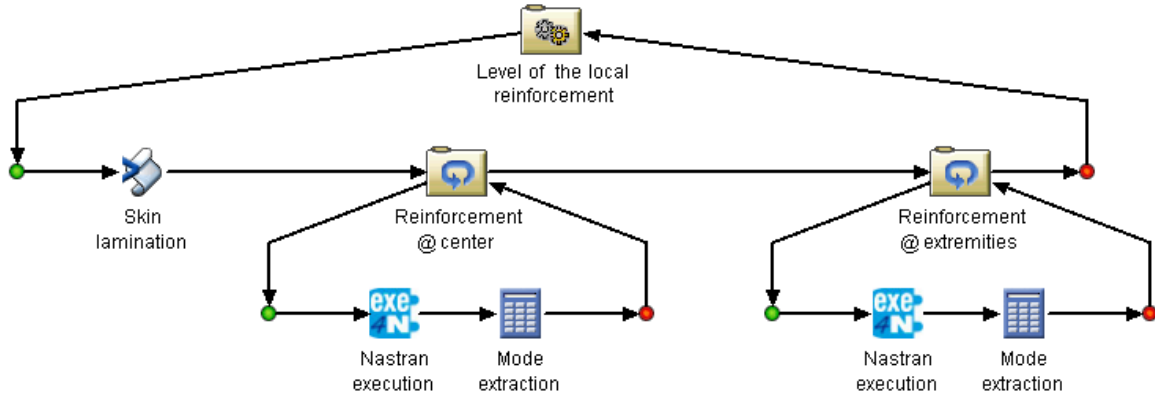
Figure 3.22: *Sim-flow* for comparing different levels of reinforcement

The inserted loops serve to create each subcase that represents different levels of reinforcement in terms of total plate height percentage. As illustrated in fig. 3.23, the correlation between the reinforcement level and the frequency does not give a precise indication about which reinforcement type is more convenient. However, when the mass–frequency relationship is plotted, the efficiency of the local reinforcement concentrated on the central part is confirmed.
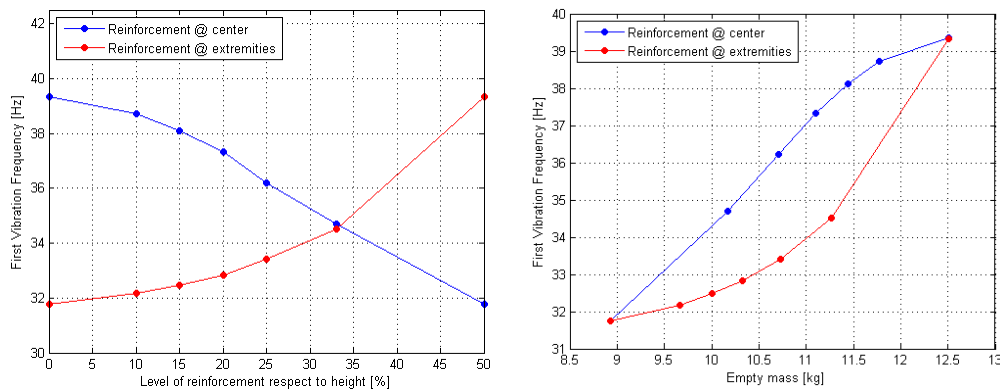
Figure 3.23: Effect of different reinforcement types on the frequency

Main model

After these two intermediate steps, the main optimization model regarding the composite sandwich can be constructed. Based on the results obtained at each step, some design variables such as the local reinforcement and ply material

types are converted to constant inputs. Reducing the number of design variables is equivalent to squeeze the design space boundaries so at the mean while to decrease the total iteration number and the entire simulation time.

Before presenting the formulation of the optimization problem, it would be useful to clarify a few concepts about lamination. As previously mentioned, the total ply number necessary to satisfy the frequency lower bound constraint is estimated by using a practical method that enables to assign numerous plies to each layer. However, this method should be developed and modified in a manner that each *PCOMP* command line is associated to a single ply. By considering the obtained results and the interested mass zone, the maximum ply number is fixed to 20 for each facing skin. Moreover, it is highlighted that the honeycomb reduction operation tends to avoid sharp corners so it follows a slope of $0.25 inch/lamina$ which gives an indication about the maximum allowable reinforcement ply number. This gradual profile reduction is not modelled in the *FEM* and the transitions between the adjacent zones follow a profile of a step function. Consequently, this transition length should be as restrained as possible in order to reduce the error committed due to the modelling. However, this fact contradicts the tendency to insert additional reinforcement layers. As a result of this, a compromise between the two approaches is found by setting a maximum transition length. In this way, the optimizer would indirectly determine the reinforcement ply number once it decides the reduction rate. This parameter is defined between 0 and 1. In other words, if the reduction rate is 1 then the whole transition length is employed in order to insert the maximum allowable reinforcement ply number. On the contrary, if this value is set to 0, then no reinforcement plies are inserted so the skin and the honeycomb thicknesses remain uniform. This mechanism would provide to the optimizer the freedom of deciding whether to utilize additional reinforcement layers or not. In the case of using extra lamina, it would also have the possibility to decide its quantity.

In chap. 3.2.2, the type of the local reinforcement is selected so in the definitive model, only the central part is reinforced. However, there is not a criterion to set the levels of the reinforcement zones in percentage of the total height. As a result of this, it would remain as a design variable for the optimization problem. In order to implement this idea, several *.bdf* files that possess different reinforcement levels are prepared and the design variable is defined as a string. Furthermore, the allowable values of this variable consist of the path list of the relevant *.bdf* files.

The main optimization problem is implemented as follows:
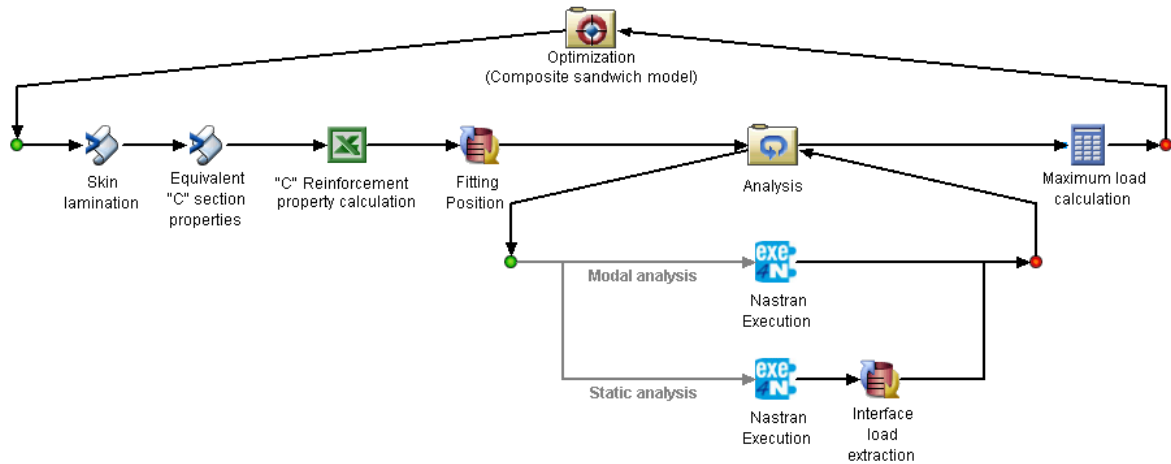
Figure 3.24: Optimization *Sim-flow* scheme for the composite sandwich model

The first block of the *Sim-flow* serves to create the arrays that contain the *PCOMP* properties of the laminates corresponding to the central part and the extremities by respecting the specified lamination instructions. However, there exists an in–consistency concerning the input–output relationship between the blocks. The *Exe4Nastran* component bases on the given template file so for this block, the dimension of the *PCOMP* properties should be kept constant. However, as the number of plies regarding both the skin and the reinforcement part are not known a priori, the dimension of that array changes at each iteration. This inconvenience is solved by creating a template file where the *PCOMP* related to the skin and local reinforcement area have the maximum allowable ply entries. In the case that the optimizer decides to insert less plies; material, thickness and the orientation angle arrays are gradually filled up to the given ply number and then a dummy thickness value that is approximately 0 is assigned to the remaining plies. In this way, such a lamina block does not contribute to the overall response as if its existence was ignored.

Even though the modelling of the "C" reinforcement elements was neglected during the previous simulations, they are inserted to the final model through the use of beam elements. The material properties of the laminate are calculated by the second block where the formulas regarding the classical lamination theory are implemented. Instead the geometrical properties are obtained through the *Excel* application. Note that the section in form of "C" should have a uniform thickness

that is equal to the global thickness of the laminate. This value which is equivalent to the total ply number of the "C" reinforcement elements is considered as one of the design variables of the problem. Similar to the skins and local reinforcement laminates, the "C" section is composed of a symmetric composite and as a result of this, the design variables are only related to the half of the laminate.
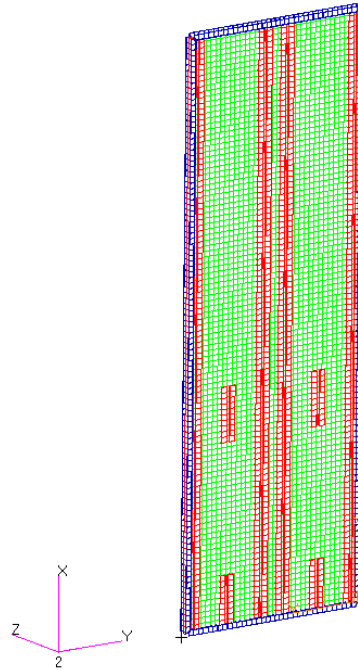
Figure 3.25: Definition of the local coordinate system for composite material

Another new component is the *Fitting position* block that introduces a slight modi-fication regarding the attachment points in order to obtain a more accurate model. Note that to create a *PCOMP* property, a local coordinate system should be properly defined. The x axis indicates the longitudinal direction. In the mean-while, it is the reference axis for defining an orientation angle different than 0°. Consequently, the y axis stands for the transverse direction and the z axis for the lamination direction. In this specific example, as fig. 3.25 shows, the orientation of the local z axis is selected parallel to the global y axis. This fact ensures that the distance between the point loads and the external surface of the plate always remains constant and independent of the plate thickness. However, it influences the relative position of the fittings respect to the modelling plane. As the tab. 3.12 indicates, a non metallic honeycomb might have higher thickness values with respect to a metallic core. Consequently, for higher honeycomb thicknesses, the position of the attachment point on the fittings should be translated more towards

the rear side. This translation operation can be done by changing the y coordinate of the constrained nodes.

Actually, this translation operation does not significantly change the natural frequencies of the global modes but has static effects in terms of constraint forces. This difference might be pejorative in the case of a load along x direction because it would increase the moment arm between the constraints and the point of application of the loads. In order to compensate this difference, a data exchanger component is used for changing the *GRID* line of the relevant nodes once the total plate thickness is calculated under the *Skin lamination* block.

Lastly, in order to complete the main model, the block for the static analysis is inserted. As in the case of the frequency, a unique loading configuration and load condition are chosen in order to proceed with the simulations. The selection bases on the worst load combinations: loading configuration $middle$ combined with a load of $20g$ along –x direction. In this way, instead of performing 24 static analysis subcases, a single one is performed. This is a strategically important move because with the introduction of the composite materials, the number of the design variables significantly increased with respect to the metallic sandwich case. Consequently, a higher quantity of iteration would be required in order to be able to span the whole design space. The saved time for a single run can be employed to increase the total iteration number.

After all these explanations, the final formulation of the optimization problem regarding the composite sandwich model can be set:

- **Case 4: Optimization of the composite sandwich model**

    <u>Objectives:</u>   Minimize M_e
    Maximize f_l^1

    <u>Constraints:</u> $f_{1_{loaded}} > 38Hz$
    $R_{x_{down}} < 20000N$ $R_{x_{up}} < 5000N$
    $R_{y_{down}} < 20000N$ $R_{y_{up}} < 10000N$
    $R_{z_{down}} < 15000N$
    $MS_{Honeycomb} > 0$
    $FI < 1$

Design variables:	Honeycomb thickness	tab. 3.12
	Ply angles (skin layers)	[0 45 –45 90]
	Ply number (skin layers)	[1:1:20]
	Ply angles (reinforcement layers)	[0 45 –45 90]
	Ply number ("C" reinforcement layers)	[2:2:14]
	Ply angles ("C" reinforcement layers)	[0 45 –45 90]
	Reduction rate	[0 0.25 0.5 0.75 1]
	Flange width	8-16 mm
	Limit of local reinforcement	[10% 33%]

Note that during the formulation of the optimization problem, in addition to the frequency and the interface load limit constraints, other new criteria are added in order to obtain a more complete static analysis. First of all, the maximum transverse shear load on the honeycomb is extracted and the shear stress is calculated by taking into account the thickness of the core block. This latter value is compared with the shear allowable of the nomex material and the safety margin is obtained. In addition to the honeycomb, the failure indexes of the *PCOMP* elements are controlled to ensure to avoid a catastrophic ply failure. Different failure theories exist for the composite materials and they are presented in app. B with details. As the flow chart in fig. B.2 indicates, the most accurate failure criteria for the analysis of unidirectional plies are the *Hashin* and *Maximum stress criteria*. The *Hashin* theory is not among the approaches used by *Nastran* to calculate the failure index and so the *Maximum stress criteria* is adopted during the static analysis. This failure theory assumes the uncoupling between the fibre and matrix failures.

3.2.3   Results

Once the preparation of the main model is terminated, the simulations are run in order to optimize the current model. Based on the results that are obtained for the metallic sandwich, the *NCGA* is not considered among the used optimization algorithms. One of the main differences between these two cases is that the composite sandwich model has much more design variables respect to the metallic one. This fact requires to increment the total iteration number in order to obtain a well defined Pareto front. To illustrate, the total iteration number for the previous configuration was around 1000 and for the new one this number goes upto 1500. This number is not known a priori but it depends on the total available time to

be dedicated to the simulations. As the number of subcases are decreased with respect to the previous case, this time is spent to do more iterations. Moreover, the population size is incremented in order to be able to span all the design space. The Pareto fronts obtained for this configuration is illustrated in fig. 3.26.
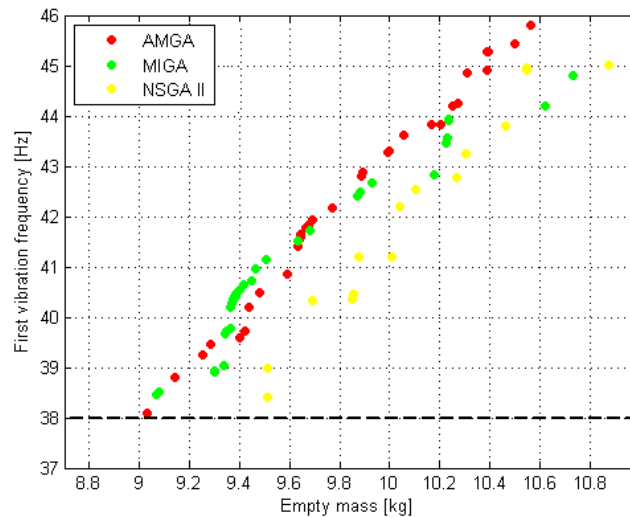
Figure 3.26: Comparison of the Pareto front of different algorithms

Algorithm	Mass $[kg]$	Frequency $[Hz]$
AMGA	9.03	38.1
MIGA	9.06	38.4
NSGA II	9.50	38.4

Table 3.15: Comparison of the best solutions of different algorithms

The results presented in fig. 3.26 and tab. 3.15 confirm that the algorithm which led to the best solution is once again *AMGA*. Moreover, the profile of the Pareto front for this algorithm is much more regular with respect to the other ones. As a result of this, *AMGA* would be the unique algorithm that will be employed during the optimization processes regarding the next configurations. When the progress of the optimization process is examined, a long design space exploration can be noted. However, as fig. 3.27 demonstrates the Pareto front is gradually obtained once the new solutions dominate the previous ones. The values that correspond to the best solution that is proposed by *AMGA* is listed in tab. 3.16.
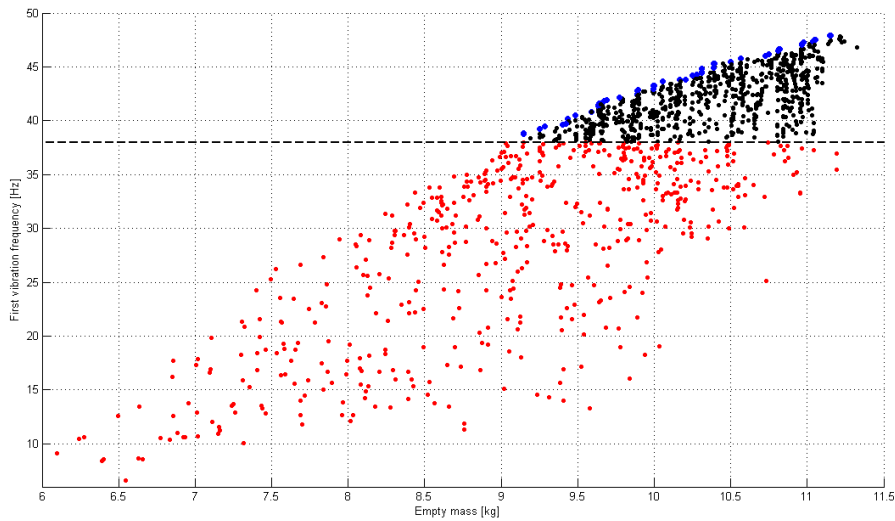
Figure 3.27: Optimization of the composite sandwich model

Design variable evaluation

Honeycomb thickness	50.66 mm
Ply angles (skin layers)	[0 0 -45 0 0 0 0 0 45 0]
Ply number (skin layers)	10
Ply angles (reinforcement layers)	[0 0 45 0]
Ply number ("C" reinforcement layers)	4
Ply angles ("C" reinforcement layers)	[0 0]
Reduction rate	0.25
Flange width	11.38 mm
Limit of local reinforcement	33%

Table 3.16: Best solution proposed for composite sandwich model

Even though it is not recommended due to risks of delamination, the optimizer tends to increment the number of consecutive plies that are positioned with an orientation angle equal to 0°. However, this tendency is coherent with the fact that the plate should be reinforced longitudinally in order to suppress the global mode corresponding to a bending out of plane. Similar to the previous case, the thickness of the honeycomb core reaches its maximum value in order to be able to increase the frequency with a minimum weight contribution. Furthermore the reduction rate is fixed to a value which is different from 0. This shows that the idea of introducing of local reinforcements has a positive impact on the objective functions. Finally, a comment on the limits of the local reinforcements can be made and it is possible to say that also the optimizer decided to divide the plate by using the same proportions selected for the "box" concept.
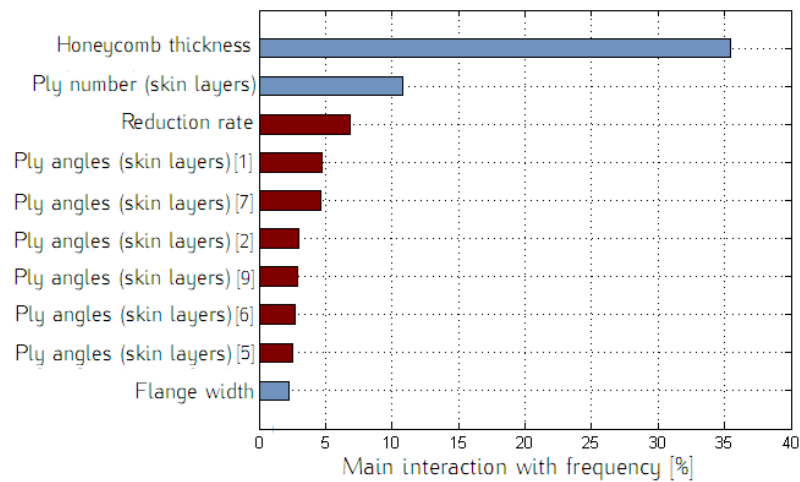
Figure 3.28: Interactions between variables and objectives

As a last step, a classification regarding the effects of the design variables on the objectives can be made. This relationship that is determined by a regression analysis of the data sets can be obtained by using *Design of experiment* process block. As fig. 3.28 indicates, the major contribution to the frequency objective comes from the honeycomb thickness. The ply numbers of the skin and the lo-cal reinforcements also have significant effects. The next set of factors which is constituted of the ply angles related to the facing skins influences the frequency between 2 and 4 %. However, the physical meaning of the correlation between various orientation angles and the frequency can not be so intuitively interpreted.

The final conclusions about this configuration concerns the feasible solution that is found by *AMGA* and that has the minimum mass value. This obtained value is slightly inferior compared to the mass target that is fixed in 2.1.2. This means that with this configuration and the listed design variables, the SAR Plate can be redesigned in a manner that the shock absorbers can be removed. As the operational frequency band does not correspond to one of the forcing frequency, the use of the shock absorbers that mainly works as a frequency filter is not necessary. Note that in order to reduce the total simulation time, the worst load cases are selected and the remaining ones are not taken into consideration. In order to be able to validate this new solution, all the remaining subcases should be implemented to ensure that they all satisfy the specified constraints.

3.3   Configuration 3: Reinforced laminate model

The composite sandwich model proposed an alternative solution to the original SAR Plate design by removing the shock absorbers for the same mass value. However, another possible configuration is taken into consideration with the scope of reaching lower mass values. The main idea behind this configuration is to construct a "tailored" structure. The use of a honeycomb core is one of the most widespread solutions used in the aerospace industry in order to gain inertia by introducing lowest weight possible. In the case of the SAR Plate Assembly, the dimensions of the honeycomb core correspond to the total plate area. This means that there might exist zones that are filled with core material even though it is not necessary. So the critical zones can be identified and reinforced in a manner to obtain the desired modal behaviour. In order to achieve this objective, a configuration that has a unique facing skin which is reinforced by the stiffeners on its rear side is going to be regarded.

3.3.1   Finite element model

The first step before constructing the FEM has been to decide where to place the local reinforcement zones and the corresponding stiffeners. As the main objective is to suppress the mode shape regarding the bending out of plane, the natural choice has been to insert stiffeners along the plate height. There also exists an-other aspect to be considered regarding the connections between the tracks and the plate. For the sandwich structure, appropriate inserts through the entire core thickness were used. Until this point, this subject has not been considered because of the fact that by using a honeycomb thickness that is higher than the original SAR Plate, the bearing problems were neglected. However, in this case, this issue becomes critical as the tracks are attached to a unique skin instead of the sum of 2 skins and the core. Consequently, the vertical straps in correspondence to the main tracks are reinforced. In this manner, the resistance of these zones are intentionally increased against the present load introduction to the plate. In addition this, 3 horizontal straps that follow the box boundaries are inserted in order to suppress the torsional mode shape. The complete reinforcement zone is illustrated in fig. 3.29.

After this decision, the reinforced zones are isolated from the rest of the structure and a new *PCOMP* property is assigned to these elements in addition to the basic skin properties. The stiffeners are placed on the reinforcement zones. The
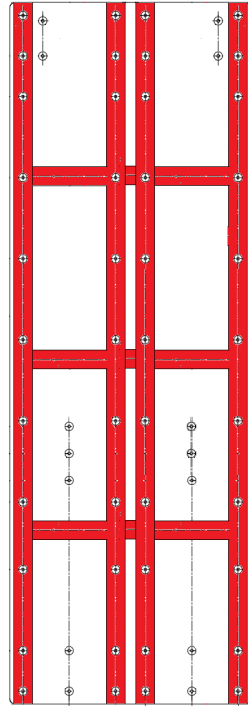
Figure 3.29: Local reinforcement zones

selection regarding the cross section of the stiffeners is based on the ease of construction and the ability to increase the inertia. Under the light of these requirements, the most convenient section has a "C" form. Obviously, the optimizer would tend to maximize the stiffener height in order to increase the inertia and satisfy the frequency constraint. Consequently, the maximum allowable stiffener height is determined in order to make a sensitivity analysis about the design space of the new configuration.

(a) Upper interface   (b) Lower interface
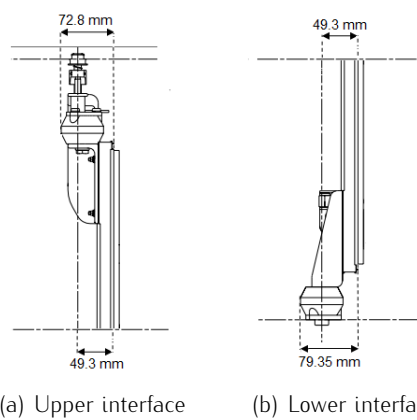
Figure 3.30: Maximum allowable beam height

As fig. 3.30 shows, even though the original SAR Plate Assembly has a honeycomb around $20mm$, the actual space that occupies along y direction is much higher. This increase is due to the fact that it is mandatory to fix the fittings on the rear side of the plate in order to leave space for the shock absorbers. However, as this new design does not include any shock absorbers, this space can be used in the favour of the structure. Including the fact that the skin and reinforcement layers introduce additional thickness, the maximum stiffener height is fixed to $70mm$ in order to be conservative.

The formulation of the fittings is kept equal to the previous cases and the position of the interface attachment points are considered fixed because the fitting is going to be fixed on the rear side of the skin and so the translation would be due to the skin thickness. As this value is negligible with respect to the honeycomb thickness, this translation operation is ignored.

(a) Front view   (b) Rear view
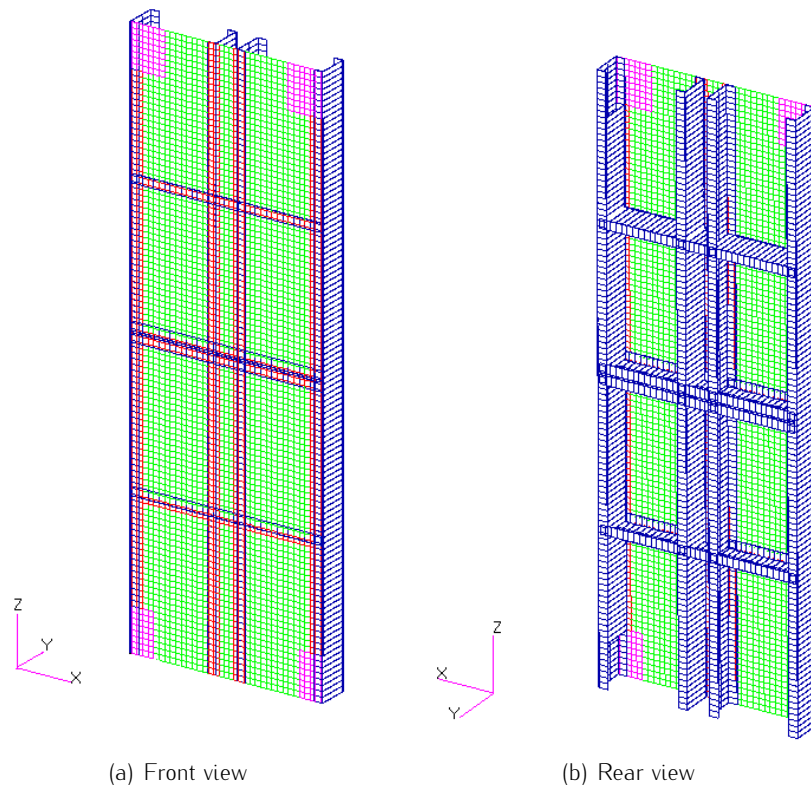
Figure 3.31: *FEM* of the reinforced laminate

Note that the stiffeners are modelled through the use of beam elements with a relevant offset that enables to make the lower flange of the stiffener and the skin

coplanar. Apart from these notions, the details related to the rest of the modelling such as material choice, constraints, fittings and introduction of the masses are the same as the previous configuration. The final *FEM* is shown in fig. 3.31.

3.3.2   Optimization model

As in the metallic and composite sandwich cases, an intermediate optimization model is constructed in order to drive the future steps. This intermediate step aims to identify the tendency of the design variables in order to satisfy the given constraints. The results of such an analysis would give clues that might serve to improve the structural choices.

Apart from the design variables associated to the skin and the reinforcement layers, additional variables such as the height, width and thickness of the stiffeners are introduced. Like in the previous case, in order to have a material compatibility, the stiffeners should be made in composite material. As a result of this, the ply number and the orientation angles of the laminate would be among the design variables of the optimization problem. Furthermore, another unknown concerning the stiffeners was its cross section shape. Among all the cross section shapes, the most appropriate ones for this current case were "C" and "I". Their efficiency depends on the fact that they can further increase the inertia of the plate by positioning flanges that are more distant from the CoG of the entire system. Between these two possibilities the "C" form is more convenient for two main reasons: the first one is the ease of manufacturing. Instead the second one is related to the formulation of the optimization problem. As there already exist the "C" reinforcements that are present around the plate, the same form and dimensions are preserved so that the number of design variables would not increase further.

As this configuration is topologically different with respect to the previous cases, this optimization step can be considered as a survey that would permit to understand the capabilities of the new design. In other words, by fixing the beam height to its maximum allowable limit, the mass-frequency relationship is analysed and the required minimum mass value that satisfies the frequency constraint is found. At this point, as illustrated in fig. 3.32, the optimization model consists of modal analysis only. After these critical decisions, the optimization problem can be formulated as follows:
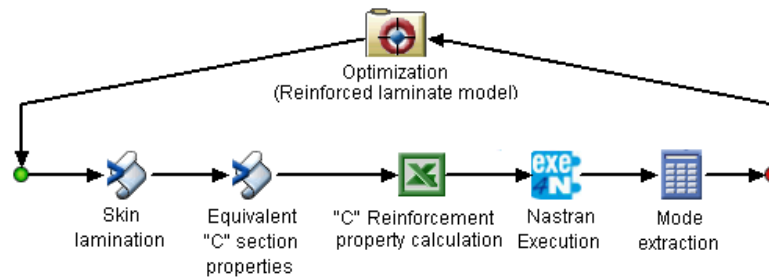
Figure 3.32: Optimization of the reinforced laminate model

- **Optimization of the reinforced composite model**

  Objectives: Minimize M_e
                           Maximize f_l^1

  Constraints: $f_{1_{loaded}} > 38 Hz$

  Design variables: Stiffener flange width   5-70 mm
                           Ply angles (skin layers)   [0 45 -45 90]
                           Ply number (skin layers)   [2:2:20]
                           Ply angles (reinforcement layers)   [0 45 -45 90]
                           Ply number (reinforcement layers)   [2:2:20]
                           Ply angles ("C" stiffener layers)   [0 45 -45 90]
                           Ply number ("C" stiffener layers)   [2:2:10]

Note that unlike in the previous cases, the design variables for defining ply num–bers are defined as even numbers only. The reason for such a convention depends on the need to construct a symmetric laminate. This condition was previously guaranteed by the presence of both an upper and lower skin. Instead this time, there is a unique skin whose variables are defined with respect to the plies that are present above or under the midplane. The properties of the remaining half are determined through a mirror operation executed by the *Skin lamination* com–ponent.

3.3.3   Results

As the optimization model only includes the modal analysis, the duration of a single iteration is significantly reduced. Moreover, based on the quality of results

that are previously obtained, *AMGA* is used as a unique algorithm. For this configuration, the total number of iterations is set to 1500. The distribution of the solutions on the design space is illustrated in fig. 3.33. Note that for this solution, the height of the stiffener web is kept constant and fixed to its maximum allowable value that is $70mm$.
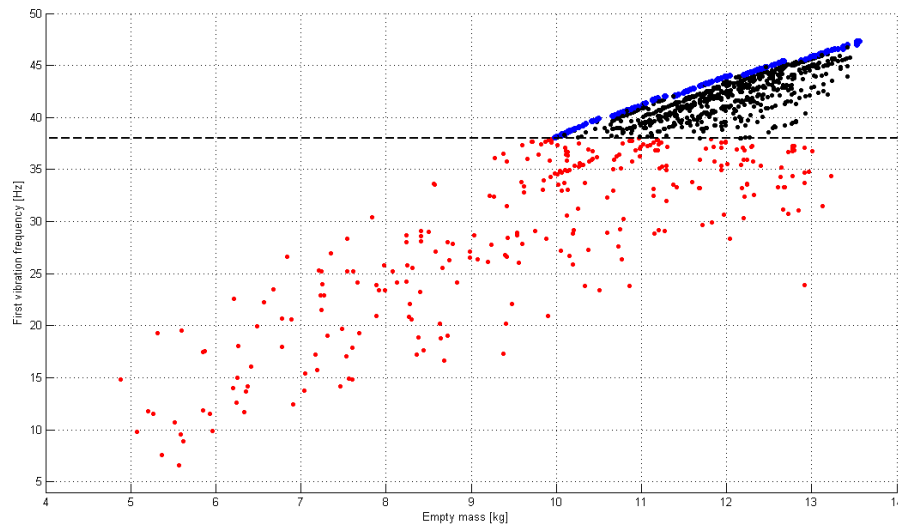
Figure 3.33: Optimization of the reinforced laminate model

Algorithm	Mass $[kg]$	Frequency $[Hz]$
AMGA	9.38	38.1

Design variable evaluation	
Stiffener flange width	60.85 mm
Ply angles (skin layers)	[0 90 –45 –45 45 –45 90 45 –45 –45]
Ply number (skin layers)	20
Ply angles (reinforcement layers)	[–45 45 0]
Ply number (reinforcement layers)	6
Ply angles ("C" reinforcement layers)	[0 0 –45 0 0 0]
Ply number ("C" reinforcement layers)	12

Table 3.17: Best solution proposed for reinforced laminate model

As the fig. 3.33 shows the Pareto front which is constituted of the non dominated solutions and represented in blue has a clear profile. Instead the black points correspond to the solutions that are dominated by the ones that form the Pareto front and lastly the red points correspond to the solutions that violate at least one of the given constraints. Similar to the previous cases, the optimization process

which initiates with a random population firstly explores the design space and then evolves towards better solutions.

The best solution that is found at the end of the optimization process has a mass value that is higher than the one that corresponds to the composite sandwich model. Consequently, the previous option is more adequate for the given objectives. However, as previously mentioned, the main scope of this configuration is to identify the most critical variables that affect the frequency. So the correlation graphics shown in fig. 3.34 give an indication about the next steps to be followed.
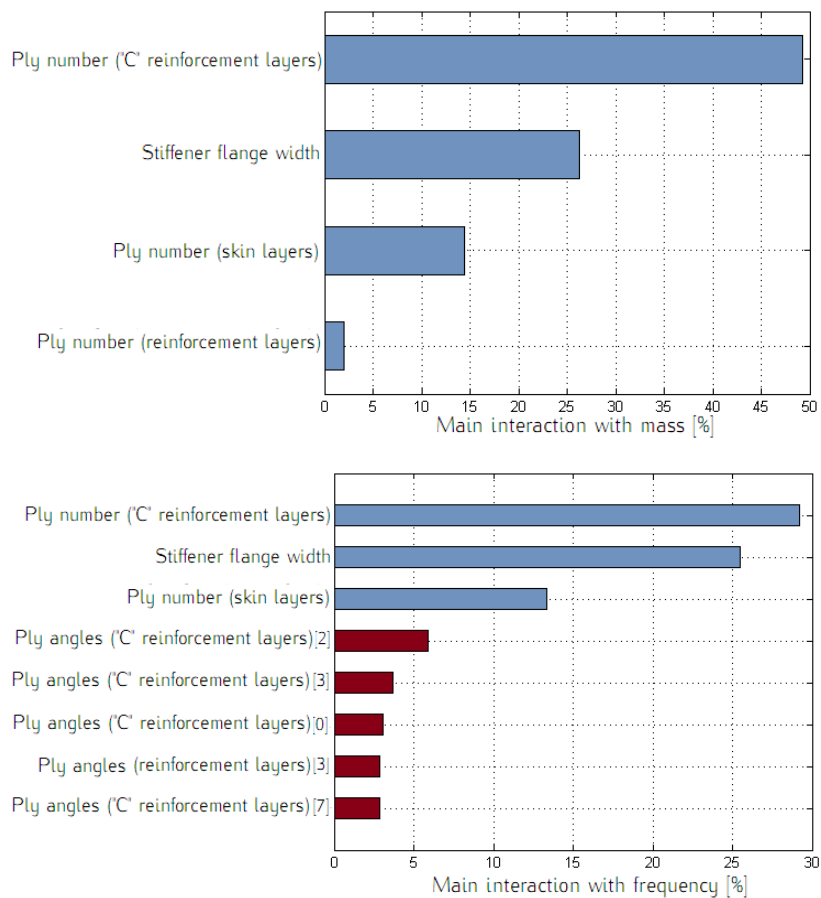
Figure 3.34: Interactions between variables and objectives

The fig. 3.34 highlights the importance of the stiffener flange width because it in–fluences the mass and the frequency in a significant way. Actually, an increasing stiffener flange width helps to reach higher natural frequency values. By consid–ering this fact, the optimizer tends to use higher flange width values in order to satisfy the frequency constraint. This situation can also be verified through the

history graph illustrated in fig. 3.35.
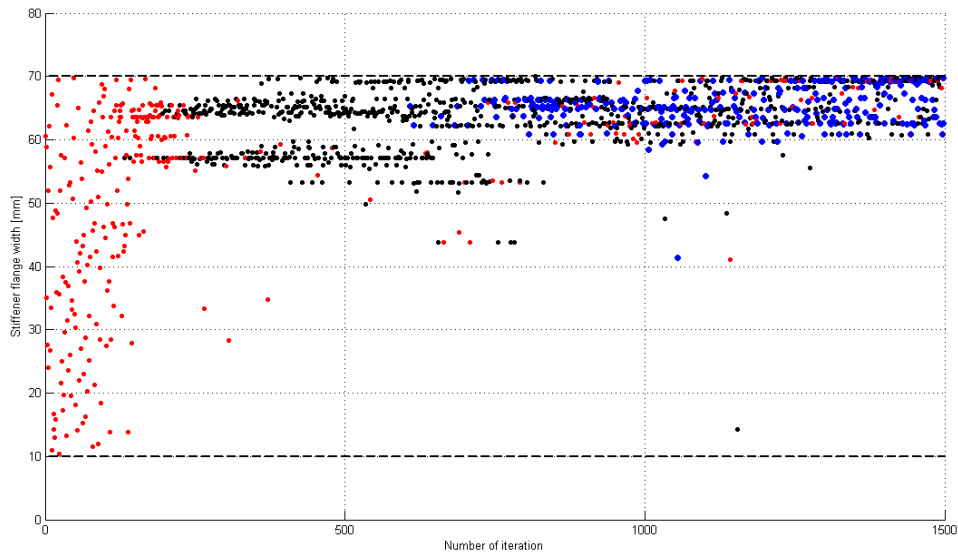
Figure 3.35: Variation of flange width during the process

It appears that the optimizer continuously changes the stiffener flange width value at the exploration phase in order to understand its effect on the objective functions. Then it tries to use values near to its upper bound in order to find feasible solutions. The system needs to increase the flange width in order to gain inertia. As a conclusion, this tendency would be the starting point of the next configuration.

3.4   Configuration 4: Reinforced closed box model

The results obtained for the 3rd configuration gave important indications about the modal behaviour of the plate and they led to further improve the model. Under the light of these indications, the 4th and final configuration is constructed. The main modification that is introduced to this model consists of a supplementary skin plate which is attached to the ends of the stiffeners. This intentional step depends on the correlations that are obtained for the previous cases. First of all, the first configuration showed that the thickness of the lower skin has an important effect on the frequency (fig. 3.12(a)) and this effect is much more significant respect to the one of the upper skin as illustrated in fig. 3.36(a). In addition this, the results related to the 3rd configuration showed that the optimizer tends to increase the flange width in order to reach higher frequencies (fig. 3.36(b)). These two clues indicate that the ideal configuration should be close to a sandwich structure. This situation highlights the efficiency of a honeycomb core that can significantly increase the natural frequency by introducing elements which have low $\frac{k}{m}$ ratio. However, in this configuration the honeycomb core would be replaced by the stiffener webs.

(a) Configuration 1   (b) Configuration 3

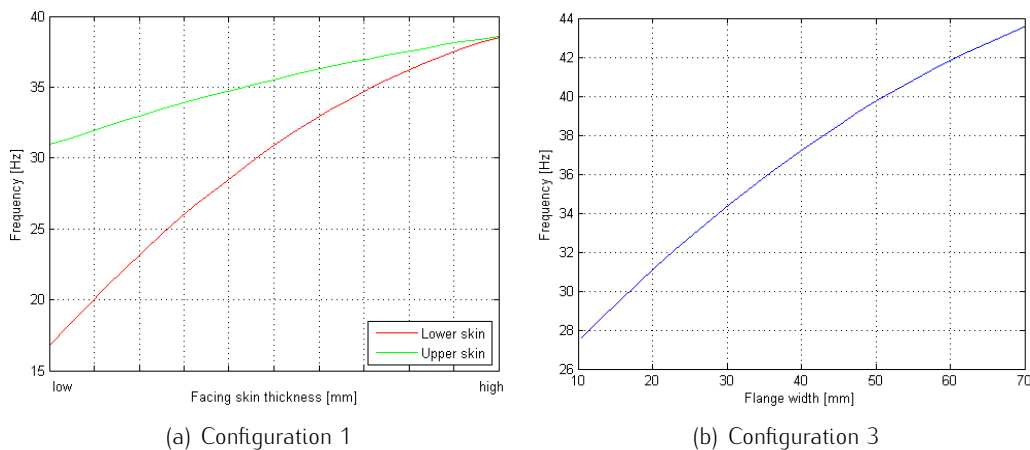**Figure 3.36:** Correlation between geometrical entities and frequency

3.4.1   Finite element model

As previously mentioned, the 3rd configuration has been a transition model in order to obtain the final one. So the *FEM* of the latter model is constructed by adding an additional surface that represents another skin. This surface is equivalently meshed as the other one. These 2 skins which are connected to

each other through stiffeners form a structure similar to a "closed box". As fig. 3.37 shows, the lower and the upper skins should be produced with their vertical extensions and connected to each other on the lateral side. The approach of having reinforcement layers near to the track lines are also adopted in this model. However, these layers are only utilized near to the upper skin in order to increase the thicknesses regarding the zones where there is a load introduction to the plate.
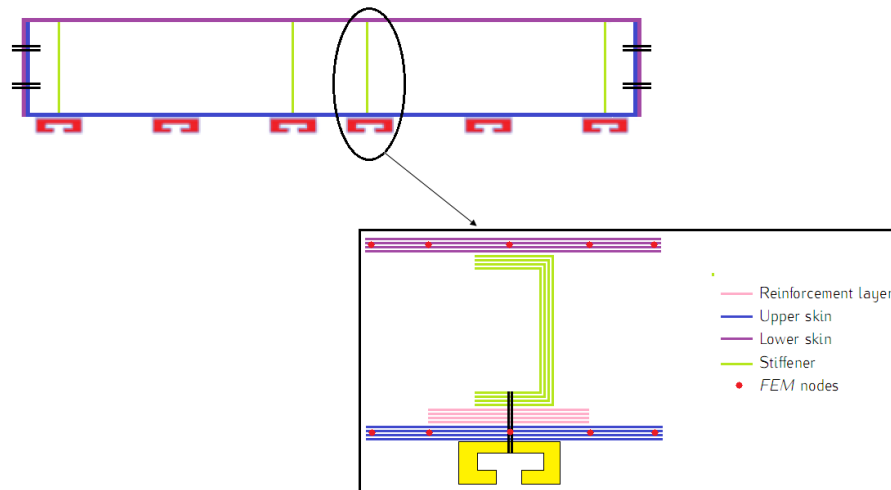
Figure 3.37: Cross section of the final configuration

The main difference that is introduced with respect to the previous model concerns the modelling of the stiffeners that were formerly modelled by beam elements. The reason for such a element type choice depends on the ease of performing any geometrical modification. However, this modelling way is not realistic for the current case due to the presence of the lower skin. A beam element which is perfect to model a stiffener introduces a mass and inertia to a line. In this case, the skins are connected to each other so this effect can not be realistically simulated by the use of such elements. Instead of mono–dimensional elements, shell elements should be used while modelling at least the web of the stiffeners. Whereas the flanges can be modelled by adopting two different approaches:

1. **Use of shell elements**: When such a way is followed, the properties of the stiffener plies should be added to the *PCOMP* of the relevant zones. Even though this might be a more realistic representation of the structure, it can be disadvantageous in terms of the optimization problem. First of all, according to this logic, the flange width should be discrete and the steps between adjacent values would be equal to the width of a shell element. Consequently, in order to increase the allowable values for a defined range,

the current mesh should be refined. This would increase the total element number as well as the time required to solve the model. Furthermore, it would also be very onerous to implement it in a parametric manner during the optimization process.

2. **Use of rod elements**: The alternative way which is quite practical consists of using mono–dimensional elements. This approach is much more convenient with respect to the other one due to the ease of modifying and implementing *PROD* property. This modelling choice is physically acceptable according to the fact that the flanges carry axial loads. Moreover, by this manner, the flange width can vary in a continuous manner without any restrictions.

After discussing the benefits and drawbacks of each modelling way, the definitive choice has been the use of rod elements. However, two equivalent models are constructed and compared with each other. The reference point has been the shell model which is more accurate. By finding close solutions in both dynamic and static terms, the use of rod elements to model the flanges of the stiffeners has been justified. The fig. 3.38 shows the *FEM* corresponding to the last configuration.
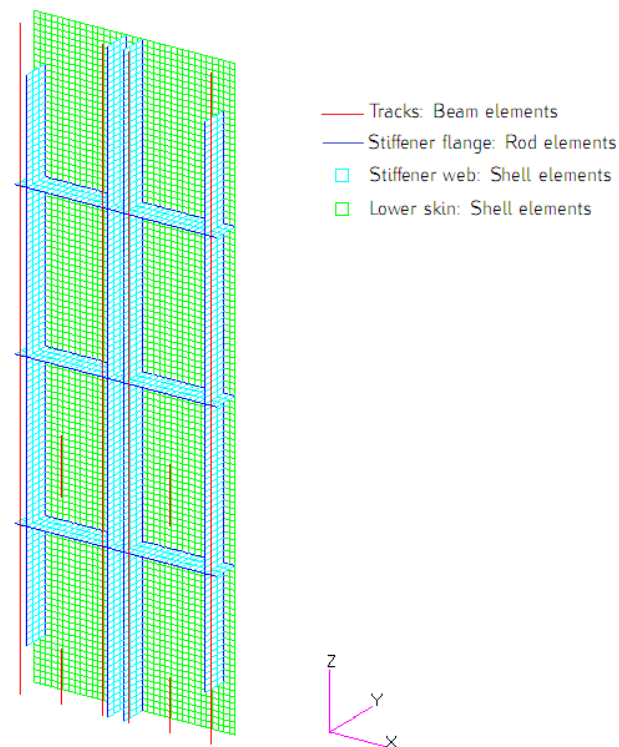

Figure 3.38: *FEM* of the last configuration without visualizing the upper skin

The main aim to construct such a model is to change the natural frequency of the entire system. This purpose is reached due to the fact that the new structure does not behave as an entire plate but as a collection of connected segments that are divided by the stiffeners. However, this kind of structure creates a particular situation which differs from the previous cases. When a modal analysis is performed, local modes with low frequencies come out in addition to the global vibration modes as illustrated in fig. 3.39.

(a) $f_l^2 = 13.9 Hz$ (b) $f_l^5 = 21.2 Hz$
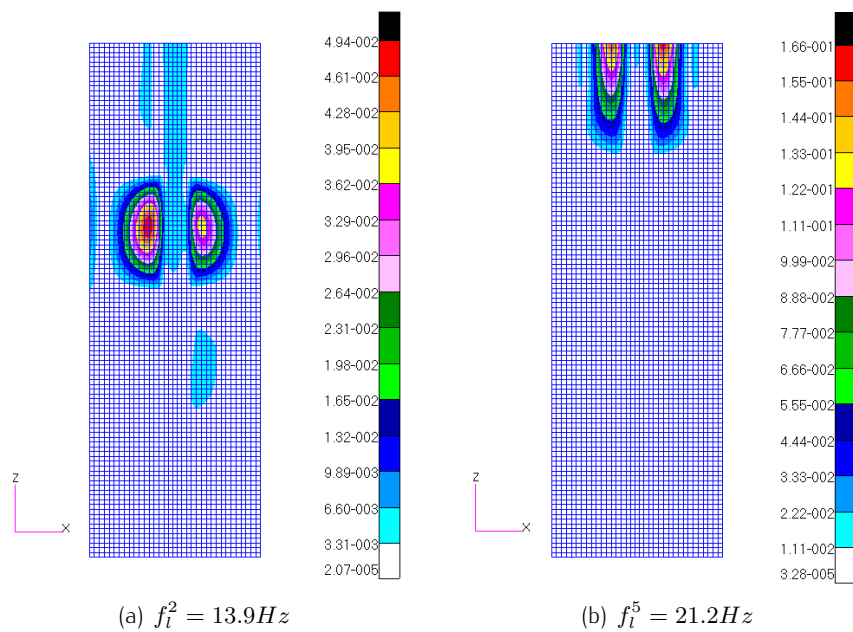
Figure 3.39: Examples of local modes

This operative problem is quite widespread for aeronautical structures where high concentrated masses are attached to thin structures like in the case of an engine attached to a wing through the pylon. The contribution of these local or panel modes to the overall dynamics is almost negligible and they can be avoided by the implementation of a modal condensation technique [17]. However, in order to be able to get such a conclusion, a verification of the current model is performed through *SOL111*. This solver serves to obtain the modal frequency response of the system based on the acceleration values of the defined nodes under dynamic loads. For this case the principal global modes are bending out of plane and torsion. Consequently, 2 subcases with dummy loads are created in order to obtain these types of deformation. Moreover, the response of the system is measured with respect to the points that would have a maximum displacement under the given load.

(a) Bending

(b) Torsion
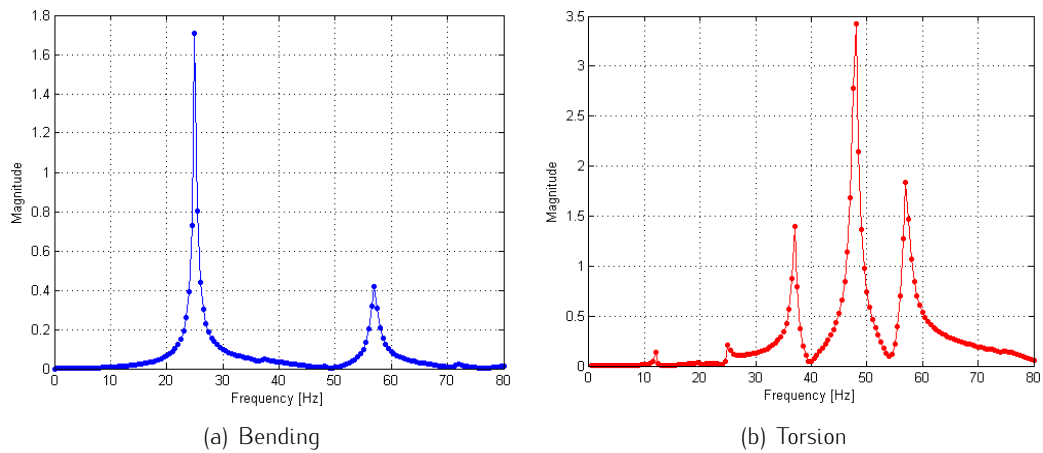
Figure 3.40: Frequency response of the system under dynamic loads

The response of the system is measured for a dynamic load interval between 0 and 80 Hz in order to consider the first 10 modes. The graphics in fig. 3.40 show that the contribution to the global bending and torsion modes are dominated by the 6th and the 8th mode respectively (fig. 3.41). This shows that the first 5 local modes that span a frequency range between 0 and 21 Hz do not participate to the overall response so they can be omitted during the optimization process. Note that these panel modes are inactive unless they are not intentionally excited.

(a) $f_l^6 = 25.0 Hz$

(b) $f_l^8 = 47.9 Hz$
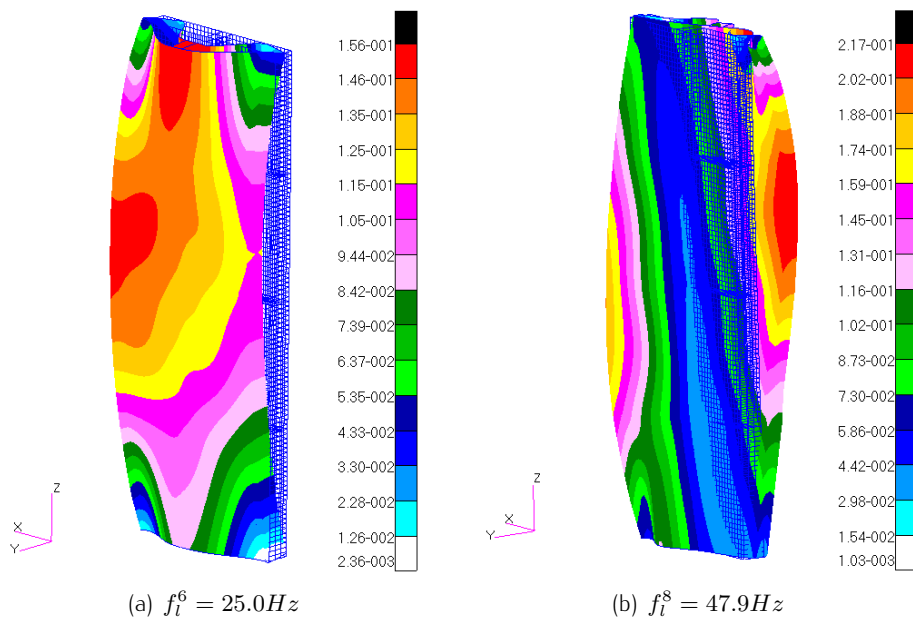
Figure 3.41: Examples of global modes

3.4.2 Optimization model

Once the definitive *FEM* is obtained, the *Work flow* of the optimization sequence is implemented. First of all, the main elements of the optimization problem such as objectives, constraints and the design variables are determined. Compared to the previous configuration, this current one has more design variables due to the inclusion of an additional facing skin. These variables depend on the geometrical properties of the stiffeners and the lamination characteristics of the composite sections. The overall optimization problem formulation can be summarized as follows:

- **Optimization of the reinforced closed box model**

  Objectives: Minimize M_e
 Maximize f_l^6

  Constraints: $f_{1_{loaded}} > 38 Hz$
  $R_{x_{down}} < 20000N$ $R_{x_{up}} < 5000N$
  $R_{y_{down}} < 20000N$ $R_{y_{up}} < 10000N$
  $R_{z_{down}} < 15000N$
  $MS_{Crippling} > 0$

  Design variables: Stiffener web height   [20:5:70] mm
  Stiffener flange width   10–50 mm
  Ply angles (lower skin layers)   [0 45 –45 90]
  Ply number (lower skin layers)   [2:2:10]
  Ply angles (upper skin layers)   [0 45 –45 90]
  Ply number (upper skin layers)   [2:2:10]
  Ply angles (reinforcement layers)   [0 45 –45 90]
  Ply number (reinforcement layers)   [2:2:10]
  Ply angles ("C" stiffener layers)   [0 45 –45 90]
  Ply number ("C" stiffener layers)   [2:2:20]

In addition to the constraints regarding the interface loads, a new check concerning the crippling analysis of the stiffeners is inserted. The absence of the reinforcement layers near to the lower skin makes this zone more critical with respect to the area in proximity to the upper skin. Consequently, in case of a compressive load condition, only this area is considered for the crippling analysis. Furthermore, the interval limits of the design variables are fixed after a rough calculation in a manner to remain in the desired mass range. Note that even though

the stiffener web height is a continuous variable, it is considered as discrete in order to be able to better analyse its effects.

After this step, this *Sim-flow* that represents the event sequence of the optimization process is constructed in *Isight* as illustrated in fig. 3.42. As this last configuration is the final one, a complete analysis is performed in dynamic and static terms.
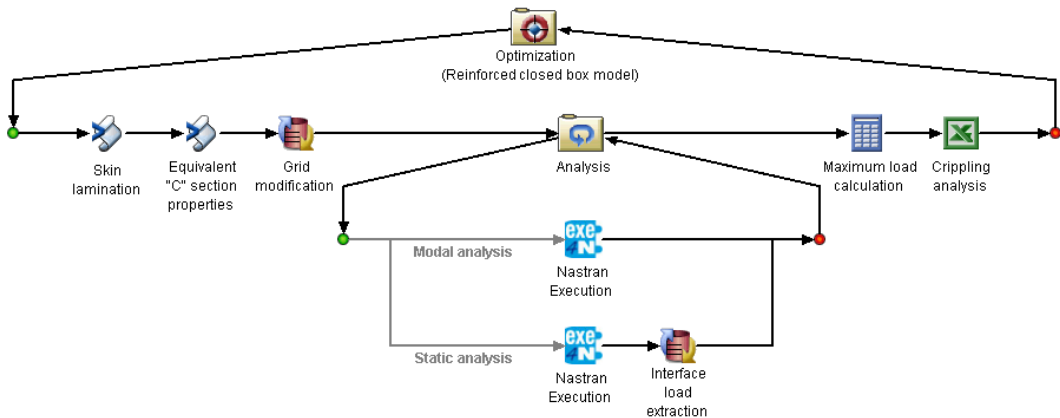

Figure 3.42: Optimization of the reinforced close box model

This represented sequence logic starts with the determination of the lamination characteristics of each laminate ie. stiffener web, reinforcement layers, upper and lower facing skins. Even though this *Skin lamination* block is present almost in all previous optimization processes, its content is different and depends on the specific conditions determined for the given configuration. For the current model, upper skin and lower skin are considered to be independent from each other but individually symmetric. In this way, optimizer would have the freedom of disposing and orienting the plies where it is necessary. Once the material, thickness and orientation angles for each laminate are determined, they are directly mapped to their corresponding arrays present in *Exe4Nastran* block. The second block calculates the material properties of the equivalent section regarding the stiffener flanges. In addition to this, their area, inertia and torsional constant are obtained then connected to the *PROD* variables. Furthermore, a new *Data Exchanger* application is employed in order to modify the *GRID* command. As the stiffener web is modelled with shell elements, the position of the nodes corresponding to these elements should be changed in order to modify the stiffener height. Firstly, in the *FEM*, the nodes along y axis are renumbered in a systematic manner. Then the total height value is passed as an input to this component which gradually changes the y coordinate of the node blocks that correspond to different height

levels present in the *.bdf* file. The *Exe4Nastran* components are configured similar to the previous cases except two different points. First one is that the block that stands for modal analysis reads the 6th natural frequency instead of the first one due to the previously explained reasons. The second point regards a new output request following the static analysis. This output corresponds to the maximum compression load on the *CROD* elements. This value is then passed to the *Excel* block where the formulas required for crippling analysis (app. A.2) are implemented. Note that in this block, the values of the tables present in fig. A.5 are discretely tabulated and then interpolated. As a result of this, at each iteration, the ultimate allowable crippling strength of the defined stiffener is calculated. Afterwards, the corresponding margin of safety is found by considering the maximum compression load on the critical elements. After this step, the cycle restarts with new design variable values.

As this optimization process comprehends both modal and static analysis, the required time for a single iteration is going to be higher with respect to the previous case. However, in order to save an important amount of time, an idea that was previously implemented for the second configuration is adopted. This approach consists of considering the pejorative combination of the overall load conditions and the loading configurations.

A last remark should be made concerning the static analysis. Unlike the second configuration, the maximum failure index of the *QUAD* elements are not included in the optimization problem as a constraint. The reason for that is the modelling of the stiffener flanges through mono dimensional elements. However, in reality, these elements are connected to the facing skins and reinforcement layers. Consequently, the stress distribution obtained in this manner can not be considered representative and so the constraint regarding the maximum failure index is temporarily ignored. Once the optimization process is terminated, the accurate *FEM* is constructed by taking into account the design variables corresponding to the best solution. Then the maximum failure index is controlled in order to verify the validity of the solution offered by the optimizer.

3.4.3   Results

The optimization strategy followed for the final configuration slightly differs from the previous cases. This change depends also on the experience that is gained

until this point. Also during this optimization process, the only algorithm that is employed is *AMGA*. The difference is that in previous cases, the starting population of the algorithm was random. This is equivalent to say that the solutions of the initial population were randomly chosen. Due to this fact, each simulation with the same parameters always gives different solutions. For a fixed generation number, it can be better or worse depending on the fitness of the solutions regarding the initial population. In order to reduce this randomness, a simulation with 1500 iterations is run and the corresponding Pareto front is obtained. Then these non dominated feasible solutions are then given as an input to the following simulation. At this point, the starting population of the new simulation would be constituted on random solutions that are combined with fit ones. Note that the ratio between random and fit points of the starting population can be regulated in a desired manner. In this way, the exploration phase would be reduced as well as the number of generation that is required to reach the best solution. This can be seen by the quantity of the red points in fig. 3.43 with respect to the black ones.
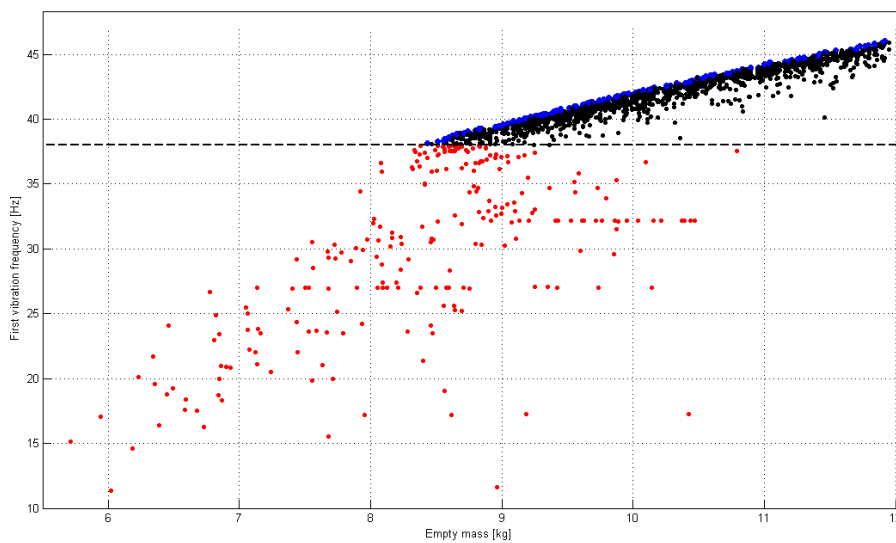
Figure 3.43: Optimization of the reinforced close box model

Algorithm	Mass $[kg]$	Frequency $[Hz]$
AMGA	8.43	38.2

Table 3.18: Mass and frequency values of the best solution

Note that the mass corresponding to best solution that is found for this configu-ration is lower than the target value. So it can be considered as an alternative

to the original design. As previously predicted, the height of the stiffener web is fixed to its maximum value in order to increase the inertia. The remaining design variables regarding the best solution are listed in tab. 3.19.

Design variable evaluation	
Stiffener web height	70 mm
Stiffener flange width	18.16 mm
Ply angles (lower skin layers)	[45 0 –45 0 0]
Ply number (lower skin layers)	10
Ply angles (upper skin layers)	[90 90 45 –45]
Ply number (upper skin layers)	8
Ply angles (reinforcement layers)	10
Ply number (reinforcement layers)	[0 0 90 0 0]
Ply angles ("C" stiffener layers)	[0 45 0 –45]
Ply number ("C" stiffener layers)	8

Table 3.19: Best solution proposed for reinforced laminate model
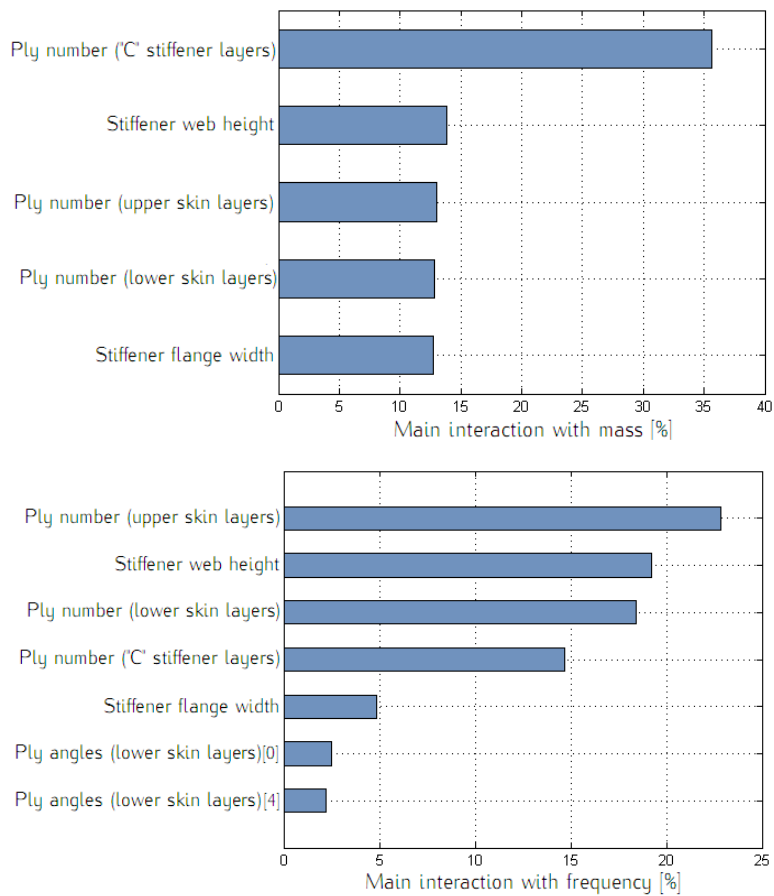

Figure 3.44: Interactions between variables and objectives

140

The classification of the most important parameters are shown in the graphs present in fig. 3.44. The most important parameters are similar to the previous cases except that for the current case, the frequency can be raised in a more efficient manner by increasing the thickness of the upper facing skin rather than the one of the lower skin. Instead the orientation angles of the plies always have lower effects with respect to the main geometric entities such ply thickness, flange width and web height.

As previously mentioned, the maximum failure index of all plies is not included among the constraints because of the fact that the current modelling that is practical for the optimization process does not accurately reflect the physicality of the stress distribution. At this point, the design variables are fixed by the optimizer and the corresponding detailed model is constructed. In this model, the flanges of the stiffeners are modelled through the use of shell elements. Once the *FEM* is constructed, static analysis is performed by including all load conditions. Then the failure index distribution is visualized in order to ensure that there is no value superior to 1.
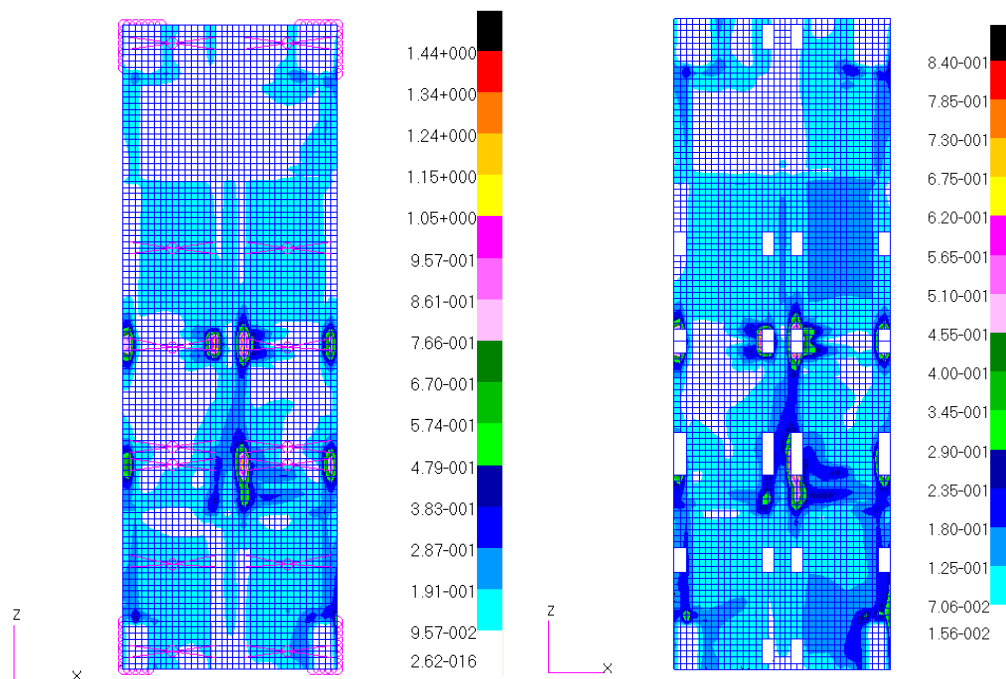

Figure 3.45: Verification of the maximum failure index

First of all, the most critical load case is determined and the maximum failure

index is visualized. This critical condition corresponds to *middle* with $20g$ along –x direction. As fig. 3.45(a) shows, the maximum failure index is superior to 1 which is equivalent to have a ply failure. However, it can be explicitly seen that these zones with highest failure indexes are the areas where a *RBE3* element is connected. The load introduction to the plate is realized through these elements and numerical singularities are present in the correspondence to these connection points. Moreover, all these connection nodes also belong to the beam elements that represent the tracks. Consequently, the load distribution is not realistic so the failure indexes are visualized once again after removing the elements around the *RBE3* connection nodes. In this way, it is verified that the maximum failure index of the remaining plate is inferior to 1 as demonstrated in fig. 3.45(b).

This encountered problem is also examined before beginning the optimization pro–cess. Actually a rough calculation is done in order to ensure to avoid bearing problems. Bearing stress can be defined as the stress resulting from the pressing of two surfaces and it is compressive in nature [18]. In order to perform such analysis, first of all the maximum shear load on the track inserts are read from the report [7]. Then the ultimate bearing strength of Vicotex 6376 unidirectional material is fixed to $556MPa$ [3]. The fastener used in order to connect the tracks to the upper facing skin has a diameter of $5mm$. By combining all these infor–mation and by supposing that the margin of safety for bearing should be superior to 0, the minimum facing skin thickness that does not create bearing problems is calculated. This value is approximately equal to $3mm$ which corresponds to 23 plies. As fig. 3.37 shows, the straps in correspondence to the tracks are composed of the plies related to upper skin, reinforcement layers and stiffener flange. For the best solution, the sum of these 3 elements is equal to 26 plies which means that it is superior to the minimum required thickness value. This lower bound concerning the bearing stress is not included in the optimization problem as a constraint due to the fact that it is just a local effect.

Once the final model is verified by a static analysis, it can be considered as the definitive solution. However, an additional analysis can be done in order to have an idea about the convergence of the solution. One of the tools that can be utilized is the evolution of the Pareto front. The Pareto points can be grouped based on their generation number and then plotted. If the points corresponding to the last generations are close to each other, this means that the solution is not evolving in a significant manner. Consequently, this generation number can be considered as

a convergence threshold for the given starting population. This situation can be verified through the graph present in fig. 3.46. Note that the quantity of Pareto points increases with number of generation and they gradually overlap with the solutions related to the previous generations.
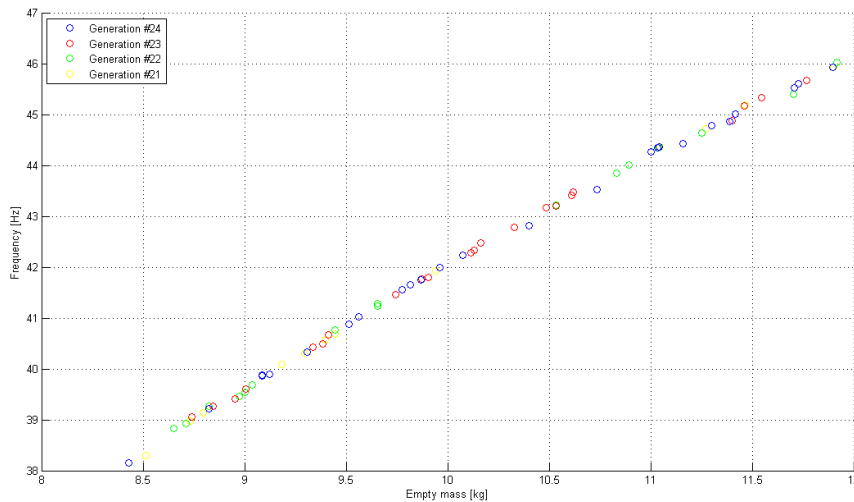

Figure 3.46: Evolution of the Pareto front

As a conclusion, a last simulation is done by changing the objective functions. As previously examined, the optimizer tends to increase the height of the stiffener web in order to gain inertia. However, this means that even though it weights less, it occupies more space inside the helicopter. This situation is not convenient either. Consequently, by keeping all the parameters equal to the last configuration, minimization of the stiffener web height is added as a 3rd objective.
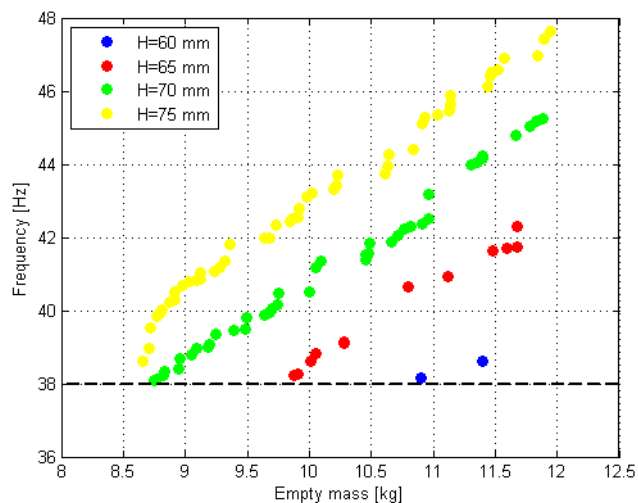

Figure 3.47: Pareto front for the new optimization problem

The fig. 3.47 highlights 2 important facts. The first one is that the optimization process and the corresponding results drastically vary with the problem formulation. This means that the first step regarding the formulation part is essential and it should be determined in a precise manner. The second conclusion is more specifically related to this current case and it concerns the effect of the stiffener web height. This effect demonstrates that different height values translate the Pareto front. Consequently, by using higher web heights, the mass can be reduced further. However, the volume that the plate occupies would automatically increase. Consequently, the maximum allowable volume should be precisely determined and the analysis should be done accordingly. Then finally a compromise between mass and volume should be found.

3.5   Overall results

After the entire optimization process applied for different configurations, some important conclusions are drawn. These final remarks can be analysed under two different groups. The first group consists of the numerical solutions that are obtained at the end of this specific optimization process regarding the SAR Plate Assembly. Instead the second group contains general key points about an optimization process.

During the entire optimization work, a work sequence is followed in order to minimize the mass of the SAR Plate Assembly by respecting the given frequency constraints. During this whole process, any considerations regarding the manufacturing and the financial part are neglected. This is because of the fact that the main scope of this thesis work is to do an optimization activity with a specific software and in the meanwhile to make a evaluation about the capabilities of this software and its possible future applications. However, while defining the variables or implementing the content of the components, a special attention is paid in order to obtain a realistic design application. The overall results that are obtained for each configuration is listed in tab. 3.20. It can be seen that the optimization process has been a gradual sequence and the last configuration has been the main focus. As the results in tab. 3.20 show the total mass of the component is approximately reduced by 7%. Note that among all the genetic algorithms present in the software, *AMGA* has been the most suitable one for this application.

Configuration No	Algorithm	Number of iteration	Total time $[h]$	Mass $[kg]$	Frequency $[Hz]$	Mass difference %
1	AMGA	1000	25.2	16.9	38.6	86.3
2	AMGA	1500	18.3	9.03	38.1	–0.4
3	AMGA	1500	4.5	9.38	38.1	3.4
4	AMGA	2500	45.5	8.43	38.2	–7.1

Table 3.20: Summary of the overall optimization process

Apart from the numerical results, the important point is the ability to integrate and automate the entire process of a structural analysis. As a result of this, a sig–nificant amount of time can be saved by omitting the repetitive manual operations that a user should do. This saved time can be spent to improve the structural details and to analyse numerous alternatives before deciding the specifications of the definitive model.

Instead the second group of conclusions can be considered as a summary of the experience that is gained during the optimization process with this specific soft–ware. Even though this software facilitates so much the use of genetic algorithms, the quality of the results highly depends on the inserted parameters. The correct setting of these parameters is therefore very important to reach the real optimum with minimum effort [19]. In order to obtain better solutions, the user should be familiar with the concepts of population size, number of generation, crossover and mutation rate. Unfortunately, there do not exist universal rules to determine these parameters and their values are unique for each problem. The first step in an optimization problem through genetic algorithms can be the determination of the time that should be dedicated to the simulations. By taking into account the time required for a single iteration, the maximum allowable iteration number can be fixed. As the total iteration time is equal to the product of the population size and number of generations, these two parameters can be set according to the nature of the problem. To illustrate, if there exist numerous design variables, the population size should be high in order to be able to span the whole design space. In the case that the results are already acceptable but a local improvement is necessary, the number of generation should be increased. In order to be able to exploit in an efficient manner from the genetic algorithms, the population size and the number of generations should be high enough to span the design space and to let the solution evolve. As a result of this, genetic algorithms are adequate for problems whose single iteration lasts few times. To illustrate, in the case of the SAR Plate

Assembly, a single iteration approximately lasts a couple of minutes. Another clue can be given concerning the cross over and mutation rate. In the case that the objective function is not smooth, a high cross over rate might help to avoid a local minimum. Instead a high mutation rate rends the search of the new solutions more random and therefore results in slow convergence [20].

Furthermore, in order to reduce the total simulation time, a specific population can be given as an input instead of starting with a random population. This initial population can be the Pareto front that is obtained from the previous simulation or it can be a design matrix prepared by a *Design of Experiment* process in a systematic manner. These two alternatives, especially the first one, can reduce the exploration process so the total time required to reach a good solution. Another efficient alternative can be to make a survey regarding the input–output sensitivity. Once the design variables that have major effects on the output are identified, the rest of the design variables can be fixed. Consequently, a new optimization simulation that would less number of variables can be run only by considering the most effective ones.

Lastly, another possibility to reach a better solution can be to adopt a different approach to the problem. According to this approach, the main focus of a genetic algorithm can be considered as exploring the design space. Then the best solution that is proposed by the genetic algorithm can be used as a starting point of a different type of algorithm that is more adequate for performing local improvements. For instance, if the design space is continuous, a gradient based method such as Sequential Quadratic Programming can be utilized; if it is discrete, Simulated Annealing Method can be efficient.

All these tips are highlighted among the results because they made an important part of the notions that influenced the work progress. Moreover, these instructions can also be beneficial for applications that are out of the structural engineering field.

Chapter 4

Conclusions

This thesis is devoted to present an application regarding the automation and optimization of a structural design process related to a helicopter component. The first aspect concerning the process integration and automation enables to significantly increase the efficiency of the entire process in terms of time and cost [48]. *Isight* can be considered as a powerful but at the meanwhile a user-friendly tool which permits to facilitate this move. Moreover, in addition to this aspect, the design solutions can be systematically improved by using its optimization tools.

In this specific example concerning the SAR Plate Assembly, a structural design process based on finite element analysis is automated. First of all, a simplified finite element model that represents the component is created and verified. The decisions during this initial modelling phase are taken in manner to facilitate its implementation during the optimization phase. In this latter stage, genetic algorithms that make part of evolutionary computing techniques are chosen due to their suitability for this kind of problem statement. The optimization process departed from the already existing design of the component and then continued in a systematic manner by taking into account the results obtained at each step. Topologically different solutions are tested and attempted to be perfected through sizing and internal parameter optimization. At the end, the main objective is achieved by reducing the mass of the entire system by 7%. It is also verified that this new design solution that does not posses any shock absorbers satisfies the frequency constraints.

The implementation of such an automated optimization process allows to test numerous configurations and to obtain a design solution that is closer to the 'optimal' one in a reasonable time period. Note that the 'optimal' solution does not always

correspond to the one that is predicted using engineering intuition and experience. In this sense, a optimizer can be more efficient by choosing the right direction to follow and by excluding the unnecessary alternatives. Consequently, in addition to decreasing the cost and time which are essential for a company, an automated optimization sequence reduces also the effort due to repetitive operations. This fact lets the analyst to focus on his human role as a planner and decision maker [31].

To conclude, this thesis work can be considered as the core of a more complete structural design process. Departing from this work, further improvements can be made by adding other two fundamental elements. The first one regards the integration of a parametric CAD approach in the *Work flow*. This step would permit a wider range of application including the models that have even more complex geometries. It is evident that constructing a parametric CAD model requires more time and effort during the initial design phase. However, as the graph in fig. 4.1 shows, its cost diminishes with time. The reason for such a variation is that the flexibility of a parametric design approach avoids the usual 'design–analysis–new design' loop between the designer and the analyst. As a result of this, such a choice can be more convenient with respect to a conventional design approach [46].
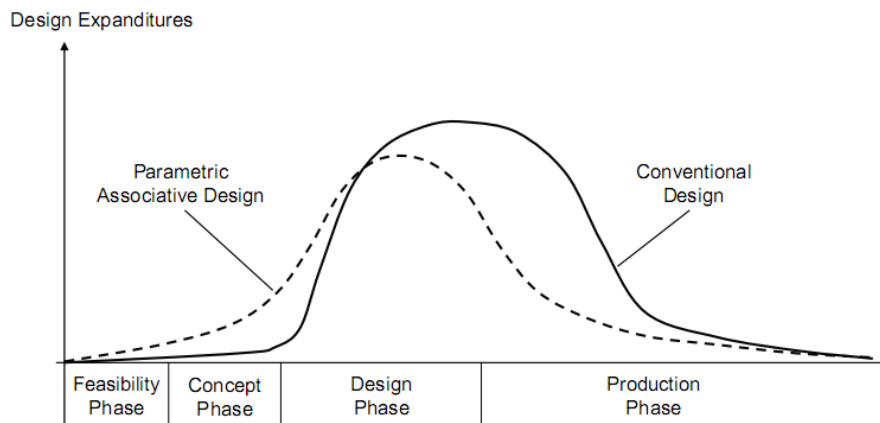

Figure 4.1: Design expenditures in an aircraft design project

After the inclusion of this new step, a more complete *Work flow* can be obtained as illustrated in fig. 4.2. Note that the input file for the finite element solver can be created through an additional software specialized in mesh morphing ([14]) or through the component of *Isight* that is reserved for finite element modelling ([45]).
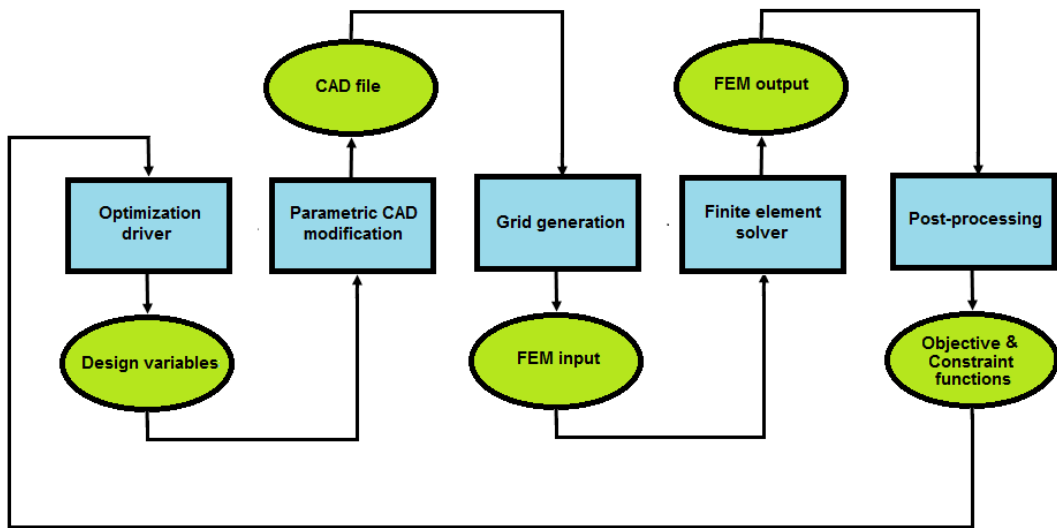
Figure 4.2: Integration and automation of a structural design process

The second element that would permit to obtain a better design allows increasing the robustness of the entire system. The implementation of a stochastic analysis like Monte Carlo simulations can lead to a more robust design that assesses the impact of known uncertainties that may depend on manufacturing, design phase, approximations and so on [47]. Once this kind of mentality is adopted for this specific field, more sophisticated multidisciplinary problems can be treated by combining the interaction between different fields.

Appendix A

Laminate analysis

A.1 Equivalent laminate properties

Applicable references: [4, 5]

In order to define a generic laminate, there exist several parameters such as the thickness, material and the orientation angles that correspond to each lamina. Based on this information at local level, it is possible to obtain the global prop-erties of the laminate. As it is mentioned in the chap. 3.2.1, the objective is to calculate an equivalent elastic modulus (E_{xx}, E_{yy}), shear modulus (G_{xy}) and Pois-son's ratio (ν_{xy}, ν_{yx}) along the principal planar directions departing from the data at lamina level. Note that the physical and mechanical properties of a lamina vary along its principal directions that are illustrated in fig. A.1:
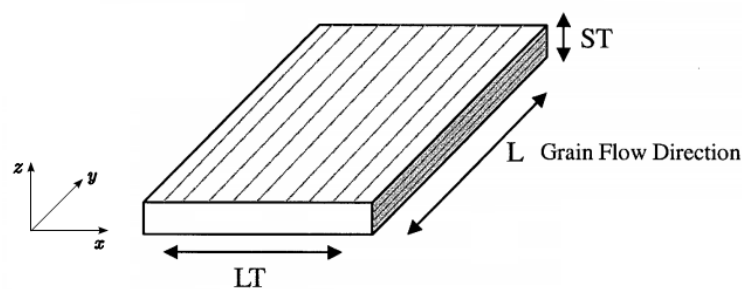

Figure A.1: Metallic material grain direction

- Longitudinal (L): Parallel to the direction of main grain flow

- Long Transverse (LT): Perpendicular to the longitudinal grain direction

- Short Transverse (ST): Shortest dimension of the component

The dimension along the short transverse direction is much smaller respect to the other remaining two directions. As a result of this, it can be assumed that a lamina is in state of plane stress which is equivalent to say that:

$$\sigma_{33} = \tau_{13} = \tau_{23} = 0$$

The next step should be to calculate the stiffness matrix for each lamina as demonstrated in the eq. A.1:

$$[C] = \begin{bmatrix} C_{11} & C_{12} & 0 \\ C_{12} & C_{22} & 0 \\ 0 & 0 & C_{66} \end{bmatrix} \tag{A.1}$$

Where:

$$\begin{cases} C_{11} = & \dfrac{E_{11}}{1 - \nu_{12}\nu_{21}} \\[2mm] C_{12} = & \dfrac{\nu_{12}E_{12}}{1 - \nu_{12}\nu_{21}} \\[2mm] C_{22} = & \dfrac{E_{22}}{1 - \nu_{12}\nu_{21}} \\[2mm] C_{66} = & G_{12} \end{cases}$$

Once the lamina stiffness matrix is obtained, its participation to the global stiffness matrix can be calculated with respect to the global laminate axis through a transformation operator that considers the orientation of the each lamina.
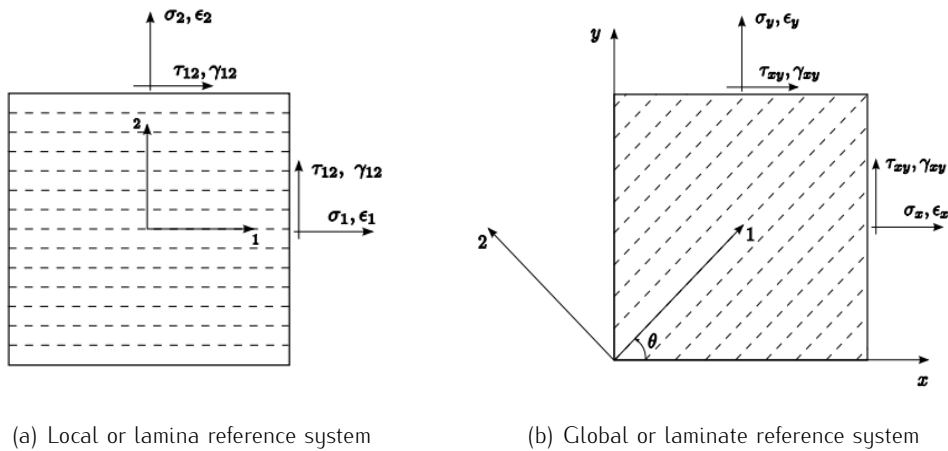

(a) Local or lamina reference system   (b) Global or laminate reference system

Figure A.2: Stress and strain components at lamina and laminate level

As the fig. A.2 shows, the subscripts $_{xx}$ and $_{yy}$ are valid for the global coordinate system whereas the terms with the subscripts $_{11}$ and $_{22}$ are represented with respect to the local reference system that is attached to each lamina. Furthermore, the transformation operator depends on the rotation angle ϑ which is defined between the longitudinal ply direction and the x axis of the global frame.

$$[Q] = \begin{bmatrix} Q_{11} & Q_{12} & Q_{16} \\ Q_{12} & Q_{22} & Q_{26} \\ Q_{16} & Q_{26} & Q_{66} \end{bmatrix} \tag{A.2}$$

Where the components of the matrix Q can be found by including the orientation angle ϑ of a lamina with respect to the global coordinate system:

$$\begin{cases} Q_{11} = & C_{11} \cos^4 \vartheta + 2(C_{12} + 2C_{66}) \sin^2 \vartheta \cos^2 \vartheta + C_{11} \sin^4 \vartheta \\ Q_{22} = & C_{11} \sin^4 \vartheta + 2(C_{12} + 2C_{66}) \sin^2 \vartheta \cos^2 \vartheta + C_{11} \cos^4 \vartheta \\ Q_{12} = & (C_{11} + C_{22} - 4C_{66}) \sin^2 \vartheta \cos^2 \vartheta + C_{12}(\sin^4 \vartheta + \cos^4 \vartheta) \\ Q_{66} = & (C_{11} + C_{22} - 2C_{12} - 2C_{66}) \sin^2 \vartheta \cos^2 \vartheta + C_{66}(\sin^4 \vartheta + \cos^4 \vartheta) \\ Q_{16} = & (C_{11} - C_{12} - 2C_{66}) \sin \vartheta \cos^3 \vartheta + (C_{12} - C_{22} + 2C_{66}) \sin^3 \vartheta \cos \vartheta \\ Q_{26} = & (C_{11} - C_{12} - 2C_{66}) \sin^3 \vartheta \cos \vartheta + (C_{12} - C_{22} + 2C_{66}) \sin \vartheta \cos^3 \vartheta \end{cases}$$

The inclusion of the effect due to the thickness of a lamina permits to obtain the constitutive equations that correlate the forces/moments per unit length (as shown in fig. A.3) to the strains/curvatures of a laminated anisotropic plate.
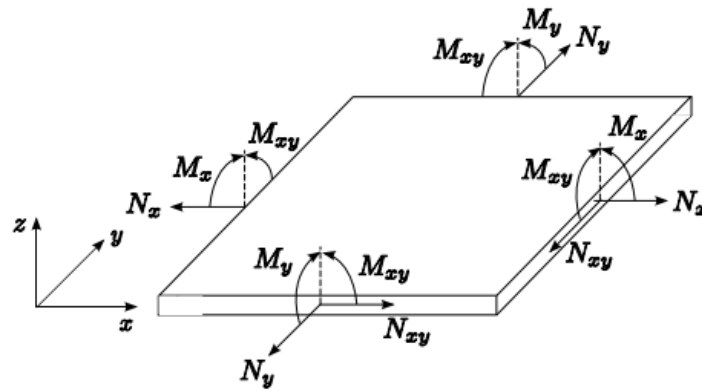

Figure A.3: Directions of the forces and moments acting on the laminate

$$
\left\{ \begin{array}{c} N_x \\ N_y \\ N_{xy} \\ M_x \\ M_y \\ M_{xy} \end{array} \right\} = \begin{bmatrix} A_{11} & A_{12} & A_{13} & B_{11} & B_{12} & B_{13} \\ A_{21} & A_{22} & A_{23} & B_{21} & B_{22} & B_{23} \\ A_{31} & A_{32} & A_{33} & B_{31} & B_{32} & B_{33} \\ B_{11} & B_{12} & B_{13} & D_{11} & D_{12} & D_{13} \\ B_{21} & B_{22} & B_{23} & D_{21} & D_{22} & D_{23} \\ B_{31} & B_{32} & B_{33} & D_{31} & D_{32} & D_{33} \end{bmatrix} \left\{ \begin{array}{c} \varepsilon_{0x} \\ \varepsilon_{0y} \\ \gamma_{0xy} \\ \chi_x \\ \chi_y \\ \chi_{xy} \end{array} \right\}
$$

$$
\left[\begin{array}{c} \{N\} \\ \hline \{M\} \end{array} \right] = \left[\begin{array}{c|c} [A] & [B] \\ \hline [B] & [D] \end{array} \right] \left[\begin{array}{c} \{\varepsilon_0\} \\ \hline \{\chi\} \end{array} \right] \tag{A.3}
$$

Where:

$$
\begin{cases}
A_{ij} = & \sum_{k=1}^{n}(Q_{ij})_k(h_k - h_{k-1}) \\[2ex]
B_{ij} = & \sum_{k=1}^{n}(Q_{ij})_k \left(\dfrac{h_k^2 - h_{k-1}^2}{2} \right) \\[2ex]
D_{ij} = & \sum_{k=1}^{n}(Q_{ij})_k \left(\dfrac{h_k^3 - h_{k-1}^3}{3} \right)
\end{cases}
$$

The matrices A, B and D all have a dimension of 3×3 because of the hypothesis of state of plane stress. The matrix A represents the membrane stiffness and the matrix D the flexural stiffness of the laminate. Instead the matrix B introduces a structural coupling between midplane curvatures and membrane forces, and similarly between membrane strains and moments [6]. In some special laminates such as a symmetric one, the matrix B becomes null. Instead, in the case of a symmetric equilibrate case, in addition to the matrix B, the components A_{13} and A_{23} are also null. Lastly, an antisymmetric equilibrate laminate (balanced) is said to be orthotropic with respect to the bending moments because its components A_{13}, A_{23}, D_{13} and D_{23} are zero.

Note that all the three matrices depend on both initial and final position of each lamina along the short transverse direction measured with respect to the midplane. The schema used for the application of this logic is shown in the fig. A.4.
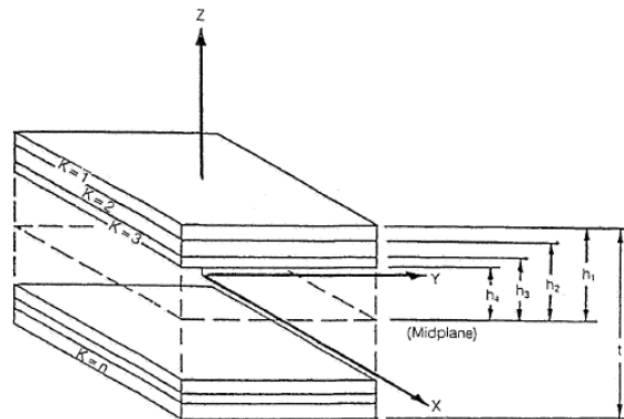
Figure A.4: Schematization of the laminate sections

According to the eq. A.4, the elastic constants of the laminate can be found once the global stiffness matrix that is composed of the matrices A, B and D is calculated.

$$E_{xx} = \frac{A_{11}A_{22} - A_{12}^2}{A_{22}t} \qquad \nu_{xy} = \frac{A_{12}}{A_{22}}$$

$$E_{yy} = \frac{A_{11}A_{22} - A_{12}^2}{A_{11}t} \qquad \nu_{yx} = \frac{A_{12}}{A_{11}} \tag{A.4}$$

$$G_{xy} = \frac{A_{66}}{t}$$

A.2 Crippling of composite sections

Applicable references: [13, 2]

An analytical formula that serves to calculate the crippling strength of the composite sections does not exist and consequently this F_{cc} value can only be calculated through semi–empirical methods. In the absence of experimental data, the eq. A.5 which is valid for metallic sections is utilized in order to estimate F_{cc}. This equation appears to give successful results also in the case of composite sections with uniform thickness:

$$F_{cc} = \frac{\sum_{i=0}^{n} F_{cc_i} b_i t_i}{\sum_{i=0}^{n} b_i t_i} \tag{A.5}$$

The ultimate allowable crippling strength F_{cc} can be calculated using the material allowable compression strength F_{cu} and other mechanical properties of the laminate. These properties belong to the equivalent material properties of the global laminate calculated as shown in chap. A.1.
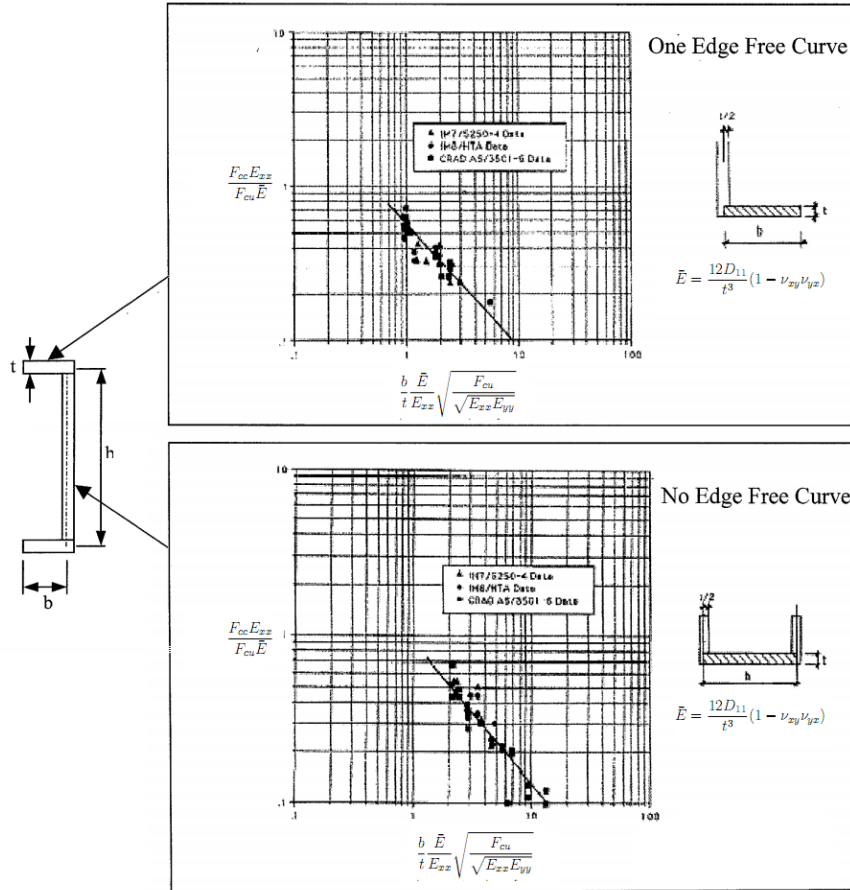

Figure A.5: Crippling strength for composite sections

The term $\dfrac{b}{t}\dfrac{\bar{E}}{E_{xx}}\sqrt{\dfrac{F_{cu}}{\sqrt{E_{xx}E_{yy}}}}$ is firstly evaluated in order to calculate the input value for the x axis and F_{cc} is calculated for each flange or web based on the graph present in fig. A.5. Then, the F_{cc} of the entire section can be obtained by using the given relation in eq. A.5. Note that finally the margin of safety for crippling can be calculated as shown in eq. A.6.

$$\boxed{MS_{ult} = \frac{F_{cc}}{\sigma_c} - 1} \tag{A.6}$$

Appendix B

Material Failure Theories for Composite Structures

Applicable references: [1, 2]

The complexity of the stress distribution throughout the fibre and the matrix regions of a composite laminate renders inefficient the use of precise analysis methods. Accordingly, two fundamental approaches have been developed in order to perform a strength analysis regarding a composite structure.

- **Ply or lamina level:** For a given load condition, the average values of the stress and strain components within each ply are calculated based on the classical Lamination Theory. Then these values are compared with either the lamina allowable or any other limit value depending on the adopted failure criteria. This model is also called "First Ply Failure" because the failure of any lamina is accepted equivalent to the complete failure of the laminate.

- **Laminate level:** Similarly, the average values of the stress and strain components within each ply are obtained using the lamination theory. However, they are compared with the laminate allowables that must be derived from experiments.

Between these two methods, the First Ply Failure is most commonly used even though it is a conservative model. Note that after the failure of the first lamina,

the residual strength of the remaining plies can be calculated. However, this approach is preferably not used during the composite design phase due to the fact that it might possibly result in unreliable or non conservative estimation of the laminate strength.

The most common failure theories concerning the composite structures may be grouped in two main categories:

Failure Mode Based	Empirical
Maximum Stress	Hill
Maximum Strain	Tsai-Wu
Hashin	Hoffman

Table B.1: Classification of the composite failure theories

Failure mode based theories treat each identifiable physical laminate failure mode such as tensile failure along fibre direction or the matrix dominated transverse failure. Instead the empirical methods attempt to combine the effects of several different failure mechanisms and create a unique function that depends on the polynomial combination of the main ply stresses or strains.

B.1   Maximum Stress and Maximum Strain Criteria

The Maximum Stress Criteria states that the failure occurs when any stress value along a material axis exceeds the allowable material strength along that direction. The Maximum Strain Criteria is equivalent to the Maximum Stress Criteria except that fact that the stress values are replaced by the corresponding strains. Generally, Maximum Stress Criteria is more frequently used due to the facility and accuracy of the stress data coming from experiments.

In addition to its simplicity, it is advantageous to use this method because the required data such as material strength values along principal laminate directions can be easily obtained from standard tests. Furthermore this approach neglects the interaction between different stress states. Consequently, a good correlation exists with the experimental data when the stress state is mainly dominated by a uni-axial loading.

The failure index based on the Maximum Stress Criteria can be calculated in the following manner:

♦ Longitudinal direction:
$$
\begin{cases}
\dfrac{\sigma_1}{X_t} & \text{if } \sigma_1 \text{ is tension} \\[2em]
\dfrac{\sigma_1}{X_c} & \text{if } \sigma_1 \text{ is compression}
\end{cases}
$$

♦ Transverse direction:
$$
\begin{cases}
\dfrac{\sigma_2}{Y_t} & \text{if } \sigma_2 \text{ is tension} \\[2em]
\dfrac{\sigma_2}{Y_c} & \text{if } \sigma_2 \text{ is compression}
\end{cases}
$$

♦ Shear: $\dfrac{\tau_{12}}{S_{12}}$

The most critical failure index is given by the following relation: $FI_{crit} = max\left(\left[\dfrac{\sigma_1}{X}, \dfrac{\sigma_2}{Y}, \dfrac{\tau_{12}}{S_{12}}\right]\right)$. Accordingly, the margin of safety [1] at ultimate load can be calculated as shown in eq. B.4.

$$
\boxed{MS_{ult} = \frac{1}{FI_{crit}} - 1}
$$

(B.1)

B.2   Hashin Failure Criteria

Hashin failure criteria is a realistic method to estimate the strength of tapes under combined stresses because it is based on experimental data. According to the tests performed on tape or unidirectional material, the tensile strength in the fibre direction depends on σ_1 and τ_{12} whereas the compressive strength is only and primarily affected by σ_1. A tensile stress σ_2 along the transverse direction leads to a failure followed by a sudden crack that is parallel to the fibre direction. Instead, in the compressive case, the crack occurs on some plane parallel to the fibre direction but not necessarily perpendicular to σ_2. Moreover, in both cases σ_1 has no effects on the failure.

---

[1] A reliable design has a positive margin of safety and consequently its failure index is inferior to unity.
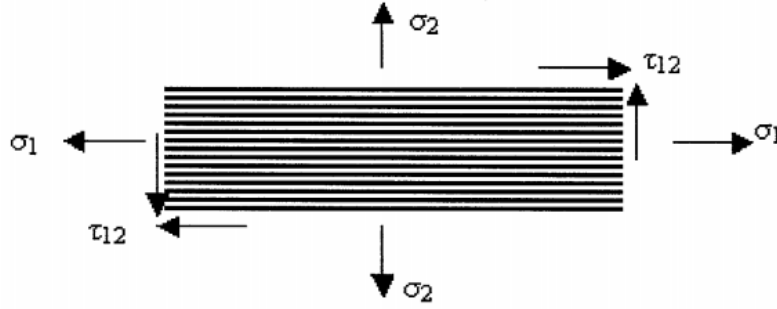
Figure B.1: Scheme for the stress vector directions

Consequently, Hashin approach identifies four failure criteria that can be handled separately and that are valid for different failure modes regarding the fibre or the matrix.

♦ Fibre modes:

$$
\begin{cases}
\text{Tensile:} \qquad FI_{ft} = \left(\dfrac{\sigma_1}{X_t}\right)^2 + \left(\dfrac{\tau_{12}}{S_{12}}\right)^2 \\[3em]
\text{Compressive:} \quad FI_{fc} = \left(\dfrac{\sigma_1}{X_c}\right)
\end{cases}
$$

♦ Matrix modes:

$$
\begin{cases}
\text{Tensile:} \qquad FI_{mt} = \left(\dfrac{\sigma_2}{Y_t}\right)^2 + \left(\dfrac{\tau_{12}}{S_{12}}\right)^2 \\[3em]
\text{Compressive:} \quad FI_{mc} = \left(\dfrac{\sigma_2}{Y_c}\right)^2 + \left(\dfrac{\tau_{12}}{S_{12}}\right)^2
\end{cases}
$$

The margins of safety corresponding to the fibre and the matrix are independently calculated for both tensile and compressive loading cases as demonstrated by eq. B.2 and eq. B.3. The critical margin of safety for the composite structure would be the lowest among the four subcases and this subcase would indicate the global failure mode of the entire structure.

$$
\boxed{
\begin{aligned}
&-\quad \text{Fiber mode (tensile):} \qquad MS_{ft_{ult}} = \frac{1}{\sqrt{FI_{ft}}} - 1 \\[2em]
&-\quad \text{Fiber mode (compressive):} \quad MS_{fc_{ult}} = \frac{1}{FI_{fc}} - 1
\end{aligned}
}
\tag{B.2}
$$

$$
\begin{array}{ll}
-\quad \text{Matrix mode (tensile):} & MS_{mt_{ult}} = \dfrac{1}{\sqrt{FI_{mt}}} - 1 \\[4mm]
-\quad \text{Matrix mode (compressive):} & MS_{mc_{ult}} \cong \dfrac{1}{\sqrt{FI_{mc}}} - 1
\end{array}
\tag{B.3}
$$

B.3   Hill, Tsai–Wu and Hoffman Failure Criteria

Unlike the Maximum Stress or Strain theory; Hill, Tsai–Wu and Hoffman failure criteria consider the interaction of plane stresses. Even though they are mostly covered by all major finite element codes, they might have some disadvantages such as instability, inaccuracy for laminates that are composed of tapes and under estimation of the actual laminate strength. The instability concept appears when a negative failure index is calculated for certain plane stress combinations. In order to avoid such inconvenience, Tsai–Wu criteria includes a stability term, F_{12} that must be evaluated experimentally. However, the difficulty to obtain such pa–rameter reduces the practical use of this theory and renders easier the application of Hill and Hoffman failure criteria.

The failure index for these interactive failure criteria can be obtained as follows:

♦ **Hill:** Lamina with equal strengths in tension and compression

$$
FI = \frac{\sigma_1^2}{X^2} - \frac{\sigma_1 \sigma_2}{X^2} + \frac{\sigma_2^2}{Y^2} + \frac{\tau_{12}^2}{S_{12}} \quad \text{where X and Y are } X = \frac{X_t + X_c}{2}, \quad Y = \frac{Y_t + Y_c}{2}
$$

♦ **Hoffman:** Lamina with unequal strengths in tension and compression

$$
FI = \left(\frac{1}{X_t} - \frac{1}{X_c} \right) \sigma_1 + \left(\frac{1}{Y_t} - \frac{1}{Y_c} \right) \sigma_2 + \frac{\sigma_1^2}{X_t X_c} + \frac{\sigma_2^2}{Y_t Y_c} + \frac{\tau_{12}^2}{S_{12}^2} - \frac{\sigma_1 \sigma_2}{X_t X_c}
$$

♦ **Tsai–Wu:** Lamina with unequal strengths in tension and compression

$$
FI = \left(\frac{1}{X_t} - \frac{1}{X_c} \right) \sigma_1 + \left(\frac{1}{Y_t} - \frac{1}{Y_c} \right) \sigma_2 + \frac{\sigma_1^2}{X_t X_c} + \frac{\sigma_2^2}{Y_t Y_c} + \frac{\tau_{12}^2}{S_{12}^2} + 2F_{12}\sigma_1 \sigma_2
$$

The margin of safety at ultimate loads for any of these interactive failure criteria can be assumed equal to:

$$MS_{ult} \cong \frac{1}{\sqrt{FI}} - 1 \qquad\qquad \text{(B.4)}$$

B.4   Analysis of un–notched composite laminates

The experience and the test results accumulated by Agusta Westland and also by the majority of the Aerospace companies demonstrate that the Tsai–Wu Criteria may significantly under estimate the strength of the component. Apart from this fact, each failure criteria might be more or less efficient depending on the laminate type (fabric versus unidirectional material) and also on the loading conditions (uni–axial versus biaxial). As a result of this, in order to be able to perform an efficient strength analysis on a composite structure, there might be the necessity of choosing the most accurate criteria for the case in investigation. A methodology regarding this problem is proposed by a flowchart presented in fig. B.2.
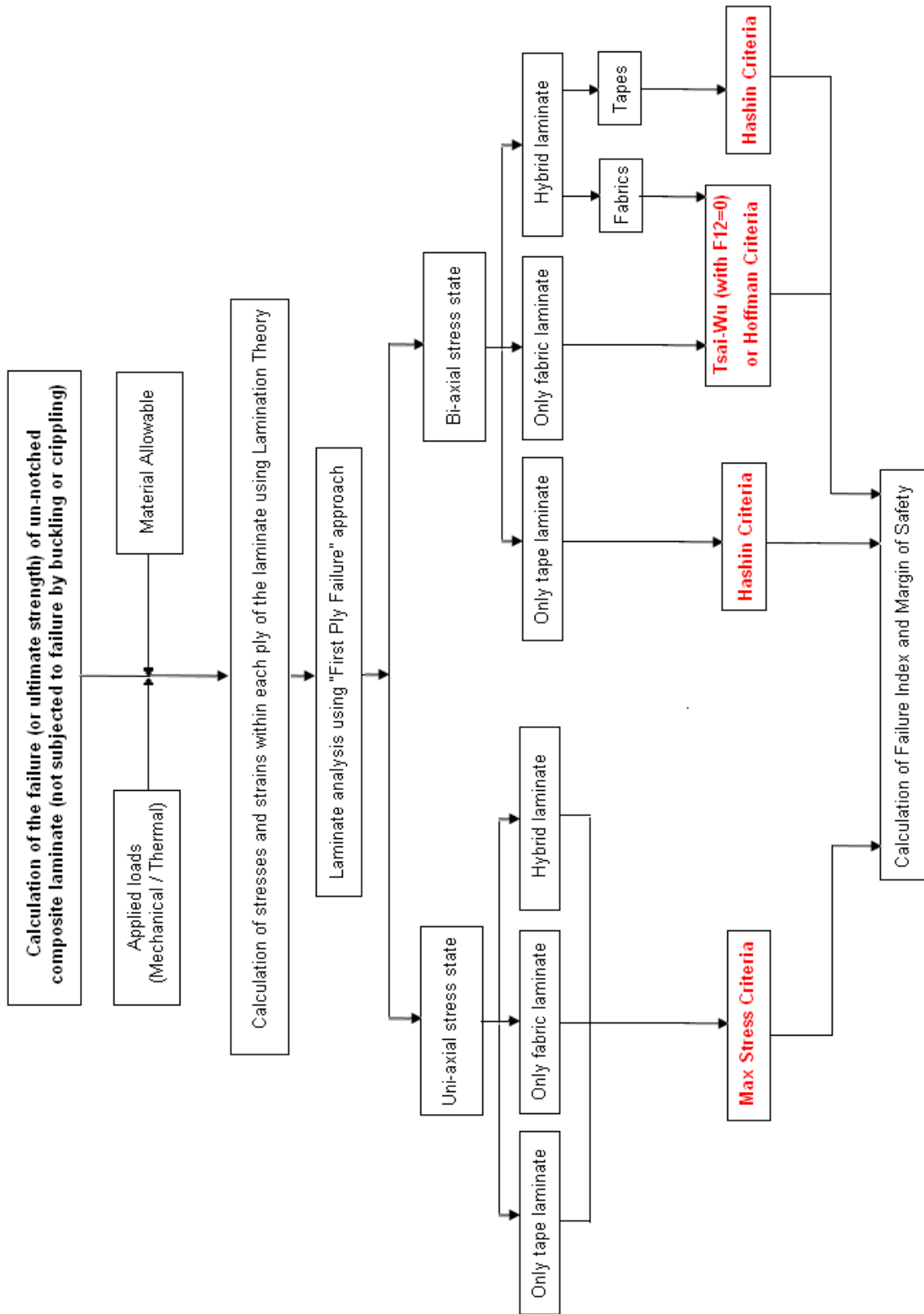
Figure B.2: Flowchart for strength analysis of un-notched composite laminates

Appendix C

Installation mechanism of SAR Plate Assembly

SAR Plate Assembly possesses a simple structural geometry but the constraints regarding the loading conditions forced the designers to plan special mechanisms around the attachment zones. These details obligate the user to follow precise steps during the installation process of the plate on the helicopter. First of all, the lower attachment points should be fixed and then the upper ones. The installation sequence can be listed as follows:

1. Sar Plate should be positioned on the floor rail

2. Lower track fittings and lower thin track fittings (fig. 2.5) should be positioned on their correct positions

3. Upper interface fittings should be connected to the upper deck by following the steps shown in fig. C.1 – fig. C.7 and in this way it would be possible to complete the installation procedure.
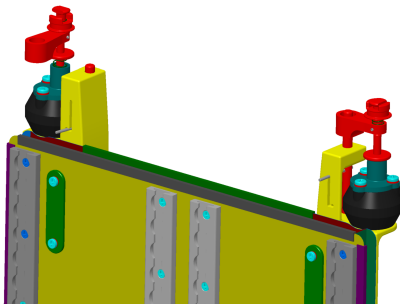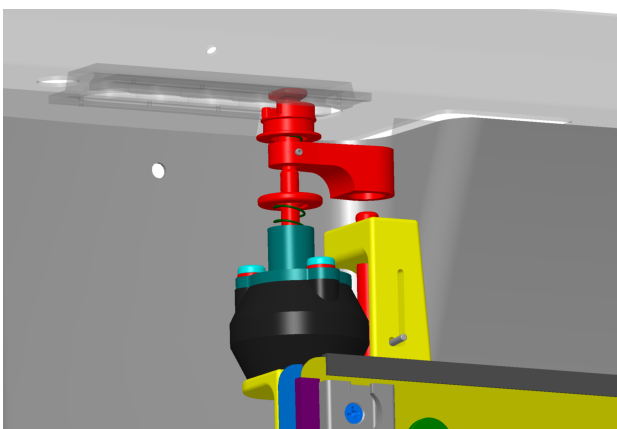

**Figure C.1:** The sliding pin is moved towards down along its guide.
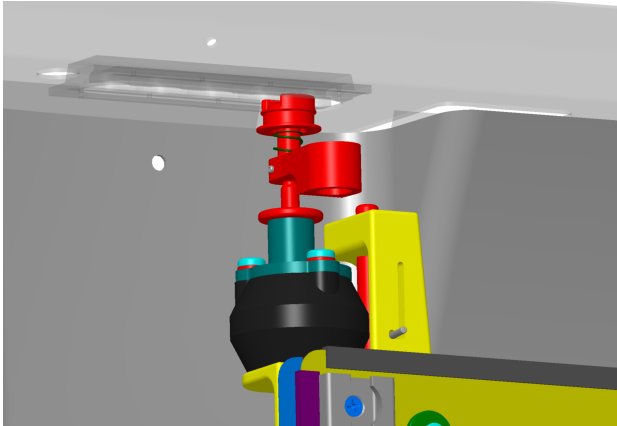
Figure C.2: The retainer is aligned with its corresponding position on the upper deck rail.
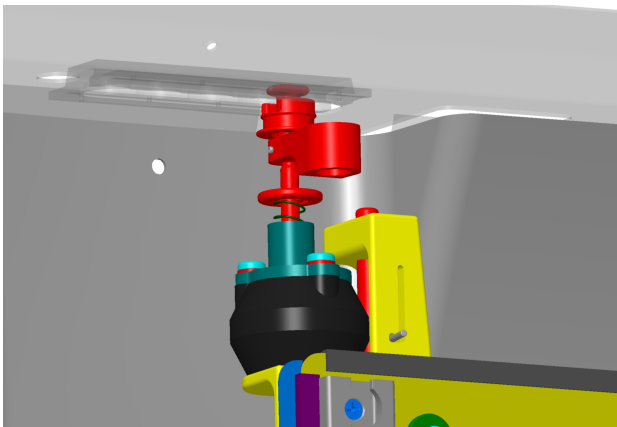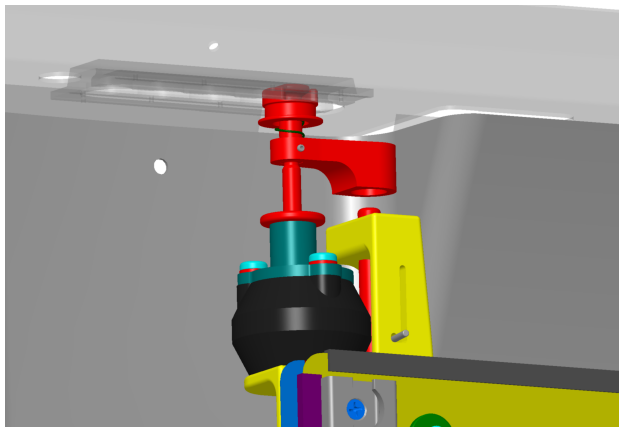

Figure C.3: The stud and the special nut are moved upwards to push the retainer and keep it vertically blocked.
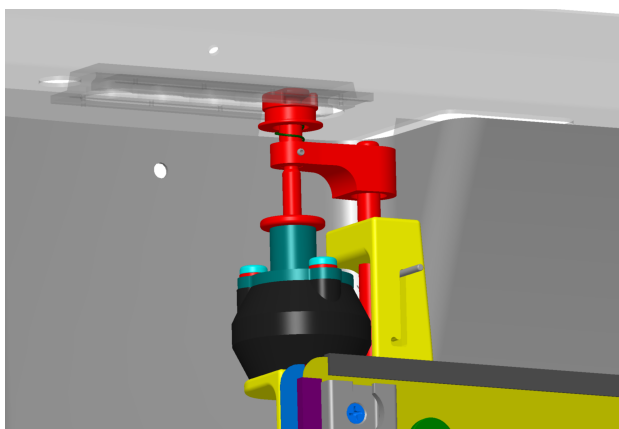

Figure C.4: The fitting is rotated 90° around the stud axis in a manner to be concentric with the sliding pin.
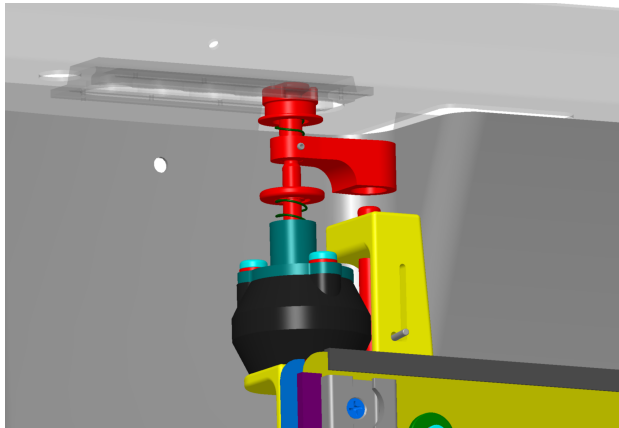
Figure C.5: With the help of a spring, the retainer is pushed into its blockage position in the track rail.

Figure C.6: In the meanwhile, the special nut is also screwed.

Figure C.7: The sliding pin is brought to its upper limit position by leaving the sliding pin return to its initial point. After this step installation procedure is terminated.
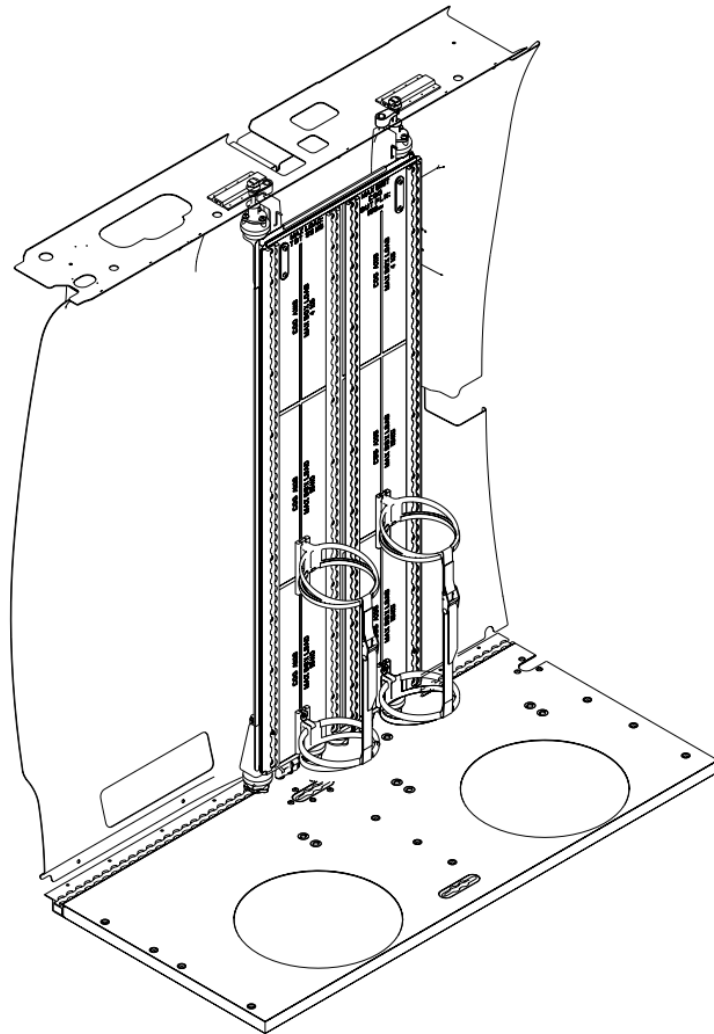
Appendix D

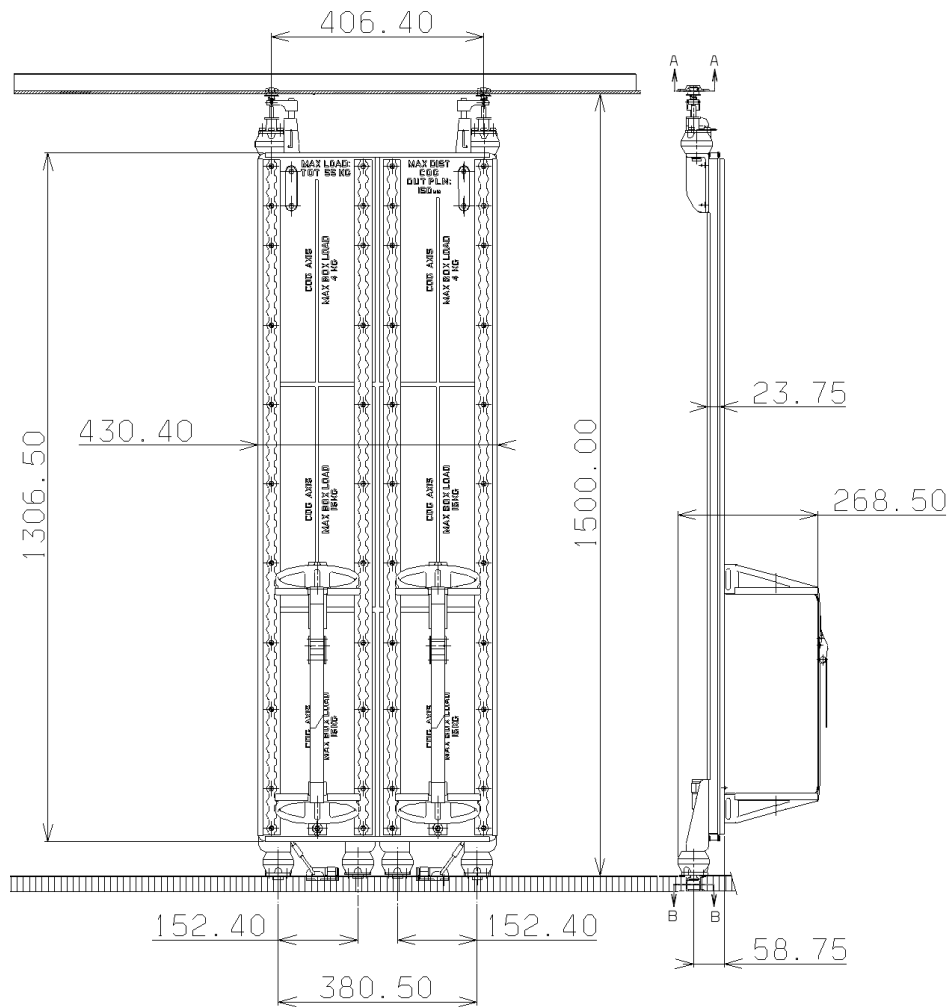# Technical drawings

Figure D.1: Isometric view of the SAR Plate

Figure D.2: Front and lateral view of the SAR Plate [*mm*]

Figure D.3: Front view of the Sar Plate and cross section views of the shock absorbers
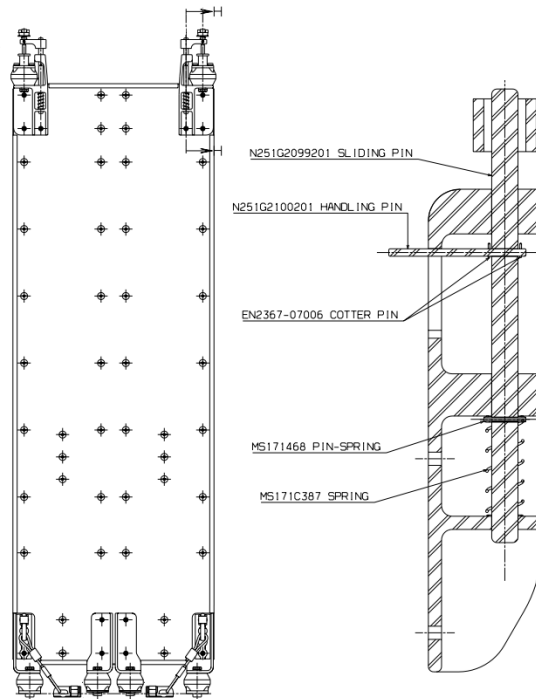
Figure D.4: Rear view of the Sar Plate and cross section view of the upper interface fitting
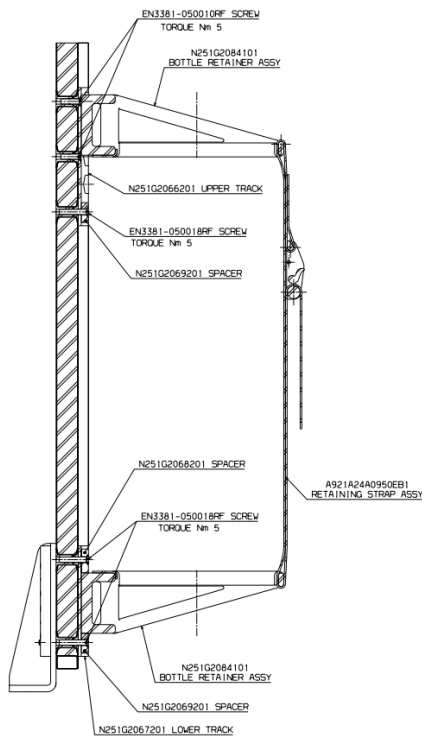

Figure D.5: Cross section view of the bottle retainers

Bibliography

[1] AW document 800-29-002/01, issue B, "Guidelines for Structural Analysis of Helicopter Airframe Structures – General", 2008.

[2] AW document 800-29-002/02, issue B, "Guidelines for Structural Analysis of Helicopter Airframe Structures – Structural Analysis Method", 2008.

[3] AW document 800-35-021, rev B, " Properties of Agusta Composite Materials", 2005.

[4] AW Program 200-90-037, issue B "Integrated Structural Analysis Program (I.S.A. Program)", 2009.

[5] AW document 200-90-037/04, issue B, "Integrated Structural Analysis Program (I.S.A. Program) – Verification Manual", 2009.

[6] Bisagni C., "Lecture notes of the course of Instability of Structures", 2008.

[7] AW document TN N251G2505E01, issue B, "NNWN SAR Plate Structural Substantiation", 2010.

[8] Paulstra, "Catalogue Gènèral", 2010.

[9] Filippone, A., "Fixed and Rotary Wing Aircraft", 2006.

[10] Mareschi, V., Chiarelli C., "Feasibility Study on Multi Disciplinary Optimization for Aerospace Application", 2008.

[11] AW document NTA-0001-07, issue E, "Preferred Commercial Dimensions for Metallic Raw Materials", 2000.

[12] AW document NTA-351A, issue A, "Honeycomb and Foams: Preferred Dimensions and Thicknesses for Agusta Programs", 2001.

[13] Bruhn, E.F., "Analysis and Design of Flight Vehicles", 1973.

[14] Recchia, V., "Development of structural optimization methodology of engine components by genetic algorithms", 2010.

[15] Dassault Systèmes, "Isight release 3.5 Component Guide", 2009.

[16] Dassault Systèmes, "Isight release 3.5 User's Guide", 2009.

[17] Ghiringhelli J.L., "Lecture notes of the course of Progetto di Strutture Aeronautiche e spaziali", 2011.

[18] Norton, R. L., "Machine Design: An Integrated Approach", 2006.

[19] Van den Braembussche R. A., Alsalihi Z., Verstraete T., "Fast Multidisciplinary Optimization of Turbomachinery Components", 2004.

[20] Sasaki D., Obayashi S., "Adaptive Range Multi Objective Genetic Algorithms and Self-Organizing Map For Multi Objective Optimization Problem", 2004.

[21] Simulia Official Website, "Isight" available at: <http://www.simulia.com/products/isight.html>, 2004.

[22] Engineous Software, "Isight-FD Design Gateway Training",2007.

[23] Koch, P., Van der Velden A., "Isight Design Optimization Methodologies ",2010.

[24] Deb, K., Fadel, G., Koch, P., Tiwari,S, "AMGA: An Archive-based Micro Genetic Algorithm for Multi-objective Optimization", 2008.

[25] Komamura, K., Ooka, R., "Optimal Design Method for Buildings and Urban Energy Systems Using Genetic Algorithms", 2007.

[26] Pitzer, T., "A Platform for Antenna Optimization with Numerical Electromagnetics Code Incorporated with Genetic Algorithms", 2006.

[27] Deb, K., "A Fast and Elitist Multiobjective Genetic Algorithm: NSGA-II", 2002.

[28] Hiroyasu, T., Miki M., Watanabe S., "Neighbourhood Cultivation Genetic Algorithm for Multi-objective Optimization Problems", 2002.

[29] Chick, J. B., "Structural Optimization of Helicopter Empennage using MSC.Nastran ", 2001.

[30] Chandra S., Kamesh J. V., Kiran S., Padmanabhan M. A., Rao J. S., "Topology Optimization of Aircraft Wing", 2008.

[31] Keller D., Kress G., "Structural Optimization", 2007.

[32] Vanderplaats, G. N., "Structural Optimization for Statics, Dynamics and Beyond ", 2006.

[33] Iyengar N. G. R., "Optimization in Structural design", 2004.

[34] Weise, T., "Global Optimization Algorithms: Theory and Application ", 2009.

[35] Obayashi, S., "Multiobjective Evolutionary Computation for Supersonic Wing Design ", 2000.

[36] Pediroda V., Poloni C., "Multi-criteria Optimization, Constraint Handling with GAs", 2000.

[37] Back, T., Naujoks B., "Some Theory of Evolution Strategies", 2000.

[38] Alsalihi Z., Van den Braembussche R. A., Verstraete T., "Fast Multidisciplinary Optimization of Turbomachinery Components", 2004.

[39] Knight D., "Multicriteria Design Optimization for Missile Air Intakes", 2004.

[40] Burns S. A., "Recent Advances in Optimal Structural Design", 2002.

[41] Michalewicz, Z., "A Survey of Constraint Handling Techniques in Evolutionary Computation Methods", 1995.

[42] Singresu S. R., "Engineering Optimization: Theory and Practice", 2009.

[43] Boccaletti C., Eleonora N., Elia S., "Deterministic and Stochastic Optimisation Algorithms in Conventional Design of Axial Flux PM Machines", 2006.

[44] Friesz, T. L., "Dynamic Optimization and Differential Games", 2010.

[45] Barner N., "Isight-Abaqus Optimization of a Ring-Stiffened Cylinder ", 2010.

[46] Amadori, K., "On Aircraft Conceptual Design: A Framework for Knowledge Based Engineering and Design Optimization ", 2008.

[47] Fernandez J. C., Pardo A., "Full Cycle Stochastic Analysis of Composite Structures under Buckling Loads. Design & Manufacturing Scatter", 2009.

[48] Williams J., "How Can We Make Best...Better: Using Abaqus and Isight to Optimize Tools for Downhole Expandable Tubulars ", 2010.